Accepted Manuscript

Hidden attractors in dynamical systems

Dawid Dudkowski, Sajad Jafari, Tomasz Kapitaniak, Nikolay V. Kuznetsov, Gennady A. Leonov, Awadhesh Prasad

PII: S0370-1573(16)30092-8
DOI: http://dx.doi.org/10.1016/j.physrep.2016.05.002
Reference: PLREP 1904

To appear in: *Physics Reports*

Accepted date: 22 May 2016

Please cite this article as: D. Dudkowski, S. Jafari, T. Kapitaniak, N.V. Kuznetsov, G.A. Leonov, A. Prasad, Hidden attractors in dynamical systems, *Physics Reports* (2016), http://dx.doi.org/10.1016/j.physrep.2016.05.002

Hidden Attractors in Dynamical Systems

Dawid Dudkowski[a], Sajad Jafari[b], Tomasz Kapitaniak[a], Nikolay V. Kuznetsov[c,d], Gennady A. Leonov[c], Awadhesh Prasad[e]

[a] *Division of Dynamics, Technical University of Lodz, Stefanowskiego 1/15, 90–924 Lodz, Poland*

[b] *Biomedical Engineering Department, Amirkabir University of Technology, Tehran 15875–4413, Iran*

[c] *Faculty of Mathematics and Mechanics, St. Petersburg State University, 198504 Peterhof, St. Petersburg, Russia*

[d] *Department of Mathematical Information Technology, University of Jyväskylä, 40014 Jyväskylä, Finland*

[e] *Department of Physics and Astrophysics, University of Delhi, Delhi 110007, India*

Abstract

Complex dynamical systems, ranging from the climate, ecosystems to financial markets and engineering applications typically have many coexisting attractors. This property of the system, is called multistability. The final state, i.e., the attractor on which the multistable system evolves strongly depends on the initial conditions. Additionally, such systems are very sensitive towards noise and system parameters so a sudden shift to a contrasting regime may occur. To understand the dynamics of these systems one has to identify all possible attractors and their basins of attraction. Recently, it has been shown that multistability is connected with the occurrence of unpredictable attractors which have been called hidden attractors. The basins of attraction of the hidden attractors do not contain unstable fixed points (if exists) and are located far away from such points. Numerical localization of the hidden attractors is not straightforward since there are no transient processes leading to them from the neighborhoods of unstable fixed points and one has to use the special analytical–numerical procedures. From the viewpoint of applications, the identification of hidden attractors is the major

Email addresses: dawid.dudkowski@p.lodz.pl (Dawid Dudkowski), sajadjafari83@gmail.com (Sajad Jafari), tomasz.kapitaniak@p.lodz.pl (Tomasz Kapitaniak), nkuznetsov239@gmail.com (Nikolay V. Kuznetsov), g.leonov@spbu.ru (Gennady A. Leonov), awadhesh.prasad@gmail.com (Awadhesh Prasad)

issue. The knowledge about the emergence and properties of hidden attractors can increase the likelihood that the system will remain on the most desirable attractor and reduce the risk of the sudden jump to undesired behavior. We review the most representative examples of hidden attractors, discuss their theoretical properties and experimental observations. We also describe numerical methods which allow identification of the hidden attractors.

Keywords: nonlinear dynamics, attractors, multistability, basins of attraction

---

Contents

1. Introduction

The climate [1–5], a number of ecosystems (e.g. the Amazon rainforest) [6–9], the human brain [10, 11], arrays of coupled lasers [12–14], financial markets [15, 16] and many applied engineering systems [17–20] are modeled by complex dynamical systems which are characterized by the existence of many coexisting attractors. This property of the systems is called multistability and refers to systems that are neither stable nor totally unstable, but that alternate between two or more mutually exclusive states (attractors) over time [21–31]. Multistable systems are very sensitive towards noise [30, 31], initial conditions [22, 24, 26] and system parameters [25].

In multistable systems, particularly in the case of the existence of attractors with very small basins or previously unidentified attractors, one can observe the sudden switch to unexpected (undesired or unknown) attractors. Such a shift can lead to the catastrophic events ranging from sudden climate changes, serious diseases to financial crises and disasters of commercial devices [32]. The spectacular example of the disaster caused by the sudden swith to the undesired attractor is the crash of aircraft YF–22 Boeing in April 1992 [33]. Generally, to keep the system on the desired attractor one

needs first to uncover all coexisting attractors and next apply an appropriate controlling scheme [24].

Most of the common examples of both chaotic and regular attractors, like that of van der Pol, Beluosov–Zhabotinsky, Lorenz, Rossler, Chua and many others are located in the neighborhoods of unstable fixed points (its basins of attraction touch/include unstable fixed points). Such attractors are called the self–exited attractors and can be easily localized numerically by the standard computational procedure (one can start with the initial conditions in a small neighborhood of the unstable fixed point on unstable manifold and observe how it is attracted) [34, 35]. The classical example of a self–excited chaotic attractor in a Duffing system was numerically constructed by Ueda in 1961, although it become well–known much later [36].

Recently, it has been shown that multistability is connected with the occurrence of unpredictable attractors [21–31] which have been called the hidden attractors [37–40]. An attractor is called the hidden attractor if its basin of attraction does not intersect with small neighborhoods of the unstable fixed point, i.e., the basins of attraction of the hidden atttractors do not touch unstable fixed points and are located far away from such points. For example, the hidden attractor is the periodic or chaotic attractor in the system without equilibria or with the only stable equilibrium (a special case of multistability and coexistence of attractors). An extensive review of control of multistability has been published by Pisarchik and Feudel [24] for the self–excited multistable attractors. However, due to existence of hidden attractors and problems with localization of them not all of the methods presented in [24] can be applied for multistable systems with hidden attractors.

The concept of hidden attractors has been suggested in connection with the discovery of unexpected attractor in Chua's circuit [37, 38, 41–46]. The dynamics of this circuit can be described by the following dimensionless equations:

$$\begin{aligned} \dot{x} &= \alpha(y - x - \psi(x)), \\ \dot{y} &= x - y + z, \\ \dot{z} &= -(\beta y + \gamma z), \\ \psi(x) &= 1/2(m_0 - m_1)(|x+1| - |x-1|), \end{aligned} \tag{1}$$

where x, y and z are state variables and $\alpha, \beta, \gamma, m_0$ and m_1 are constant [47]. For $\alpha = 9.3515908493, \beta = 14.7903198054, \gamma = 0.0160739649, m_0 = -1.1384111956$ and $m_1 = -0.7224511209$ system (1) has two coexisting double scroll attractors shown in Fig. 1, while for $\alpha = 8.5, \beta = 14.28, \gamma = 0, m_0 = -8/7$ and $m_1 = -5/7$ it evolves on two symmetric Rossler–like attractors

shown in Fig. 2. The attractors shown in Figs. 1 – 2 are self–excited as they can be easily reached from the neighborhoods of unstable fixed points F_0, S_1 and S_2. On the other hand, the attractor shown in Fig. 3 ($\alpha = 8.4562218418, \beta = 12.0732335925, \gamma = 0.0051631393, m_0 = -0.1767573476$ and $m_1 = -1.1467573476$) is hidden. One can see that its basin does not touch any of the unstable points $S_{1,2}$. Stable fixed point F_0 attracts trajectories (shown in black) from stable manifolds ${M_{1,2}}^{st}$ of two saddle points $S_{1,2}$ while the trajectories starting from unstable manifolds ${M_{1,2}}^{unst}$ (shown in red) tend to infinity. The comparison of Figs. 1 – 3 exhibits the main differences between the self–excited and hidden attractors.

Contrary to the self–excited attractors the localization of hidden attractors is not straightforward since there are no similar transient processes leading to such attractors from the neighborhoods of the unstable fixed points [44, 48]. For numerical uncovering of hidden attractors it is necessary to develop special analytical–numerical procedures. This paper reviews the current state of art in the research on multistable systems with hidden attractors from the physical point of view (other reviews like e.g. [40] discuss hidden attractors from the strict mathematical point) and point out the directions of further studies. New examples of hidden attractors, numerical procedures for finding them as well as methods of controlling multistable systems are presented. Experimental evidence of the existence of hidden attractors is given. We try to unify the approaches of rare attractors, rare events [49] and basin stability [50].

This review paper is organized as follows. Section 2 gives examples of the hidden attractors and categorize them according to the structure of systems' equations. The relation between hidden and rare attractors is discussed in Sec. 3. In Sec. 4 we describe the methods for detection of hidden attractors and introduce their main properties. In addition to various numerical methods we describe the recently developed approach of perpetual points [51, 52]. Section 5 describes the dynamics of the coupled systems with hidden attractors. The examples of the experimental realizations of the systems with hidden attractors are given in Sec. 6. Finally, this review is summarized in Sec. 7.

2. Hidden attractors: widespread objects in dynamical systems

Consider a dynamical system

$$\dot{X} = F(X, p), \tag{2}$$

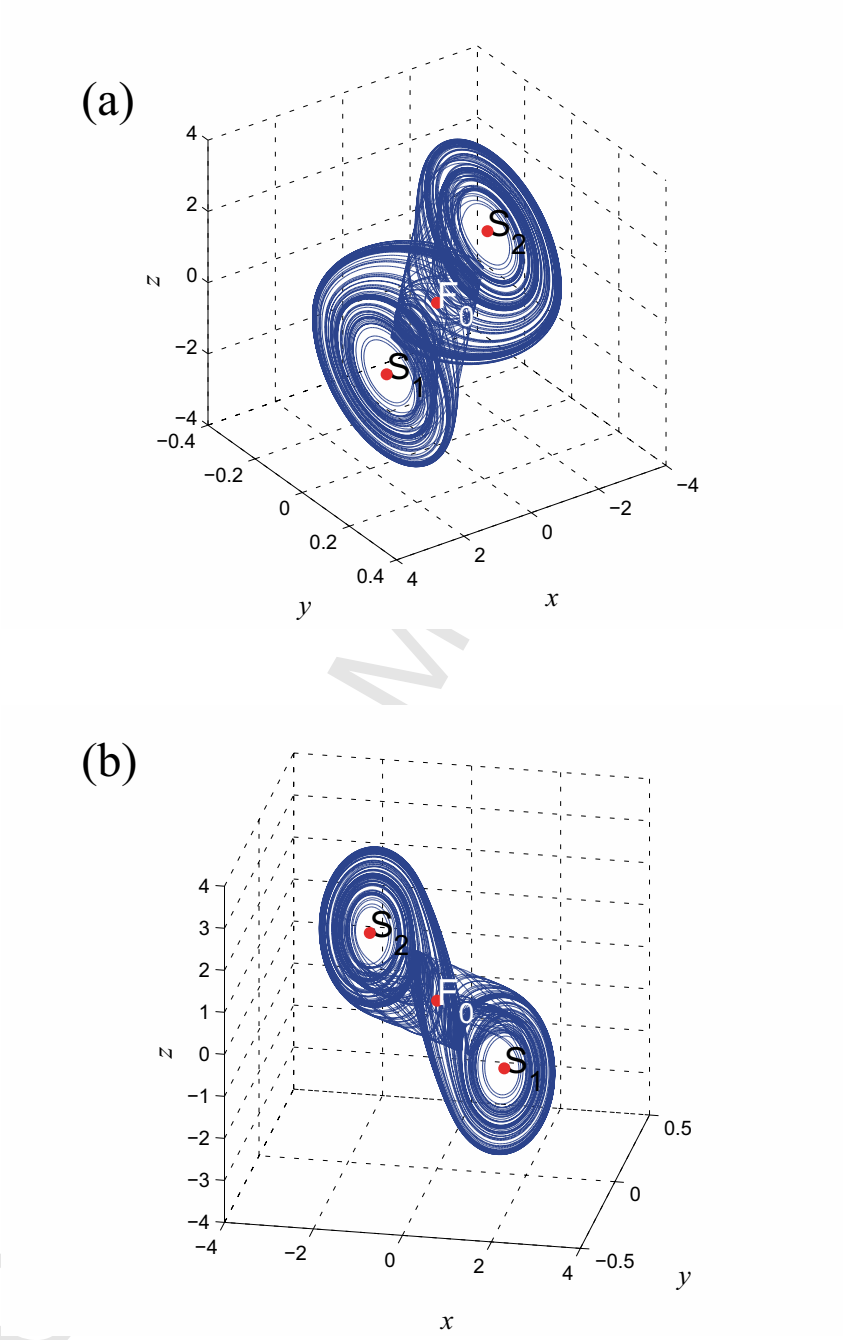

Figure 1: (color online). Double–scroll self–excited Chua attractors for parameters $\alpha = 9.3515908493$, $\beta = 14.7903198054$, $\gamma = 0.0160739649$, $m_0 = -1.1384111956$, $m_1 = -0.7224511209$. In (a) the localization from vicinity of fixed point F_0 is shown, while in (b) the localization from vicinity of fixed point S_1 is presented.

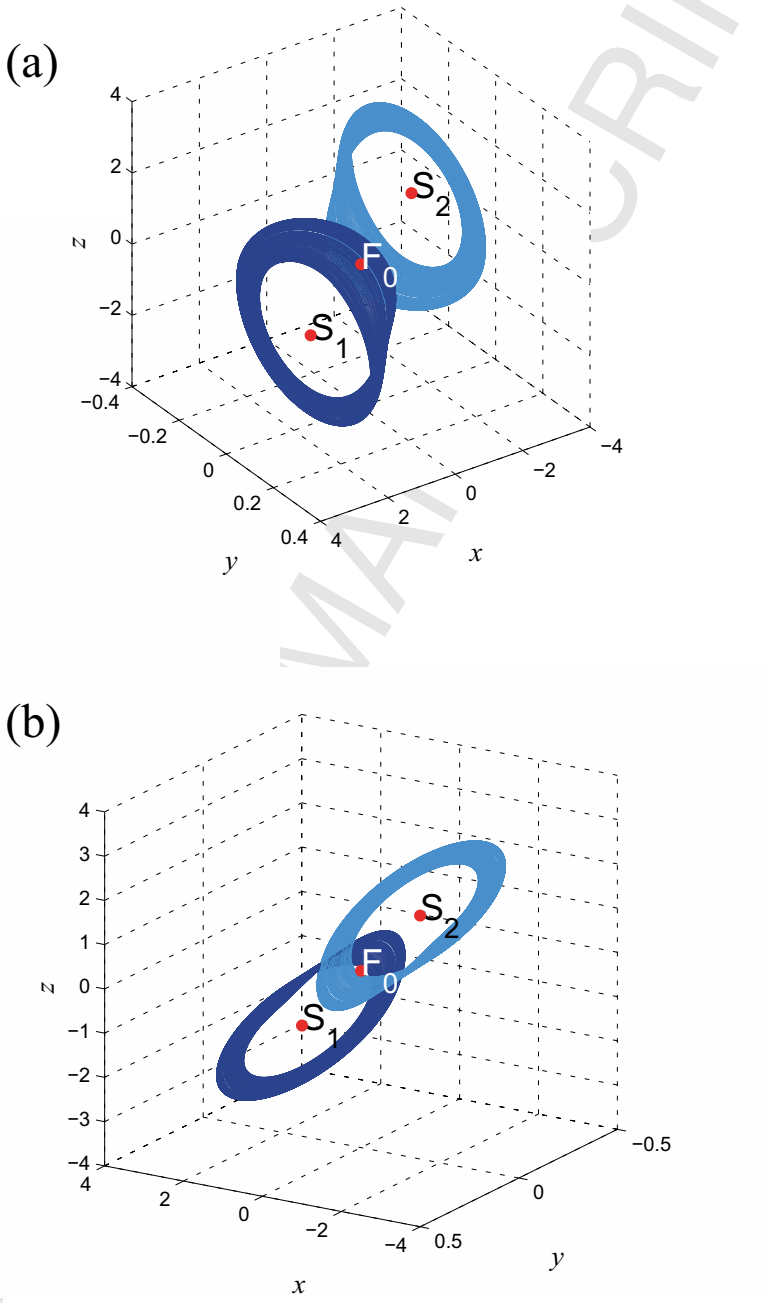

Figure 2: (color online). Two symmetric Rossler–like self–excited Chua attractors for parameters $\alpha = 8.5$, $\beta = 14.28$, $\gamma = 0$, $m_0 = -8/7$, $m_1 = -5/7$. The localization from vicinity of fixed point F_0 is shown (two views (a) and (b)).

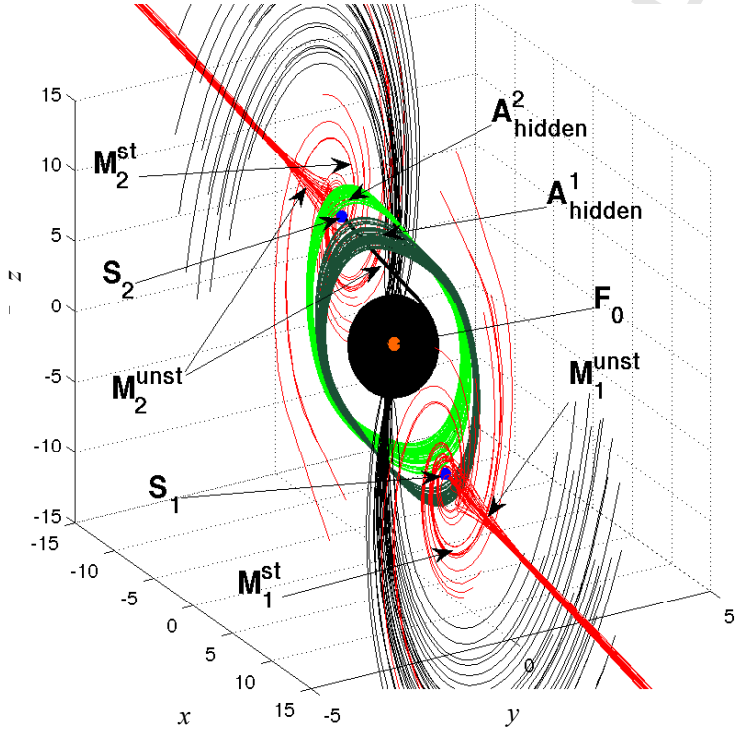

Figure 3: (color online). Symmetric hidden chaotic attractors ($A^{1,2}_{hidden}$ – green domain) in the classical Chua circuit: locally stable zero equilibrium F_0 (orange dot) attracts trajectories (black) from stable manifolds $M^{st}_{1,2}$ of two saddle points $S_{1,2}$ (blue dots); trajectories (red) from unstable manifolds $M^{unst}_{1,2}$ tend to infinity; $\alpha = 8.4562$, $\beta = 12.0732$, $\gamma = 0.0052$, $m_0 = -0.1768$, $m_1 = -1.1468$.

where $X \in \mathbb{R}^n, t \in \mathbb{R}$ and $p \in \mathbb{R}^k$ is the vector of system parameters. From a computational point of view, it is natural to introduce the following classification of attractors:

Definition 1. *[37, 38, 40, 53] An attractor is called a self–excited attractor if its basin of attraction intersects with any open neighborhood of an unstable fixed point. Otherwise it is called a hidden attractor.*

The basin of attraction for a hidden attractor is not connected with any unstable fixed point. For example, the hidden attractors are observed in the systems with no unstable fixed points or with one stable fixed point (a special case of multistability). In many practical systems (e.g. Chua

circuit described in Sec. 1) various self–excited attractors coexist with hidden attractor (of attractors).

In this Section we describe typical examples of hidden attractors. We start with simple flows and continue to present the real physical systems.

2.1. Hilbert's 16th problem

The problem of analyzing hidden periodic oscillations first arose in the second part of Hilbert's 16th problem (1900), which considered the number and mutual disposition of limit cycles in two–dimensional polynomial systems [54]. The first nontrivial results have been obtained by Bautin (see, e.g. [55]) and have been devoted to the theoretical construction of three nested limit cycles around one equilibrium in quadratic systems. Bautin's method can only be used to construct nested, small–amplitude limit cycles, which can hardly be computed and visualized. However, recently an analytical approach has been developed, which can be used to effectively visualize nested, normal amplitude limit cycles in quadratic systems [40, 56, 57].

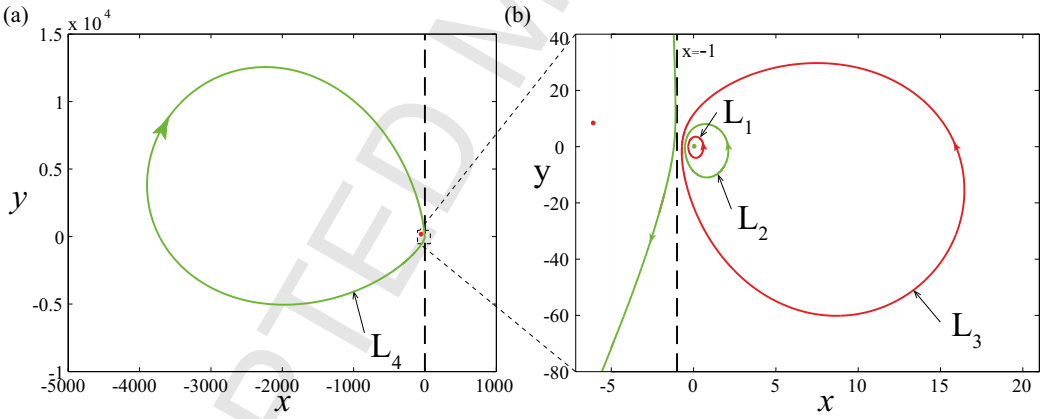

Figure 4: (color online). Visualization of four limit cycles $L_1 - L_4$ (green color represents stable and red represents unstable) in a two–dimensional polynomial quadratic system (3) for the coefficients $a_1 = b_1 = \beta_1 = -1$, $c_1 = \alpha_1 = 0$, $b_2 = -2.2$, $c_2 = -0.7, a_2 = 10$, $\alpha_2 = 72.7778$, and $\beta_2 = -0.0015$. One limit cycle L_4 (self–excited attractor) around an unstable equilibrium (red dot) is shown in (a), while the localization of three nested limit cycles ($L_{1,2,3}$; L_2 is a hidden attractor) around stable zero equilibrium (green dot) is presented in (b).

For example, let us consider the following system:

$$\begin{aligned} \dot{x} &= -(a_1x^2 + b_1xy + c_1y^2 + \alpha_1x + \beta_1y), \\ \dot{y} &= -(a_2x^2 + b_2xy + c_2y^2 + \alpha_2x + \beta_2y). \end{aligned} \tag{3}$$

Typical limit cycles of system (3) are shown in Fig. 4. The cycles $L_1 - L_4$ are presented in green (stable) and red (unstable). The fixed point $(0, 0)$ is stable as well as the orbits L_2 and L_4. Attractor L_2 is hidden as its basin located between unstable cycles L_1 and L_3 does not contain unstable fixed points.

2.2. Flows without fixed points (equilibria)

The works of Nosè [58] and Hoover [59] in 1984–85 have led the study of the following dynamical system without equilibria

$$\begin{aligned} \dot{x} &= y, \\ \dot{y} &= -x - yz, \\ \dot{z} &= \alpha(y^2 - 1), \end{aligned} \tag{4}$$

and its various modifications, where hidden chaotic oscillations can be found (see, e.g. [60–64]). This example motivates further construction and study of various artificial chaotic systems without equilibria.

Let us consider the system proposed by Wei [65]

$$\begin{aligned} \dot{x} &= -y, \\ \dot{y} &= x + z, \\ \dot{z} &= 2y^2 + xz - 0.35, \end{aligned} \tag{5}$$

which is a modification of the Sprott case D system [61]. As system (5) has no fixed points, the chaotic attractor shown in Fig. 5 is hidden.

Jafari and Sprott [66] have performed systematic search to find the simplest three–dimensional chaotic systems with quadratic nonlinearities and no equilibria. Seventeen simple systems that show chaos have been found. As an example, the attractor of the system

$$\begin{aligned} \dot{x} &= y, \\ \dot{y} &= -x + z, \\ \dot{z} &= -0.8x^2 + z^2 + 2, \end{aligned} \tag{6}$$

is shown in Fig. 6.

Other examples of chaotic and hyperchaotic systems with no equilibrium and hidden attractors can be found in [51, 67–73].

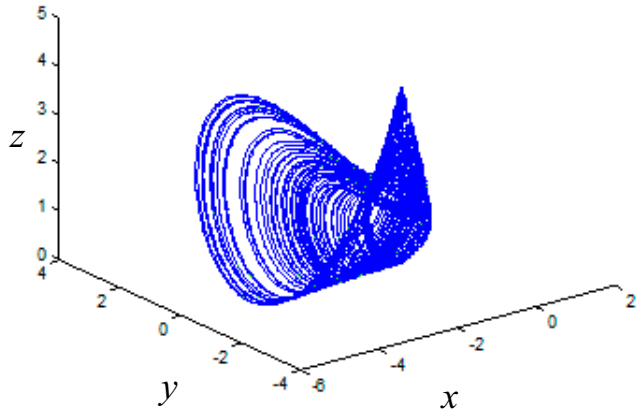

Figure 5: (color online). Attractor of the system (5) with initial conditions (-1.6,0.82,1.9).

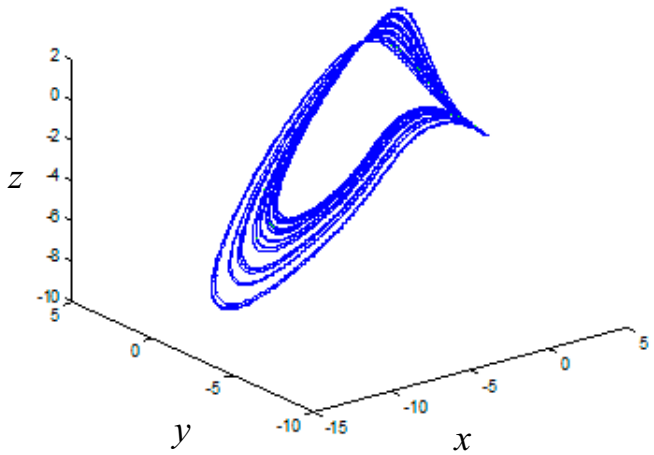

Figure 6: (color online). Attractor of system (6) with initial conditions (0,2.3,0).

2.3. Flows with stable fixed point (equilibrium)

The example of such unusual chaotic flow (with only one stable equilibrium) has been designed by Wang and Chen [74]. They have considered the

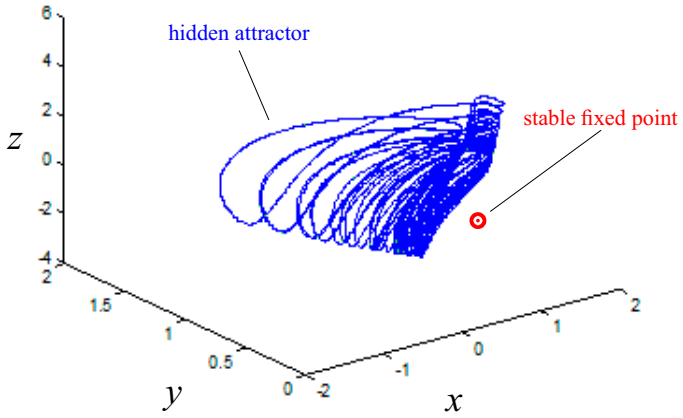

Figure 7: (color online). Attractor of the system (7) with initial conditions (0,0,0).

following system:

$$\begin{aligned} \dot{x} &= yz + 0.006, \\ \dot{y} &= x^2 - y, \\ \dot{z} &= 1 - 4x. \end{aligned} \tag{7}$$

Its hidden attractor is shown in Fig. 7.

Later Jafari and Sprott have identified 23 simple systems with this property. To do that, they have performed systematic computer search for chaos in three–dimensional autonomous systems with quadratic nonlinearities and a single equilibrium (stable according to the Routh–Hurwitz criterion). System

$$\begin{aligned} \dot{x} &= y, \\ \dot{y} &= z, \\ \dot{z} &= -x - 0.6y + z^2 - 0.4xy, \end{aligned} \tag{8}$$

is one of the simplest cases which have been found in this way. The equilibrium of this system is at (0,0,0) and its attractor is illustrated in Fig. 8. At least one point attractor coexists with a hidden strange attractor for these types of chaotic flows. Other chaotic and hyperchaotic systems with stable equilibrium have been described in [71, 75–82].

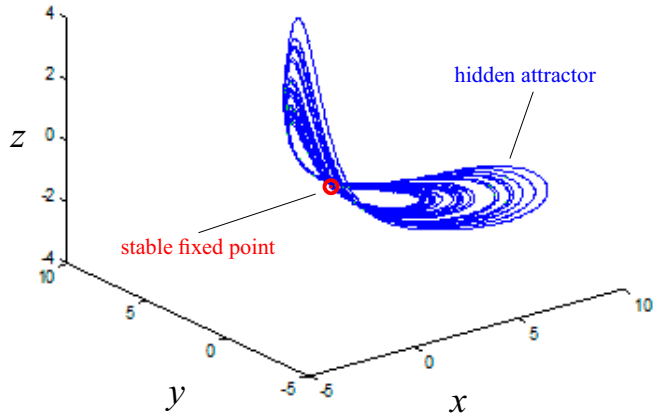

Figure 8: (color online). Attractor of the system (8) with initial conditions (4,-2,0).

2.4. Flows with a line of fixed points (equilibria)

After proposing a chaotic system with any number of equilibria by Wang and Chen in [73], Jafari and Sprott in [83] have introduced simple chaotic systems with a line of equilibria. They have been inspired by the structure of the conservative Sprott case A system [61] and have considered a general parametric form of it with quadratic nonlinearities. With exhaustive computer search, nine simple cases have been found. The system given by the following equations:

$$\begin{aligned} \dot{x} &= y, \\ \dot{y} &= -x + yz, \\ \dot{z} &= -x - 15xy - xz, \end{aligned} \tag{9}$$

is an especially simple example with only six terms. System (9) has a line of stable fixed points (equilibria) at $(0, 0, z^*)$, where $z^* \in \mathbb{R}$, with no other equilibria (in other words the z–axis is the line equilibrium of this system). Its attractor is shown in Fig. 9.

The strange attractor of this system is hidden, from computational point of view, since there are uncountably many unstable points on the equilibrium line of which only a tiny portion intersects the basin of the chaotic attractor. Thus the equilibria cannot help in finding the attractor(s) because we don't know which part of the equilibria may be the desired part.

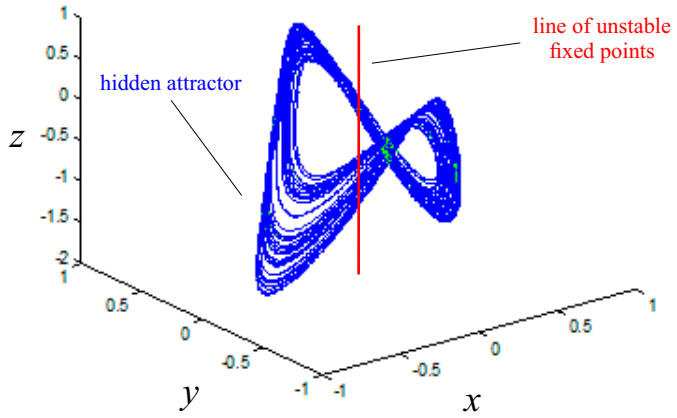

Figure 9: (color online). Attractor of the system (9) with initial conditions (0,0.5,0.5).

2.5. Electromechanical system without equilibria

Hidden attractors appear naturally in systems without equilibria, describing various mechanical and electromechanical models with rotation and electrical circuits with cylindrical phase space. One of the first such examples has been described by Arnold Sommerfeld in 1902 [84]. He has studied the oscillations caused by a motor driving an unbalanced weight and discovered the resonance capture (Sommerfeld effect). The Sommerfeld effect of the capture phenomenon represents the failure of a rotating mechanical system to be spun up by a torque–limited rotor to a desired rotational velocity due to its resonant interaction with another part of the system [85, 86].

As an example, let us consider the model studied in [87], i.e., the translational oscillator–rotational actuator, which consists of a cart (of mass M) attached to a wall by a spring of stiffness k_2. An unbalanced rotor (where m is the rotating eccentric mass, while l is the length from the axis of rotation) which is connected to the cart is actuated by a DC motor, where $u = N(t)$ is the motor torque. The scheme of the model is shown in Fig. 10.

The dynamics of the system is given by the following equations

$$\begin{cases} (M+m)\ddot{x} + k_1\dot{x} + ml(\ddot{\theta}\cos\theta - \dot{\theta}^2\sin\theta) + k_2 x = 0, \\ J\ddot{\theta} + k_3\dot{\theta} + ml\ddot{x}\cos\theta = u, \end{cases} \tag{10}$$

where J is the moment of inertia, k_1, k_3 are the damping coefficients, and

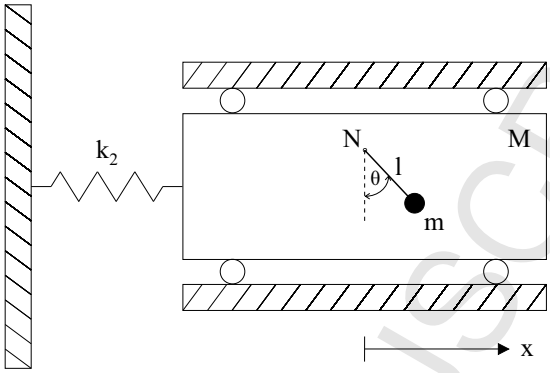

Figure 10: The translational oscillator–rotational actuator model in the horizontal plane [87].

M, m, l, k_2, u are as in the description of the model presented above. The x variable is the displacement of the cart from its equilibrium, while θ is the rotational angle of the rotor.

In Fig. 11 the hidden attractors in the model (10) are presented for the fixed parameters $J = 0.014, M = 10.5, m = 1.5, l = 0.04, k_3 = 0.005, k_2 = 5300, k_1 = 5$ and u considered as the control one. In the space $(x, \dot{x}, \dot{\theta})$ there is a hidden attractor for $u = 0.49$ shown in Fig. 11(a), where the red curve corresponds to the regular start of the system, i.e. zero initial conditions, and is attracted by an attractor. For $u = 0.48$ there are two coexisting hidden attractors presented in Fig. 11(b). The blue curve corresponds to the regular start of the system, i.e. zero initial conditions and demonstrates the Sommerfeld effect, while the red curve is attracted to the desired operation of the system.

2.6. Electromechanical model of the drilling system

In the works [89, 90] a double–mass mathematical model of the drilling system is studied by the group of researchers from the Eindhoven University of Technology. This mathematical model is based on an experimental setup. It consists of upper and lower discs connected with each other by a steel string. The upper disc is actuated by a DC motor and there is also a brake device which is used for modelling of the friction force which acts on the lower disc. The model is described by the following differential equations

$$\begin{aligned} &J_u\ddot{\theta}_u + k_\theta(\theta_u - \theta_l) + b(\dot{\theta}_u - \dot{\theta}_l) + T_{fu}(\dot{\theta}_u) - k_m v = 0, \\ &J_l\ddot{\theta}_l - k_\theta(\theta_u - \theta_l) - b(\dot{\theta}_u - \dot{\theta}_l) + T_{fl}(\dot{\theta}_l) = 0. \end{aligned} \tag{11}$$

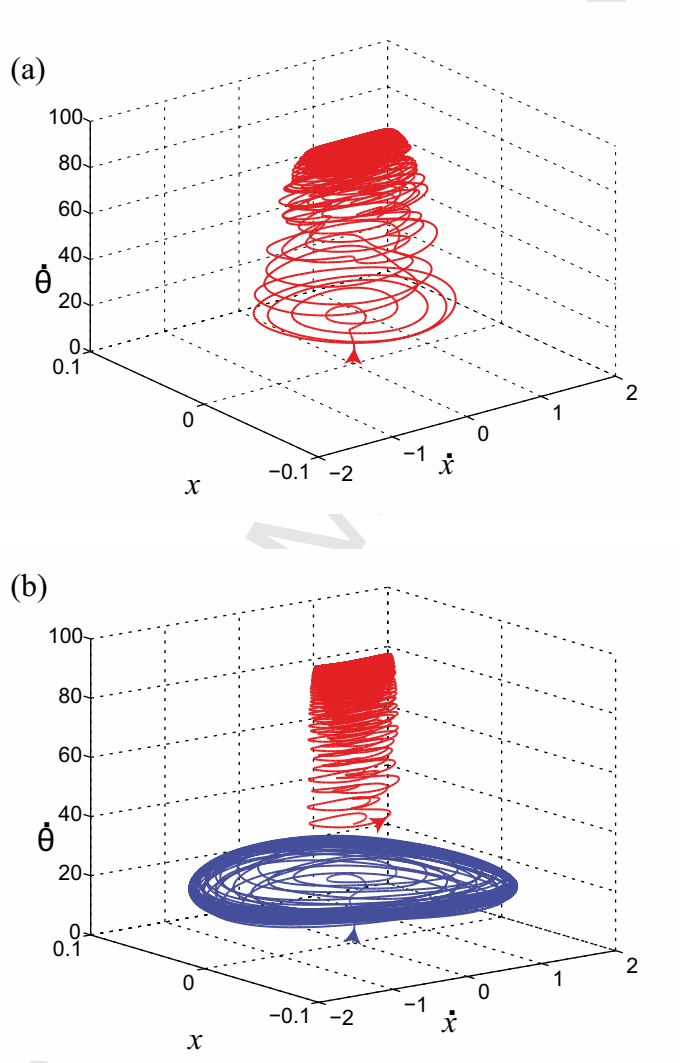

Figure 11: (color online). Hidden attractors and multistability in the electromechanical model without equilibria (10). The control parameter equals to $u = 0.49$ (a) and $u = 0.48$ (b) respectively [88] .

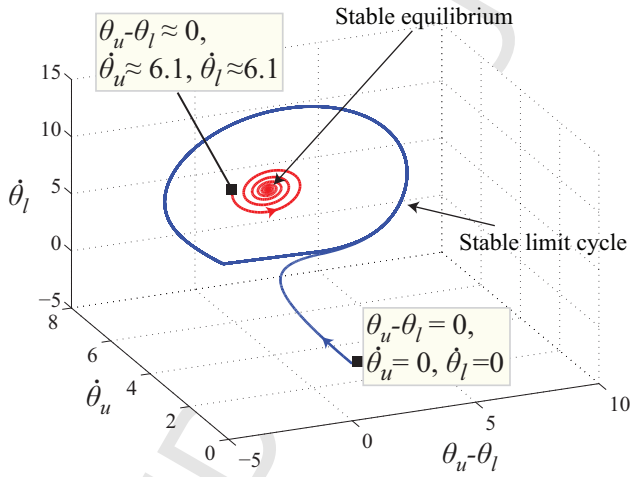

Figure 12: (color online). Hidden attractor and multistability in the drilling model (11). In the space $(\theta_u - \theta_u, \dot{\theta}_u, \dot{\theta}_l)$ a hidden periodic attractor coexists with a stable stationary point (the red curve is attracted to a stable stationary point and corresponds to the start of drilling, i.e. the friction is applied to the model, after starting the motor; the blue curve is attracted to a stable limit cycle and corresponds to the start of the system with friction applied). Parameters: $k_m = 4.3228; J_u = 0.4765; T_{su} = 0.37975; \Delta T_{su} = -0.00575; b_u = 2.4245; \Delta b_u = -0.0084; k_\theta = 0.075; b = 0; J_l = 0.035; T_{sl} = 0.26; T_{cl} = 0.05; \omega_{sl} = 2.2; \delta_{sl} = 1.5; b_l = 0.009; u = 3.5$ [88].

Here θ_u and θ_l are angular displacements of upper and lower discs; J_u and J_l are constant inertia torques; b is rotational friction (damping); k_θ is the torsional spring stiffness; k_m is the motor constant; v is the constant input voltage; $T_{fu}(\dot{\theta}_u)$ and $T_{fl}(\dot{\theta}_l)$ are friction torques acting on the upper and the lower discs. The torque $T_{fl}(\dot{\theta}_l)$ appears due to the friction between the drill bit (lower disc) and the bedrock to be drilled. $T_{fu}(\dot{\theta}_u) - k_m v$ is a result of the influence of the drive part on the drill–string. The drive part of the model, considered above, is a linear combination of constant input voltage and friction torque $T_{fu}(\dot{\theta}_u)$ acting on the upper disc. The friction model, which has been found experimentally [89, 90], is as follows:

$$T_{fl}(\omega + \dot{\theta}_l) \in \begin{cases} T_{cl}(\omega + \dot{\theta}_l)\mathrm{sign}(\omega + \dot{\theta}_l), & \omega + \dot{\theta}_l \neq 0 \\ [-T_0, T_0], & \omega + \dot{\theta}_l = 0, \end{cases} \tag{12}$$

where

$$T_{cl}(\omega + \dot{\theta}_l) = \tfrac{T_0}{T_{sl}}(T_{pl} + (T_{sl} - T_{pl})e^{-|\frac{\omega + \dot{\theta}_l}{\omega_{sl}}|^{\delta_{sl}}} + b_l|\omega + \dot{\theta}_l|). \tag{13}$$

Here T_0, T_{sl}, T_{pl}, ω_{sl}, δ_{sl}, and b_l are nonnegative coefficients. T_0 is an additional parameter for changing the drilling medium.

In the above dynamical model of the drilling system there are two natural transition processes: the first is to start the motor and then to begin drilling (i.e. to add friction to the model), the second is to apply friction to the model and then to start the motor (also it corresponds to the sudden changes in the friction). The first transition process leads to the normal operation (i.e. the corresponding trajectory is attracted to the stable stationary point), while the second transition process may lead to a hidden oscillation (see Fig. 12).

Similar behavior and hidden periodic attractors are also found in the drilling systems driven by induction motors with a wound rotor or salient pole synchronous motors [91–94].

2.7. Rabinovich system

In 1978 one of the oldest known chaotic system, where a hidden attractor can be found,

$$\begin{cases} \dot{x} = hy - \nu_1 x - yz, \\ \dot{y} = hx - \nu_2 y + xz, \\ \dot{z} = -z + xy, \end{cases} \tag{14}$$

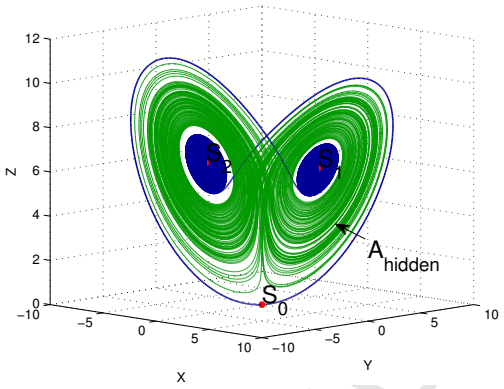

Figure 13: (color online). Hidden attractor in the Rabinovich system (14). Parameters: $r = 6.8, a = -0.5, \sigma = ra, b = 1$ [95].

was suggested by Mikhail Rabinovich [96, 97]. The Rabinovich system (14) describes the interaction of three resonantly coupled plasma waves two of them being parametrically excited. Here parameter h is proportional to the pumping amplitude and parameters ν_1 and ν_2 are normalized dumping decrements.

By the linear transformation (see, e.g. [98]): $x \to \nu_1\nu_2 h^{-1} y, y \to \nu_1 x, z \to \nu_1\nu_2 h^{-1} z, t \to \nu_1^{-1} t$ the Rabinovich system (14) is transformed to the form of generalized Lorenz system

$$\begin{cases} \dot{x} = -\sigma(x - y) - ayz, \\ \dot{y} = rx - y - xz, \\ \dot{z} = -bz + xy, \end{cases} \tag{15}$$

where

$$\sigma = \nu_1^{-1}\nu_2,\ b = \nu_1^{-1},\ a = -\nu_2^2 h^{-2},\ r = \nu_1^{-1}\nu_2^{-1}h^2. \tag{16}$$

System (15) with $a = 0$ coincides with the classical Lorenz system [99]. Remark that for classical parameters $\sigma = 10, \beta = 8/3, \rho = 28$ the Lorenz attractor is self–excited with respect to all three equilibria and $\sigma = 10, \beta = 8/3, \rho = 24.5$ is self–excited with respect to zero unstable equilibrium only.

System (15) was also used to describe the following physical processes: the convective fluid motion inside rotating ellipsoid, the rotation of rigid body in viscous fluid, the gyrostat dynamics, the convection of horizontal layer of fluid making harmonic oscillations and the model of Kolmogorov's flow.

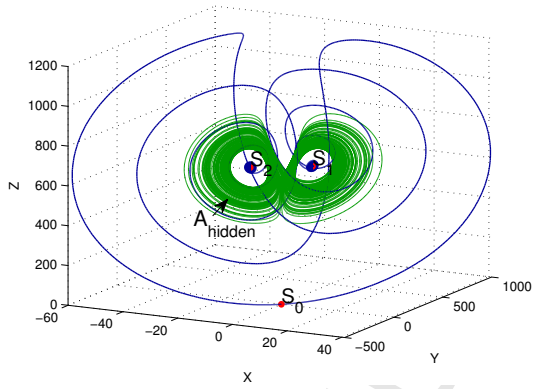

Figure 14: (color online). Hidden attractor in the Gluhovsky–Dolzhansky system (17). Parameters: $r = 700, a = 0.0052, \sigma = ra, b = 1$ [53, 102].

Note that since parameters ν_1, ν_2, h are positive then from (16) the parameter a is negative. Also, due to (16) one can obtain the following relation between σ, a and r: $\sigma = -ar$. For $a < 0$ if $r < 1$, then (15) has a unique equilibrium $\mathrm{S}_0^* = (0, 0, 0)$, which is globally asymptotically Lyapunov stable [98, 100]. If $r > 1$, then system (15) has three equilibria: $\mathrm{S}_0^* = (0, 0, 0)$ and $\mathrm{S}_{1,2}^* = (\pm x_1, \pm y_1, z_1)$. Here $x_1 = \frac{\sigma\sqrt{\xi}}{\sigma + a\xi}, y_1 = \sqrt{\xi}, z_1 = \frac{\sigma\xi}{\sigma + a\xi}$, $\xi = \frac{\sigma}{2a^2}\left(a(r-2) - \sigma + \sqrt{(\sigma - ar)^2 + 4a\sigma}\right)$. For $r = 6.8$ and $a = -0.5$ the equilibria $S_{1,2}^*$ attract the unstable separatrices of the saddle zero equilibrium, at the same time a hidden attractor can be computed in the system (see Fig. 13) [95, 101].

2.8. Gluhovsky–Dolzhansky system

In 1980 another Lorenz–like system, where a hidden attractor can be found,

$$\begin{cases} \dot{x} = -\sigma x + z + a_0 yz, \\ \dot{y} = R - y - xz, \\ \dot{z} = -z + xy, \end{cases} \tag{17}$$

was suggested by Alexander Gluhovsky and Felix Dolzhansky [103]. This model describes convective fluid motion, a rigid body rotation in a resisting medium and the forced motion of a gyrostat.

By the change of variables $x \to x$, $y \to R - \frac{\sigma}{a_0 R + 1} z$, $z \to \frac{\sigma}{a_0 R + 1} y$ system (17) takes the form of the generalized Lorenz system (15) with parame-

ters $b = 1, \quad A = \frac{a_0\sigma^2}{(a_0R+1)^2}, \quad r = \frac{R}{\sigma}(a_0R+1)$. For $r = 700, a = 0.0052, \sigma = ra$, and $b = 1$ the equilibria $S_{1,2}$ attract the unstable separatrices of the saddle zero equilibrium, at the same time a hidden attractor can be computed in the system (see Fig. 14) [53, 102].

2.9. Rabinovich–Fabricant model

Mikhail Rabinovich and Anatoly Fabrikant [104] introduced and analyzed from a physical point of view a model describing the stochasticity arising from the modulation instability in a non–equilibrium dissipative medium. This is a simplification of a complex nonlinear parabolic equation modelling different physical systems, such as: the Tollmien–Schlichting waves in hydrodynamic flows, wind waves on water, concentration waves during chemical reactions in a medium, where diffusion occurs, Langmuir waves in plasma, etc. [104]. The Rabinovich–Fabrikant model is described by the following equations:

$$\begin{aligned} \dot{x}_1 &= x_2\left(x_3 - 1 + x_1^2\right) + ax_1, \\ \dot{x}_2 &= x_1\left(3x_3 + 1 - x_1^2\right) + ax_2, \\ \dot{x}_3 &= -2x_3\left(b + x_1x_2\right), \end{aligned} \tag{18}$$

where two constant parameters $a, b > 0$. For $a < b$, the system is dissipative. The system is equivariant with respect to the symmetry [104, 105] $T(x_1, x_2, x_3) \to (-x_1, x_2, x_3)$ and has five equilibria

$$X_0^* = (0,\, 0,\, 0), \tag{19}$$

$$X_{1,2}^* = \left(\pm x_+,\, \mp\frac{b}{x_+},\, 1 - \left(1 - \frac{a}{b}\right)x_+^2\right), \tag{20}$$

$$X_{3,4}^* = \left(\pm x_-,\, \mp\frac{b}{x_-},\, 1 - \left(1 - \frac{a}{b}\right)x_-^2\right), \tag{21}$$

where

$$x_\pm = \sqrt{\frac{1 \pm \sqrt{1 - ab\left(1 - \frac{3a}{4b}\right)}}{2\left(1 - \frac{3a}{4b}\right)}}.$$

According to the article [105], we consider $a = 0.1$, $b \in (b_{min},\, b^*)$ and take the values of b for which in the phase space there are a chaotic attractor besides the stable equilibria $X_{1,2}^*$. In order to integrate system (18) we use the LIL method of order 4 (MATLAB code taken from [106]).

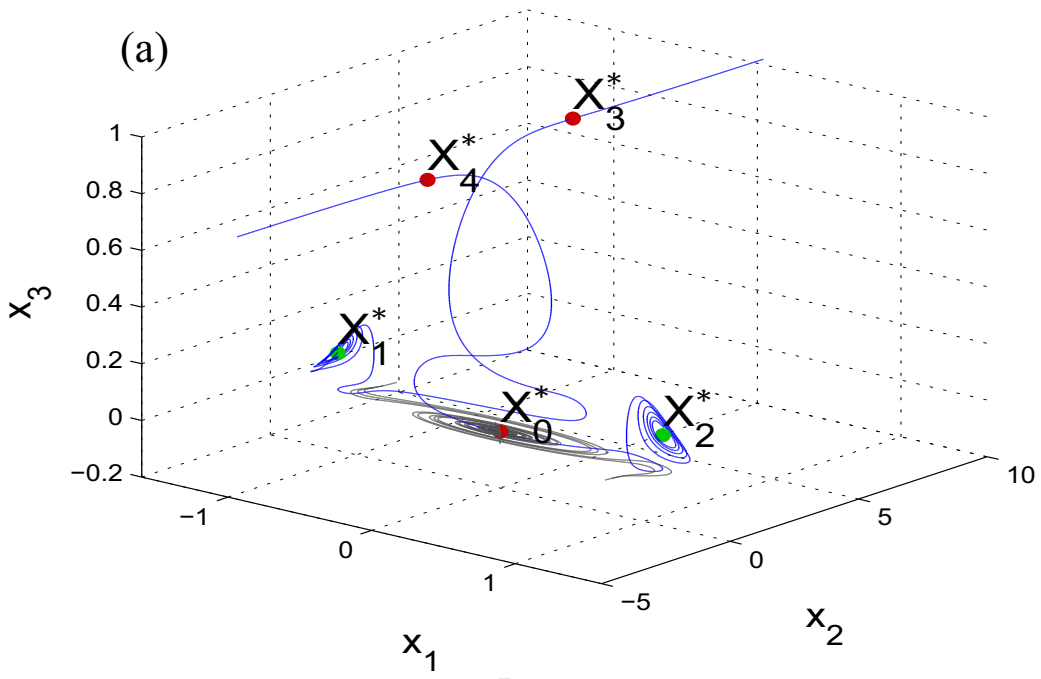

Figure 15: (color online). Parameters $a = 0.1$, $b = 0.2715$. (a) Blue curves – separatrices of the $X^*_{3,4}$ with initial conditions on 1D unstable manifolds, grey curves – trajectory with initial condition on 2D unstable manifold of X^*_0. (b) Grey sphere – δ–vicinity of X^*_0, $\delta = 0.05$; green curves – trajectories that attract to equilibrium X^*_1; purple curves – trajectories that attract to equilibrium X^*_2; orange curves – trajectories that tend to ∞ [107].

For parameters $a = 0.1$, $b = 0.2715$. it is known analytically that 1) equilibrium X^*_0 is a saddle–focus with 1D stable and 2D unstable manifolds; 2) equilibria $X^*_{1,2}$ are stable focus–nodes; 3) equilibria $X^*_{3,4}$ are saddle–foci with 2D stable and 1D unstable manifolds.

Numerical simulations show that trajectories with initial data from the δ–vicinity of X_0 on the 2D unstable manifold tend to ∞ as $t \to +\infty$ (see Fig. 15(a), grey curves). Separatrices of $X^*_{3,4}$ either tend to ∞ as $t \to +\infty$ or attract to the stable equilibria $X^*_{1,2}$ (see Fig. 15(a), blue curves).

Around equilibrium X_0 we choose a small sphere with radius δ (in our experiment $\delta = 0.05$) and take N random initial points on it (in our experiment $N = 50$). Using LIL solver we integrate system (18) with these initial points in order to explore the obtained trajectories. We repeat this

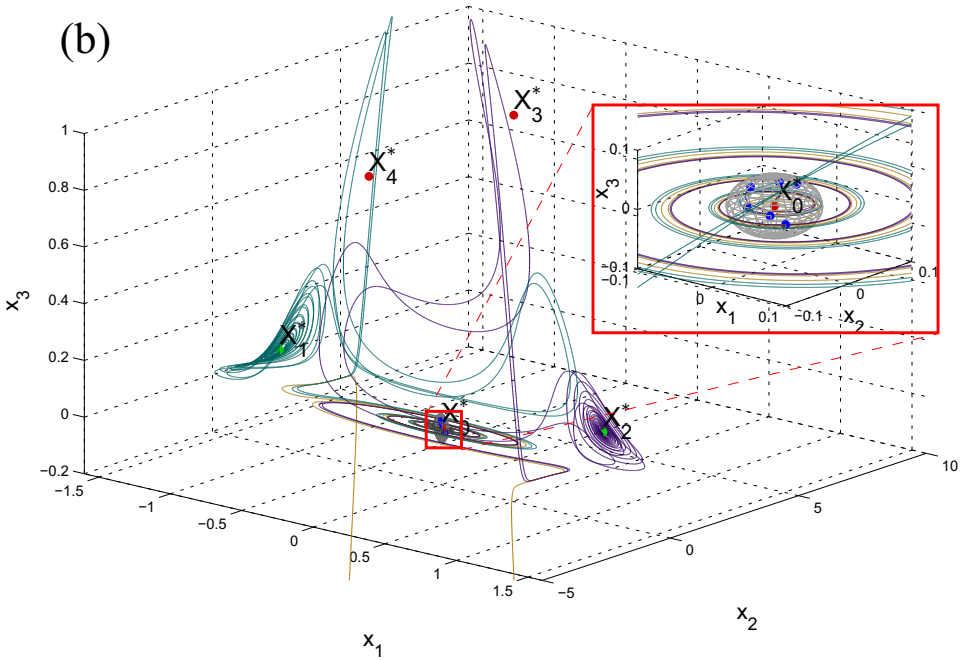

Fig. 15 (continued)

procedure several times in order to get different initial points for trajectories on the sphere. We get the following results: all obtained trajectories either tend to ∞, or attract to the stable equilibria $X^*_{1,2}$ and do not attract to the chaotic attractor (see Fig. 15(b)). This gives us the reason to say [107] (but very carefully, taking into account all the difficulties arising in the numerical investigation of this system) that the chaotic attractor obtained in system (18) is hidden (see Fig. 16).

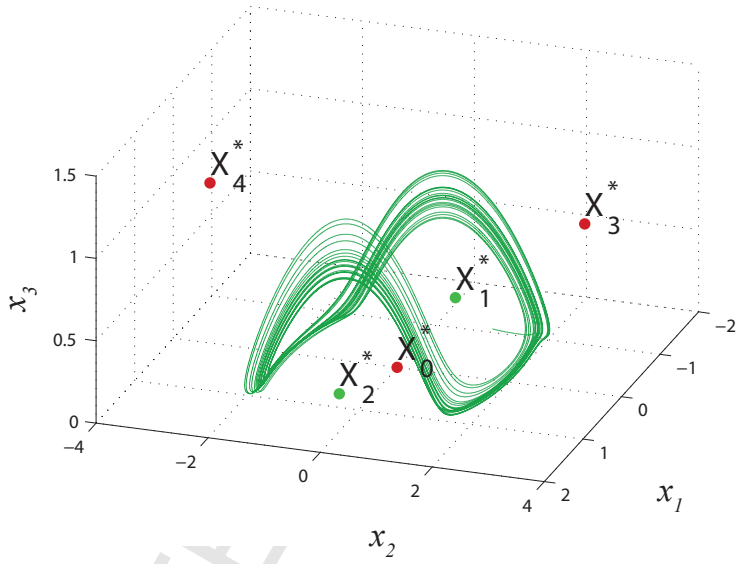

Figure 16: (color online). Parameters $a = 0.1$, $b = 0.2715$. Hidden attractor in the Rabinovich–Fabricant system (18) [107].

Other examples of hidden attractors can be found in [46, 52, 68–73, 76–78, 81–83, 91–94, 107–135].

3. Rare attractors and basin stability

Let us consider the externally excited Van der Pol–Duffing oscillator, given by the equation

$$\ddot{x}(t) - \alpha(1 - x^2(t))\dot{x}(t) + x^3(t) = F\sin(\omega t), \tag{22}$$

where α, ω, F are the positive constants that determine the multistability of the system. In our calculations we have assumed $\alpha = 0.2$, $F = 1.0$, and consider ω as the control parameter. The system in non–autonomous and its attractor can be identified as the projection on $(x, \dot{x})$ plane.

The influence of ω parameter on the dynamics of the considered oscillator can be observed in Fig. 17. In each subfigure, the basins of attraction of coexisting attractors for fixed ω value are shown. Each basin is presented by a different color, while the black points on them denote the points of the corresponding Poincare maps. In Fig. 17(a) the basins of attractors A_T, A_{7T}, two A_{9T} and A_{11T} are shown in green, yellow, blue, red and pink colors respectively. For each of the described states, the lower index kT denotes the period of solution, where $T = 2\pi/\omega$, and $k \in \mathbb{N}$. As it can be seen, the green basin (period T solution) is the dominant one for initial conditions in the neighbourhood of $(0, 1)$ point. As the initial conditions are further away from this point, the competition between A_T and A_{11T} states (green and pink) increases. When we decrease the parameter to $\omega = 0.962$, in Fig. 17(b) one can observe that the Neimark–Sucker bifurcation occured for the states A_T and A_{7T} from the previous subfigure, and as the result two tori appear – A_Q and A_{Q7}, with green and yellow basins respectively. The coexisting periodic solutions are A_{21T}, A_{35T} and two A_{9T}, with corresponding grey, white, blue and red basins of attraction. With further decrease of the control parameter, at $\omega = 0.955$ (Fig. 17(c)) the chaotic attractor A_{Ch} is born, which basin shown in green color is clearly the dominant one in the whole range of the considered initial conditions. One can also observe a quasiperiodic attractor A_Q with yellow basin and three periodic orbits – two A_{21T} (brown and orange), and A_{35T} (the white one). Finally, in the last subfigure Fig. 17(d) for $\omega = 0.945$ only three attrators coexist: the A_{7T} with corresponding yellow basin, and two A_{14T} shown in violet and green. The latter state is the dominant one. It should be emphasized that for different values of the control parameter ω many similar structures, with variety of coexisting attractors, have been found.

As it can be seen, the basins of attraction of some of the states shown in Fig. 17 are very small in comparison with the basins of other attractors coexisting in the system (22). For example, in subfigure Fig. 17(d) the basin of A_{7T} (yellow) is extremally smaller than the basin of A_{14T}, denoted by the green color. This type of property of the coexisting attractors has been described by Zakrzhevsky et al. [136], and is known as the concept of rare attractors. In [25] we have proposed the definition of rare attractors and

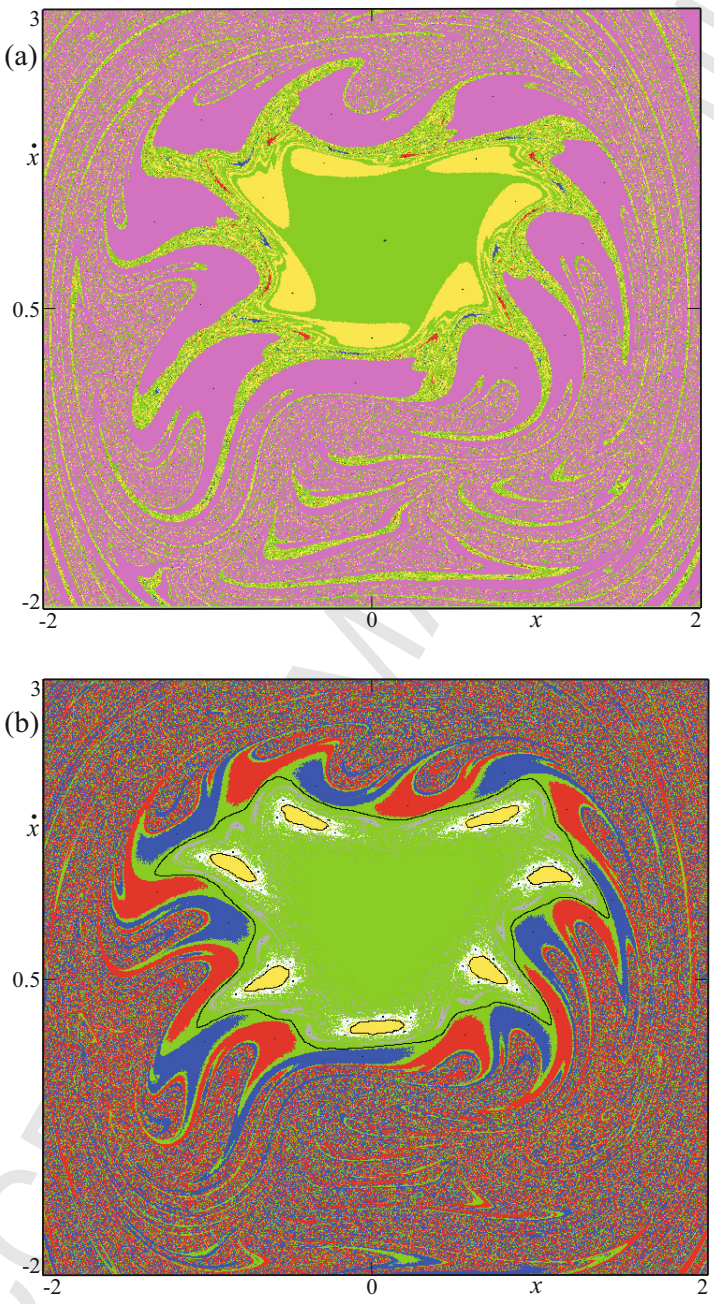

Figure 17: (color online). Basins of attraction of system (22) for different control parameter values ω. Decreasing from the top to the bottom, $\omega = 0.975, 0.962, 0.955, 0.945$ respectively. The basin of each state is shown with different color and the black dots on them denote the points of the corresponding Poincare maps [25].

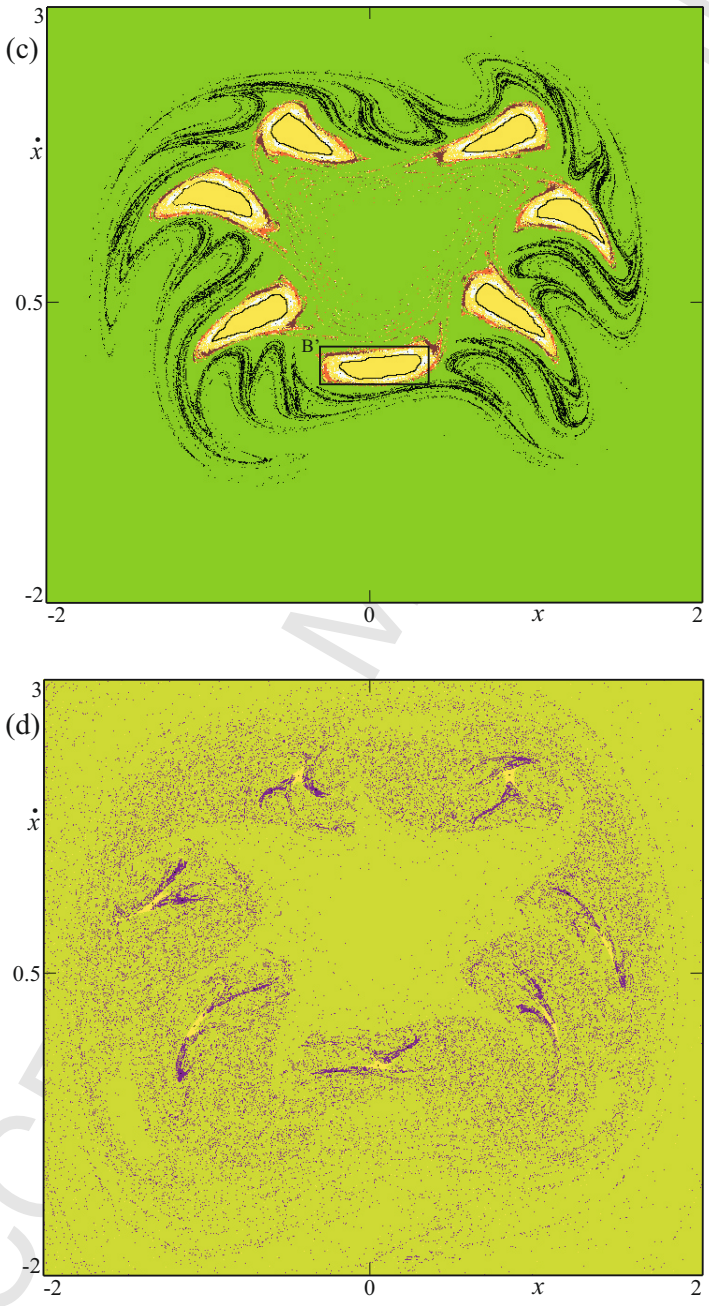

Fig. 17 (continued)

described their creation in system (22). Consider the dynamical system (2) (cf. Sec. 2). Let $B \subset \mathbb{R}^n$ be a set of all possible initial conditions and $C \subset \mathbb{R}^k$ be a set of accessible system parameters. Assume that attractor A_p exists for $p \in C_A \subset C$ and has a basin of attraction $\beta(A_p)$. Assuming that the initial conditions and the system parameters are chosen independently, the probability that the system is on attractor A_p is equal to

$$p(\{A_p : p \in C_A\}) = \frac{\mu(C_A)}{\mu(C)\mu(B)} \int_{C_A} \mu(\beta(A_p))dp, \tag{23}$$

where μ is a set measure (e.g. Lebesgue measure). If $p(\{A_p : p \in C_A\})$ is small (i.e., $p(\{A_p : p \in C_A\}) << 1$) attractor A_p is called the rare one. According to the introduced definition, we can indicate the rare attractors of the considered oscillator for the set of initial conditions as in Fig. 17, i.e., $B = [-2, 2] \times [-2, 3]$. In Fig. 17(a) two A_{9T} rare attractors coexist (blue and red basins), while in Fig. 17(b) rare A_{21T} and A_{35T} orbits are present, with corresponding grey and white basins respectively. Three coexisting rare states can be observed in Fig. 17(c) – two A_{21T} (brown and orange basins) and the A_{35T} one (white basin). Finally, in Fig. 17(d) single rare solution A_{7T} with yellow basin of attraction is shown.

As one can notice, the concept of rare attractors is strongly related with the considered set of accessible system parameters C, as well as the set of possible initial conditions B. As an example let us consider the torus A_{7Q} shown in Fig. 17(c), with corresponding yellow basin of attraction. For simplicity, let $C = C_A = \{0.955\}$. If we consider the set of possible initial conditions as in subfigure, i.e., $B = [-2, 2] \times [-2, 3]$, then according to the formula (23) the probability of occurrence of solution A_{7Q} equals $p(A_{7Q}) = 0.0519$, and this attractor can be considered as the rare one. For the chaotic attractor A_{Ch}, which is the dominant one (green basin), the probability is equal to $p(A_{Ch}) = 0.9227$. Nonetheless, the 'rare' property of coexisting attractors can change for different sets of possible initial conditions. We have considered the second set $B' = [-0.34, 0.33] \times [-0.15, 0.17]$ (shown as the inset in subfigure), for which the occurrence of the quasiperiodic state A_{7Q} is the highest and equals $p(A_{7Q}) = 0.6982$. The second most probable attractor is the periodic one A_{35T} (white basin) with $p(A_{35T}) = 0.1207$, while the previously dominant chaotic state A_{Ch} is now the rare one with probability at $p(A_{Ch}) = 0.0785$. In Table (1) the probabilities of occurrence for all attractors in Fig. 17(c) are shown, in both cases of the initial conditions sets B and B'.

Attractor (color of basin)	$p(A)$ for B	$p(A)$ for B'
Chaotic A_{Ch} (green)	0.9227	0.0785
Torus A_{Q7} (yellow)	0.0519	0.6982
Periodic A_{21T} (brown)	0.0087	0.0522
Periodic A_{35T} (white)	0.0086	0.1207
Periodic A_{21T} (orange)	0.0081	0.0504

Table 1: Probabilities of occurrence of coexisting attractors shown in Fig. 17(c) ($\omega = 0.955$) for two sets of possible initial conditions: $B = [-2, 2] \times [-2, 3]$ and $B' = [-0.34, 0.33] \times [-0.15, 0.17]$ [25].

The definition of hidden attractors introduced so far in Sec. 1 refers to the autonomous system, but it can also be generalized to the non–autonomous dynamical systems (see, e.g. [53]). Let us consider Poincare map P, where points are taken by the period of external excitation $2\pi/\omega$, i.e. $P = \{(x(t), \dot{x}(t)) : t = 2n\pi/\omega, n = 0, 1, \ldots\}$. We call the attractor of the system (22) hidden if its basin of attraction does not touch the neighbourhood of the equilibrium on such defined Poincare section. Consequently, the attractor is self–excited if its basin of attraction contains the fixed point of map P. For example, in the Fig. 17(a) for $\omega = 0.975$ we have two fixed points on Poincare section – the stable $(x, \dot{x}) = (0.072, 1.055)$ (A_T solution) with green basin of attraction and the unstable $(x, \dot{x}) = (0, 0)$ equilibrium. The trajectory beginning near the unstable equilibrium gets attracted to A_{11T} solution (pink basin) and so it is the self–excited orbit. By definition, the rest of the attractors, i.e., A_{7T} and two A_{9T} (yellow, blue and red basins respectively) are the hidden ones. In the considered case, two A_{9T} states are also rare, as it has been described previously. As we can see, there are no peculiar relations between the hidden and rare properties of the attractors, i.e., the state can be hidden but not rare (rare, but not hidden), as well as hidden and rare simultaneously. Both these properties depend on the dynamics of the system and are independent of each other.

The existence of rare attractors shows that the linear stability analysis is not sufficient to quantify how stable a particular attractor is against non–small perturbations. Quantification of stability in this sense requires the complete knowledge of the basin of attraction. This allows to identify permissible perturbations. As in many dynamical systems attractors basins are intricate entries which are especially hard to explore in high–dimensions. Menck et al. [50] introduced the concept of basin stability of attractor A.

The likehood of the return to the attractor after any random (non–small perturbations) SA has been taken as the measure of the basin stability. To illustrate this concept let us go back to the examples shown in Table (1). If one considers that the perturbations to attractor A are limited to sets B and B' then the values of $p(A)$ in both columns of the table represent the measures of the basin stability of attractor A. The concept of basin stability is particularly useful in the analysis of high–dimensional systems (e.g. networks) as: (i) it follows the probabilistic approach that is compatible with the natural uncertainty about the strength and direction of perturbations; (ii) it provides a measure of stability that is clearly defined and easy to calculate.

4. Detection and main properties of hidden attractors

4.1. Localization of hidden attractors

4.1.1. Synthesis of scenario of hidden attractor birth based on homotopy and continuation

One of the effective methods for the numerical localization of hidden attractors is based on a *homotopy* and *numerical continuation*. We construct a sequence of similar systems such that the initial data for numerically computing the oscillating solution (starting oscillation) can be obtained analytically for the first (starting) system. For example, it is often possible to consider a starting system with a self–excited starting oscillation. Then we numerically track the transformation of the starting oscillation while passing between the systems.

In a scenario of transition to chaos in the dynamical system there is typically parameter $\lambda \in [a_1, a_2]$, the variation of which gives the scenario. We can also artificially introduce parameter λ, let it vary in the interval $[a_1, a_2]$ (where $\lambda = a_2$ corresponds to the initial system) and choose parameter a_1 such that we can analytically or computationally find a certain nontrivial attractor when $\lambda = a_1$ (this attractor has often a simple form, e.g., periodic). That is, instead of analyzing the scenario of a transition into chaos, we can synthesize it. Further, we consider the sequence $\lambda_j,\ \lambda_1 = a_1,\ \lambda_m = a_2,\ \lambda_j \in [a_1, a_2]$ such that the distance between λ_j and λ_{j+1} is sufficiently small. Then we numerically investigate the changes to the shape of the attractor obtained for $\lambda_1 = a_1$. If the change in λ (from λ_j to λ_{j+1}) does not cause a loss of the stability bifurcation of the considered attractor, then the attractor for $\lambda_m = a_2$ (at the end of procedure) is localized. The application of this method is demonstrated below.

4.1.2. Chua circuit: from self–excited periodic to hidden chaotic attractor

Let us consider the Chua's system in the form

$$\frac{d\mathbf{x}}{dt} = \mathbf{P}\mathbf{x} + \mathbf{q}\psi(\mathbf{r}\mathbf{x}), \quad \mathbf{x} \in \mathbb{R}^3. \tag{24}$$

Here

$$\mathbf{P} = \begin{pmatrix} -\alpha(m_1+1) & \alpha & 0 \\ 1 & -1 & 1 \\ 0 & -\beta & -\gamma \end{pmatrix}, \ \mathbf{q} = \begin{pmatrix} -\alpha \\ 0 \\ 0 \end{pmatrix}, \ \mathbf{r} = \begin{pmatrix} 1 \\ 0 \\ 0 \end{pmatrix},$$

$\psi(\sigma) = 1/2(m_0 - m_1)(|\sigma+1| - |\sigma-1|)$.

Introduce coefficient k and small parameter ε and represent system (24) as

$$\frac{d\mathbf{x}}{dt} = \mathbf{P_0}\mathbf{x} + \mathbf{q}\varepsilon\varphi(\mathbf{r}\mathbf{x}), \tag{25}$$

where

$$\mathbf{P_0} = \mathbf{P} + k\mathbf{q}\mathbf{r} = \begin{pmatrix} -\alpha(m_1+1+k) & \alpha & 0 \\ 1 & -1 & 1 \\ 0 & -\beta & -\gamma \end{pmatrix}, \ \lambda_{1,2}^{\mathbf{P}_0} = \pm i\omega_0, \ \lambda_3^{\mathbf{P}_0} = -d,$$

$\varphi(\sigma) = \psi(\sigma) - k\sigma = 1/2(m_0 - m_1)(|\sigma+1| - |\sigma-1|) - k\sigma$.

By the nonsingular linear transformation $\mathbf{x} = \mathbf{S}\mathbf{y}$ system (25) is reduced to the form

$$\frac{d\mathbf{y}}{dt} = \mathbf{A}\mathbf{y} + \mathbf{b}\varepsilon\varphi(\mathbf{c}\mathbf{y}), \tag{26}$$

where

$$\mathbf{A} = \begin{pmatrix} 0 & -\omega_0 & 0 \\ \omega_0 & 0 & 0 \\ 0 & 0 & -d \end{pmatrix}, \ \mathbf{b} = \begin{pmatrix} b_1 \\ b_2 \\ 1 \end{pmatrix}, \ \mathbf{c} = \begin{pmatrix} 1 \\ 0 \\ -h \end{pmatrix}.$$

The transfer function $W_{\mathbf{A}}(p)$ of system (26) can be represented as

$$W_{\mathbf{A}}(p) = \frac{-b_1 p + b_2\omega_0}{p^2 + \omega_0^2} + \frac{h}{p+d}.$$

Further, using the equality of transfer functions of systems (25) and (26), one can obtain

$$W_{\mathbf{A}}(p) = \mathbf{r}(\mathbf{P}_0 - p\mathbf{I})^{-1}\mathbf{q}.$$

This implies the following relations

$$k = \frac{-\alpha(m_1 + m_1\gamma + \gamma) + \omega_0^2 - \gamma - \beta}{\alpha(1+\gamma)}, d = \frac{\alpha + \omega_0^2 - \beta + 1 + \gamma + \gamma^2}{1+\gamma},$$
$$h = \frac{\alpha(\gamma + \beta - (1+\gamma)d + d^2)}{\omega_0^2 + d^2}, b_1 = \frac{\alpha(\gamma + \beta - \omega_0^2 - (1+\gamma)d)}{\omega_0^2 + d^2}, \tag{27}$$
$$b_2 = \frac{\alpha\big((1+\gamma-d)\omega_0^2 + (\gamma+\beta)d\big)}{\omega_0(\omega_0^2 + d^2)}.$$

Since by the nonsingular linear transformation $\mathbf{x} = \mathbf{S}\mathbf{y}$ system (25) can be reduced to the form (26), for the matrix $\mathbf{S}$ the following relations

$$\mathbf{A} = \mathbf{S}^{-1}\mathbf{P_0}\mathbf{S}, \quad \mathbf{b} = \mathbf{S}^{-1}\mathbf{q}, \quad \mathbf{c} = \mathbf{r}\mathbf{S} \tag{28}$$

are valid. Having solved these matrix equations, one can obtain the transformation matrix

$$\mathbf{S} = \begin{pmatrix} s_{11} & s_{12} & s_{13} \\ s_{21} & s_{22} & s_{23} \\ s_{31} & s_{32} & s_{33} \end{pmatrix}'$$

where

$$s_{11} = 1, \quad s_{12} = 0, \quad s_{13} = -h,$$
$$s_{21} = m_1 + 1 + k, \quad s_{22} = -\frac{\omega_0}{\alpha}, \quad s_{23} = -\frac{h(\alpha(m_1 + 1 + k) - d)}{\alpha},$$
$$s_{31} = \frac{\alpha(m_1 + k) - \omega_0^2}{\alpha}, \quad s_{32} = -\frac{\alpha(\beta+\gamma)(m_1+k) + \alpha\beta - \gamma\omega_0^2}{\alpha\omega_0},$$
$$s_{33} = h\frac{\alpha(m_1+k)(d-1) + d(1+\alpha-d)}{\alpha}.$$

Introduce the following describing function

$$\Phi(a) = \int_0^{2\pi/\omega_0} \varphi\big(\cos(\omega_0 t)a\big)\cos(\omega_0 t)dt. \tag{29}$$

Theorem 1. *Suppose that there exists a number $a_0 > 0$, $a_0 \neq |\nu_i|$, such that the conditions*

$$\Phi(a_0) = 0, \quad b_1\frac{d\Phi(a)}{da}\bigg|_{a=a_0} < 0 \tag{30}$$

are satisfied. Then for sufficiently small $\varepsilon > 0$ system (26) *has a periodic solution of the form*

$$\begin{aligned} y_1(t) &= \cos(\omega_0 t) y_1(0) + O(\varepsilon), \\ y_2(t) &= \sin(\omega_0 t) y_1(0) + O(\varepsilon), \qquad t \in [0, T] \\ y_3(t) &= \exp(-d_3 t) y_3(0) + O(\varepsilon), \end{aligned} \tag{31}$$

with the initial data

$$y_1(0) = a_0 + O(\varepsilon),\ y_2(0) = 0,\ y_3(0) = O(\varepsilon) \tag{32}$$

and with the period

$$T = \frac{2\pi}{\omega_0} + O(\varepsilon).$$

Theorem 1 describes the procedure of the search for stable periodic solutions by the standard describing the function method (see, e.g., generalization of the theorem in [40, 137]).

By (32), for sufficiently small ε at the first step of multistage localization procedure one obtains the initial data

$$\mathbf{x}(0) = \mathbf{S}\mathbf{y}(0) = \mathbf{S} \begin{pmatrix} a_0 \\ 0 \\ 0 \end{pmatrix} = \begin{pmatrix} a_0 s_{11} \\ a_0 s_{21} \\ a_0 s_{31} \end{pmatrix}.$$

Returning to Chua's system denotations, for the determination of the initial data of starting the solution for multistage procedure, it can be obtained

$$x(0) = a_0,\ y(0) = a_0(m_1 + 1 + k),\ z(0) = a_0 \frac{\alpha(m_1 + k) - \omega_0^2}{\alpha}. \tag{33}$$

Consider system (25) with the parameters

$$\alpha = 8.4562,\ \beta = 12.0732,\ \gamma = 0.0052,\ m_0 = -0.1768,\ m_1 = -1.1468. \tag{34}$$

Note that for the considered values of parameters there are three equilibria in the system: a locally stable zero equilibrium and two saddle equilibria. Now let us apply the above procedure of hidden attractors localization to Chua's system (24) with parameters (34). For this purpose, compute a starting frequency and a coefficient of harmonic linearization:

$$\omega_0 = 2.0392, \quad k = 0.2098\,.$$

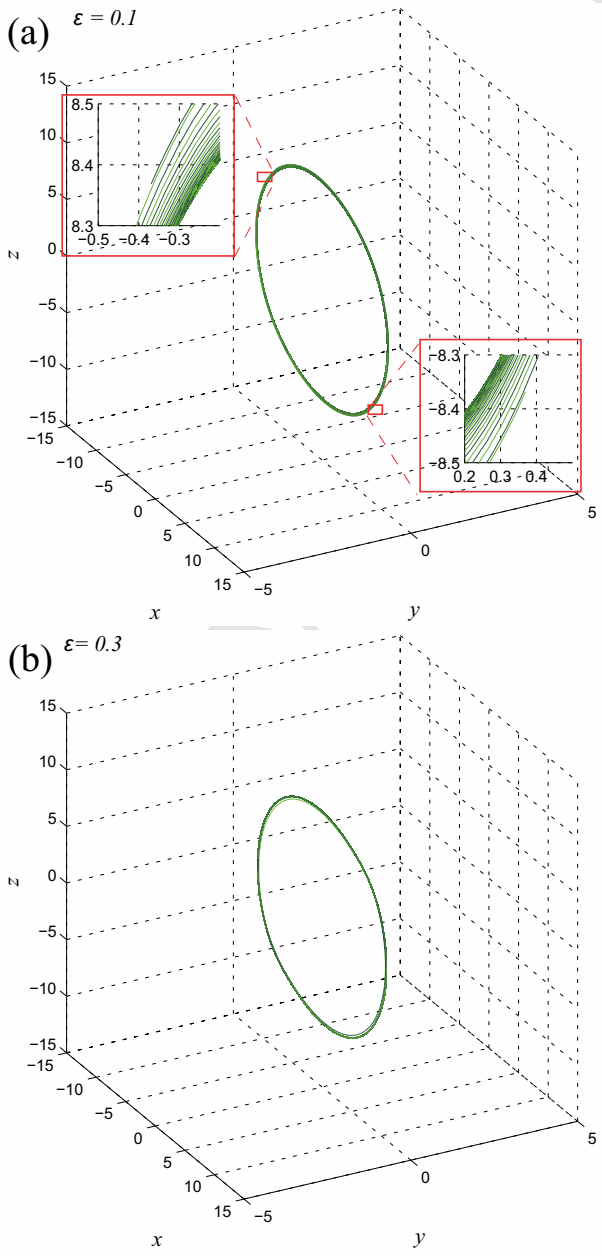

Figure 18: (color online). A road to chaos: the localization of hidden chaotic Chua attractors. The attractors with corresponding trajectories obtained for different ε values are shown. Increasing from (a) to (f), $\varepsilon = 0.1, 0.3, 0.5, 0.8, 0.9, 1.0$ respectively.

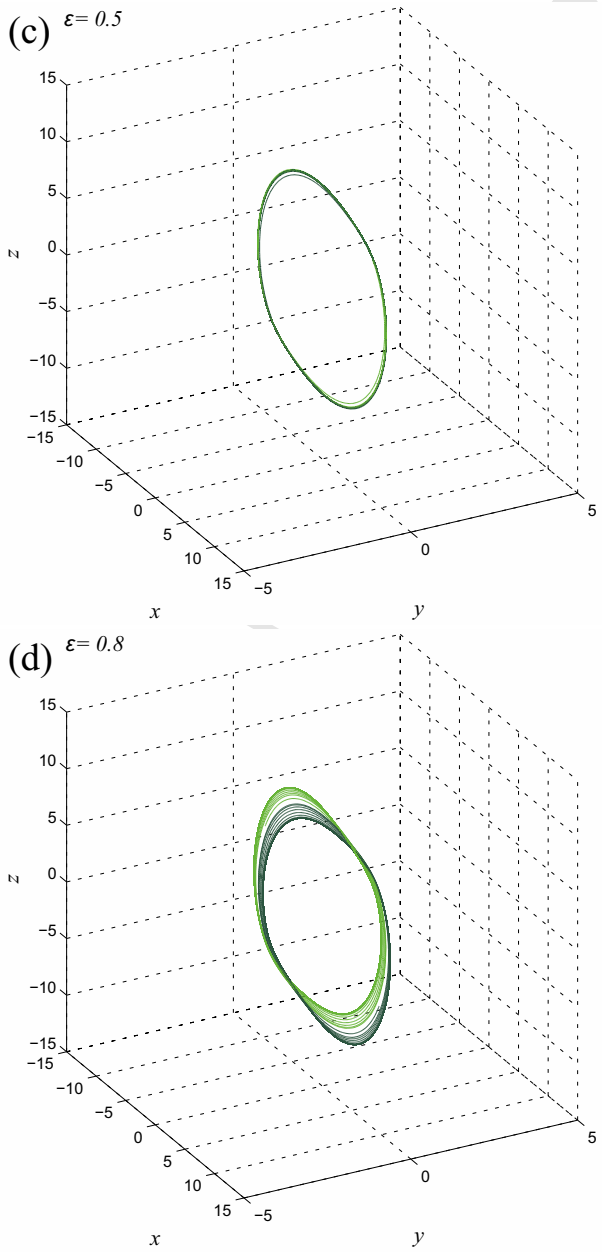

Fig. 18 (continued)

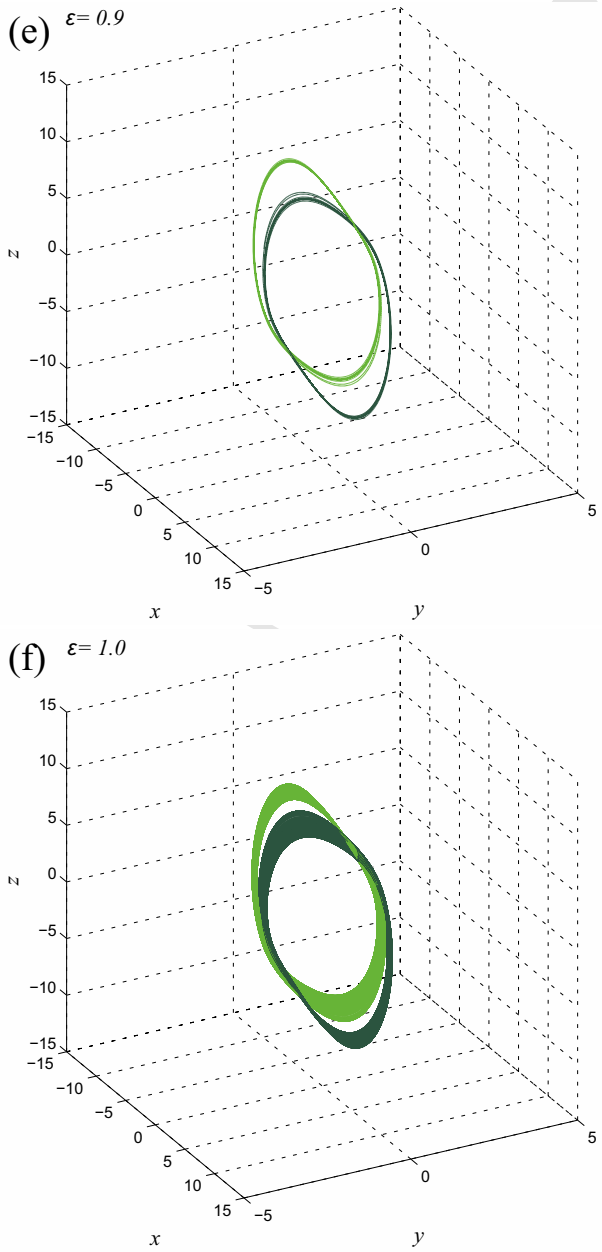

Fig. 18 (continued)

Then, we compute the solutions of system (25) with nonlinearity $\varepsilon\varphi(x) = \varepsilon(\psi(x) - kx)$, sequentially increasing ε from value $\varepsilon_1 = 0.1$ to $\varepsilon_{10} = 1$ with step 0.1. By (27) and (33) the initial data can be obtained

$$x(0) = 9.4287, y(0) = 0.5945, z(0) = -13.4705$$

for the first step of multistage procedure for the construction of solutions. For $\varepsilon_1 = 0.1$, after a transient process the computational procedure reaches starting oscillation $\mathbf{x}^1(t)$. Further, by the numerical procedure and the sequential transformation $\mathbf{x}^j(t)$ with increasing parameter ε_j, for original Chua's system (24) set $\mathcal{A}_{\text{hidden}}$ is computed.

The results of the procedure are shown in Fig. 18. For each ε value the attractors of the system (25) are presented (in Fig. 18(a) one can observe the enlargement of the trajectories leading to the symmetric attractor). The dynamics changes from periodic through quasiperiodic, to finally obtaining the chaotic behaviour (Chua attractors of the Rossler–like type shown in Fig. 18(f)). The observed states can be unique (symmetric attractor obtained for $\varepsilon = 0.1, 0.3, 0.5$) or two symmetric states ($\varepsilon = 0.8, 0.9, 1.0$) can coexist.

Also the hidden attractors were computed in modified Chua systems with smooth nonlinearity $tanh(\cdot)$ [39] and with nonlinearity $sign(\cdot)$ [45].

To present the probability of occurrence of coexisting attractors in Chua system we have performed the following experiment. Let us consider the 3D sphere B that contains hidden attractors and generate a bunch of random points in it. Then we integrate Chua system using obtained random points as initial conditions. There are three possibilities for the current obtained trajectory:
(i) it will be attracted to the stable equilibrium F_0,
(ii) it will be attracted to one of the hidden attractors,
(iii) it will go to infinity.
The sphere $B = (x^2 + y^2 + z^2) \leq 10$ and the possible attractors are shown in Fig. 19.

In our experiment we have generated 1000 of random initial conditions from the sphere B. Obtained probabilities of occurence of states (i)–(iii) are shown in Table (2).

According to our calculations, the probability that the system will go to infinity is the dominant one. About 9 % of the time one of the hidden atractors will be obtained and in 0.4 % of cases the trajectory will be attracted to the fixed point. As one can see, because of the rare character of hidden

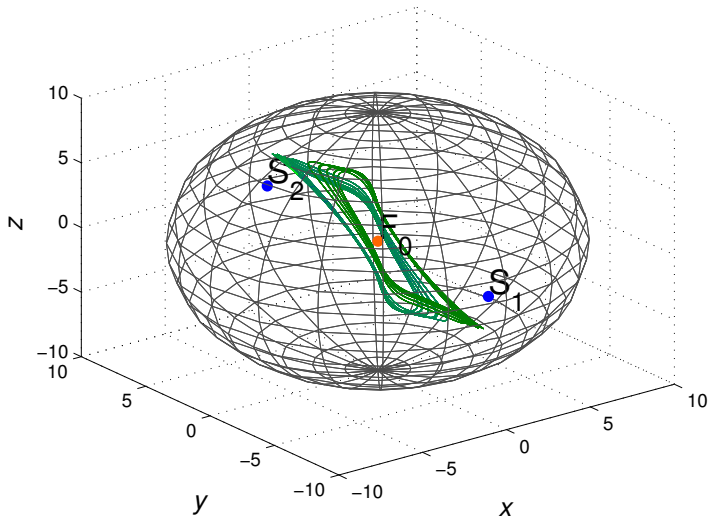

Figure 19: (color online). Sphere $B = (x^2 + y^2 + z^2) \leq 10$ and the possible attractors of the Chua system.

Attractor	$p(A)$ for B
Stable zero equilibrium	0.004
Hidden attractors (union of two symmetric attractors)	0.087
Infinity	0.899

Table 2: Probabilities of occurrence of attractors (zero equilibrium, hidden attractors, infinity) in Chua system with $\alpha = 8.4562, \beta = 12.0732, \gamma = 0.0052, m_0 = -0.1768, m_1 = -1.1468$ for the set of possible initial conditions: $B = (x^2 + y^2 + z^2) \leq 10$.

attractors (cf. Sec. 3) it is hard to obtain these states from the random data and so the special methods like the one presented above are very important.

4.1.3. Gluhovsky–Dolzhansky system: from self–excited to hidden chaotic attractor

Let us determine the stationary points of the Gluhovsky–Dolzhansky system introduced in Sec. 2, i.e.

$$\begin{cases} \dot{x} = -\sigma(x - y) - ayz, \\ \dot{y} = rx - y - xz, \\ \dot{z} = -bz + xy, \end{cases} \tag{35}$$

We can show that for positive parameters, if $r < 1$, system (35) has unique equilibrium $\mathrm{S}_0 = (0, 0, 0)$, which is globally asymptotically Lyapunov stable [100]. If $r > 1$, then (35) possesses three equilibria: saddle $\mathrm{S}_0 = (0, 0, 0)$ and symmetric (with respect to $z = 0$) equilibria

$$\mathrm{S}_{1,2} = (\pm x_1^*, \pm y_1^*, z_1^*), \tag{36}$$

where

$$x_1^* = \frac{\sigma\sqrt{\xi}}{\sigma + a\xi}, \quad y_1^* = \sqrt{\xi}, \quad z_1^* = \frac{\sigma\xi}{\sigma 1 + a\xi},$$

and

$$\xi = \frac{\sigma}{2a^2}\left[a(r-2) - \sigma + \sqrt{(\sigma - ar)^2 + 4a\sigma}\right].$$

Following [103], we let $\sigma = 4$ and define the stability domain of equilibria $S_{1,2}$. Using the Routh–Hurwitz criterion we can obtain that equilibria $S_{1,2}$ are stable if

$$8a^2r^3 + a(7a - 64)r^2 + (288a + 128)r + 256a - 2048 < 0. \tag{37}$$

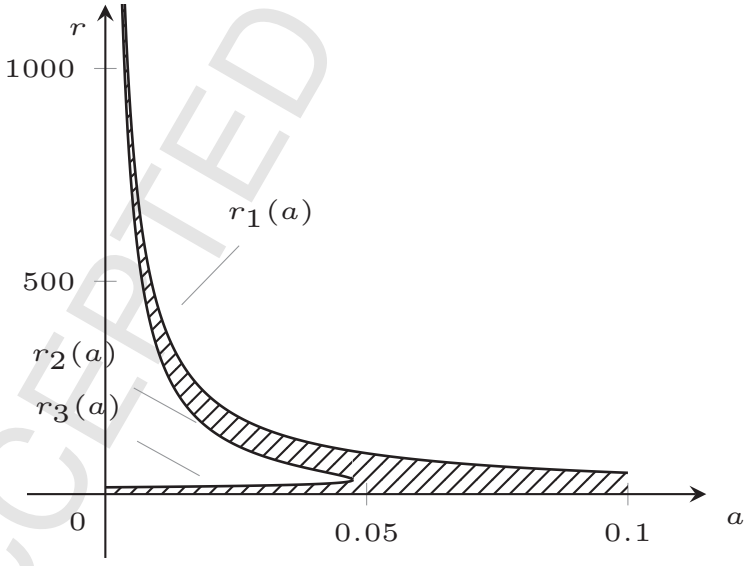

Figure 20: The stability domain of equilibria $S_{1,2}$ for $\sigma = 4$ [53].

The discriminant of the left–hand side of (37) has only one positive real root, $a^* \approx 0.04735$. So the roots of the polynomial in (37) are as follows. For

$0 < a < a^*$, there are three real roots $r_1(a) > r_2(a) > r_3(a)$; for $a = a^*$, there are two real roots: $r_1(a)$ and $r_2(a) = r_3(a)$; for $a > a^*$, there is one real root $r_1(a)$. Thus, for $0 < a < a^*$, equilibria $S_{1,2}$ are stable for $r < r_3(a)$ and for $r_2(a) < r < r_1(a)$; and for $a > a^*$ equilibria $S_{1,2}$ are stable for $r < r_1(a)$ (see Fig. 20).

Let us construct a line segment on the plane (a, r) that intersects a boundary of the stability domain of equilibria $S_{1,2}$ (see Fig. 21). We choose point $P_1(r = 700, a = 0.0052)$ as the end point of the line segment. The eigenvalues for the equilibria of system (35) that correspond to the parameter P_1 are the following:

$$\begin{aligned} S_0: &\quad 50.4741, \quad -1, \quad -55.4741, \\ S_{1,2}: &\quad -0.1087 \pm 10.4543\mathrm{i}, \quad -5.7826. \end{aligned}$$

This means that equilibria $S_{1,2}$ become stable focus–nodes. Now we choose point $P_0(r = 687.5, a = 0.0052)$ as the initial point of the line segment. This point corresponds to the parameters for which system (35) has a self–excited attractor, which can be computed using the standard computational procedure. Then, we choose a sufficiently small partition step for the line segment and compute a chaotic attractor in the phase space of system (35) at each iteration of the procedure. The last computed point at each step is used as the initial point for the computation at the next step (the computation time must be sufficiently large).

In our experiment the length of the path was 2.5 and there were 6 iterations. Here for the selected path and partition, we can visualize a hidden attractor of system (35) (see Fig. 22). The results of continuation procedure are given in [102].

Note that the choice of path and its partitions in the continuation procedure is not trivial. For example, a similar procedure does not lead to a hidden attractor for the following path on the plane (a, r). Consider $r = 33.51541181$, $a = 0.04735056...$ (the rightmost point on the stability domain) and take starting point P_2: $r = 33.51541181$, $a = 0.046$ near it (Fig. 21). If we use the partition step 0.001, then there are no hidden attractors after crossing the boundary of the stability domain. For example, if the end point is P_3: $r = 33.51541181$, $a = 0.048$, there is no chaotic attractor but only trivial attractors (equilibria $S_{1,2}$).

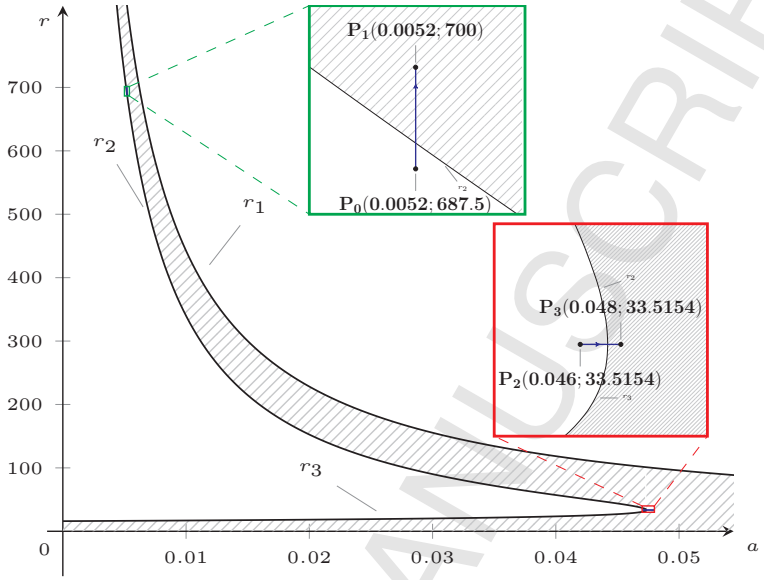

Figure 21: (color online). Paths $[P_0, P_1]$ and $[P_2, P_3]$ in the plane of parameters $\{a, r\}$ used in the continuation procedure [53].

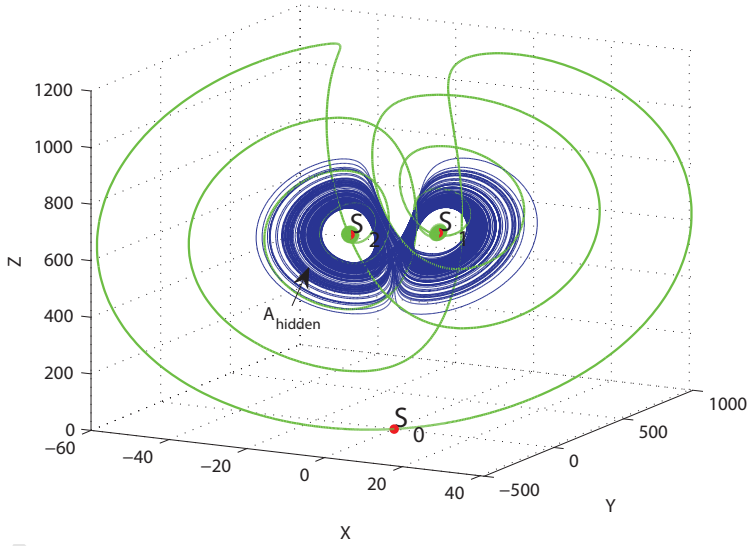

Figure 22: (color online). Hidden attractor (blue) coexists with B–attractor (green outgoing separatrix of saddle S_0 attracted to red equilibria $S_{1,2}$) [53].

4.1.4. Analytical localization of attractor in dissipative dynamical systems

In the previous sections, we have considered the numerical localization of various self–excited and hidden attractors of system (35). It is natural to question if these attractors (or the union of attractors) are the only attractors (the monostable system) or if other coexisting attractors can be found (the multistable system).

Consider an autonomous differential equation (2) (cf. Sec. 2). Suppose, that any solution $X(t, X_0)$ of (2) such that $X(0, X_0) = x$ and $X_0 \in \mathbb{R}^n$ exists for $t \in [0, \infty)$ and is unique. Similarly, one can consider the dynamical system generated by a difference equation

$$X(t+1) = F(X(t)), \quad t = 0, 1, \ldots \tag{38}$$

Here the existence and the uniqueness are satisfied for all $t \geq 0$.

The *dissipativity* property is important when proving the monostability of the dynamical system and gives an analytical localization of the attractor in the phase space. The dissipativity of the system, on one hand, proves that there are no trajectories that tend to infinity as $t \to +\infty$ in the phase space and on the other hand, can be used to determine the boundaries of the domain that all trajectories enter within a finite time.

Let us introduce the following notation.

A set $B_0 \subset \mathbb{R}^n$ is said to be *absorbing* for the dynamical system if for any $\mathrm{X}_0 \in \mathbb{R}^n$ there exists $T = T(\mathrm{X}_0)$ such that $\mathrm{X}(t, \mathrm{X}_0) \in B_0$ for any $t \geq T$.

Note that the trajectory $\mathrm{X}(t, \mathrm{X}_0)$ with $\mathrm{X}_0 \in B_0$ may leave B_0 for only the finite time before it returns and stays inside for $t \geq T$.

In [138] the ball $B_R = \{\mathrm{X} \in \mathbb{R}^n : |\mathrm{X}| < R\}$ has been regarded as an absorbing set. In this case, if there exists $R > 0$ such that

$$\limsup_{t \to \infty} |\mathrm{X}(t, \mathrm{X}_0)| < R, \quad \text{for any } \mathrm{X}_0 \in \mathbb{R}^n,$$

then it is said that a dynamical system is *dissipative in the sense of Levinson* and R is called *a radius of dissipativity*.

We can effectively prove dissipativity by constructing Lyapunov function [139, 140]. Consider a sufficient condition of dissipativity [141]. Suppose that there exists continuously differentiable function $V(\mathrm{X}) : \mathbb{R}^n \to \mathbb{R}$, possessing the following properties:

I. $\lim_{|\mathrm{X}| \to \infty} V(\mathrm{X}) = +\infty$, and

II. there exist numbers R and $\varkappa$ such that for any solution $\mathrm{X}(t, \mathrm{X}_0)$, the condition $|\mathrm{X}(t, \mathrm{X}_0)| > R$ implies that $\dot{V}(\mathrm{X}(t, \mathrm{X}_0)) \leq -\varkappa$.

Then if $\eta > 0$ is such that $B_0 = \{\mathrm{X} \in \mathbb{R}^n \mid V(\mathrm{X}) \leq \eta\} \supset \{\mathrm{X} \in \mathbb{R}^n \mid ||\mathrm{X}|| < R\}$, the set B_0 is a compact absorbing set.

More general theorems, connected with the application of Lyapunov functions to the proof of dissipativity for dynamical systems can be found in [142, 143].

It is known that Lorenz system is dissipative (it is sufficient to choose Lyapunov function $V(x, y, z) = \frac{1}{2}(x^2 + y^2 + (z - r - \sigma)^2)$). However, for example, one of Rossler systems is not dissipative in the sense of Levinson [144] because the outgoing separatrix is unbounded. In the general case, there is an art in the construction of Lyapunov functions which prove dissipativity.

4.1.5. Gluhovsky–Dolzhansky system: Analytical localization of self–excited and hidden attractors

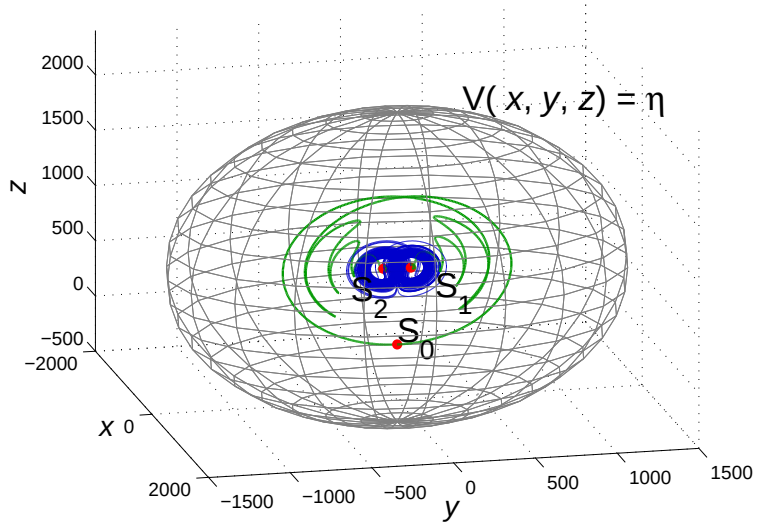

Figure 23: (color online). Absorbing set (grey), hidden attractor (blue), and global B–attractor (blue, green and red) for system (35) with the parameters $r = 700$, $\sigma = 4$, and $a = 0.0052$. $\eta \approx 247230.5$ [53].

Using Lyapunov function approach one can show that Gluhovsky–Dolzhansky system (35) is dissipative (see, e.g. [53]). The proof is based on Lyapunov function

$$V(x, y, z) = \frac{1}{2}\left(x^2 + y^2 + (a + 1)\left(z - \frac{\sigma + r}{a + 1}\right)^2\right) \geq 0.$$

For an arbitrary solution $\mathrm{x}(t) = (x(t), y(t), z(t))$ of system (35) we have

$$\begin{aligned}\dot{V}(x,y,z) &= x(-\sigma x + \sigma y - ayz) + y(rx - y - xz) + ((a+1)z - (\sigma + r))(-z + xy) \\ &= -\sigma x^2 - y^2 - (a+1)z^2 + (\sigma + r)z.\end{aligned}$$

Suppose that $\varepsilon \in (0, (a+1))$, $c = \min\{\sigma, 1, (a+1) - \varepsilon\} > 0$, and $x^2 + y^2 + z^2 \geq R^2$. Then positive $\varkappa$ exists such that

$$\dot{V}(x,y,z) \leq -cR^2 + \frac{(\sigma + r)^2}{4\varepsilon} < -\varkappa \quad \text{for} \quad R^2 > \frac{1}{c}\frac{(\sigma + r)^2}{4\varepsilon}.$$

We choose a number $\eta > 0$ such that

$$\{(x,y,z) \mid V(x,y,z) \leq \eta\} \supset \left\{(x,y,z) \mid x^2 + y^2 + z^2 \leq R^2\right\},$$

i.e., the relation $x^2 + y^2 + z^2 \leq R^2$ implies that

$$x^2 + y^2 + (a+1)\left(z - \frac{\sigma + r}{a+1}\right)^2 = x^2 + y^2 + z^2 + az^2 - 2(\sigma + r)z + \frac{(\sigma + r)^2}{a+1} \leq 2\eta.$$

Since

$$-2(\sigma + r)z \;\leq\; 2(\sigma + r)|z| \;\leq\; 2(\sigma + r)R,$$

if we choose $\eta > 0$ such that

$$(a+1)R^2 + 2(\sigma + r)R + \frac{(\sigma + r)^2}{a+1} \leq 2\eta, \quad \text{i.e.} \quad \eta \geq \frac{1}{2}(a+1)\left(R + \frac{\sigma + r}{a+1}\right)^2,$$

then system (35) has a compact absorbing set

$$B_0 = \left\{(x,y,z) : V(x,y,z) = \frac{1}{2}\left(x^2 + y^2 + (a+1)\left(z - \frac{\sigma + r}{a+1}\right)^2\right) \leq \eta\right\},$$

which contains all existing self–excited and hidden attractors of the system.

For example, for $\sigma > 1, r > 1, a < 1$ we can choose $R = \dfrac{\sigma + r}{a+1}$ and $\eta = 2(a+1)R^2$ (see Fig. 23). Note that for system (35) the ellipsoidal absorbing set B_0 can be improved using special additional transformations and Yudovich's theorem (see, e.g. [145]), similarly to [146] for the Lorenz system.

4.1.6. Perpetual points and its connection with hidden attractors

The fixed points of any dynamical system are the ones where velocity and acceleration of the system simultaneously become zero. If the existing fixed points are unstable then we may get either oscillating solutions or unbounded ones. If there are oscillating solutions then the fixed points are considered to be important points in phase space for locating the oscillating attractors, i.e. these unstable fixed points are considered as reference points and the initial conditions near to the fixed points lead to the attractors. However, for the systems having hidden attractors we don't have such unstable fixed points. Therefore a natural question can be asked as "Is there an reference point for hidden attractors similar to the fixed point for self–excited attractors?". In this section we show numerical results which suggest that there are points, termed as perpetual points, which could be considered as reference points of hidden attractors.

Consider a general dynamical system (2) (cf. Sec. 2). The fixed points correspond to where $\dot{X} = 0$, i.e. $F(X^*, p) = 0$ where $*$ stands for the fixed points. Let us consider the derivative of Eq. (2) with respect to time, i.e.

$$\begin{aligned} \ddot{X} &= F_{X^T}(X, p) \cdot F(X, p) \\ &= G(X, p) \end{aligned} \tag{39}$$

where $G = F_{X^T}(X, p) \cdot F(X, p)$ may be termed as the acceleration vector (here T stands for transpose of the vector). This shows the variation of acceleration in phase space.

Similar to the fixed points estimation where we set velocity vector zero, we can also get a set of points where $\ddot{X} = G(X_{PP}, p) = 0$ in Eq. (39), i.e. the points corresponding to the zero acceleration. At these points velocity $\dot{X}$ may be either zero or nonzero. This set includes the fixed points (X^*) with zero velocity as well as a subset of new points with nonzero velocity. These nonzero velocity points are termed as perpetual points, X_{PP} [51, 52, 147]. The velocity at these points is either maximum or minimum or of inflection behavior [51]. It has been also observed that these points are important for better understanding of transient dynamics in the phase space. These points also show the bifurcation behavior, similar to the fixed points, as the parameters of the system vary – for details see [51, 52, 147].

The understanding of hidden attractors (cf. Sec. 2), as compared to the excitable ones, is difficult due to the absence of the fixed points. To locate the hidden attractors in a given system is even more difficult. However, the

perpetual points could be used to locate the hidden oscillating attractors, rare attractors as well as coexisting attractors [51, 52], in both single and coupled oscillators [52].

The reason why perpetual points lead to hidden states is still not well understood and more analysis has to be made in this area. Nevertheless, we present some argumentation in the particular type of the systems, i.e. the ones for which the potential is known.

Let us consider the dynamical equation of the dumped oscillator, for which the potential energy function is defined, i.e.

$$\ddot{x} + \alpha\dot{x} + \frac{d}{dx}V(x) = 0, \tag{40}$$

where V is the potential and α is the dumping coefficient. Denoting $x_1 := x$ and $x_2 := \dot{x}$ as the position and velocity of the oscillator respectively, the equations of fixed and perpetual points are as follows.

Fixed points:

$$\begin{cases} x_2 = 0, \\ \frac{d}{dx_1}V(x_1) = 0. \end{cases} \tag{41}$$

Perpetual points:

$$\begin{cases} \alpha x_2 - \frac{d}{dx_1}V(x_1) = 0, \\ (\frac{d^2}{dx_1^2}V(x_1))x_2 = 0. \end{cases} \tag{42}$$

Considering the relation (42) we can observe that $x_2 \neq 0$ because otherwise from the first equation $\frac{d}{dx_1}V(x_1) = 0$ and the solution will be the fixed point. Hence, $\frac{d^2}{dx_1^2}V(x_1) = 0$ and $\frac{d}{dx_1}V(x_1) \neq 0$ (otherwise it will also be the equilibrium). Thus, the perpetual point of system (40) is also an inflection point of the potential energy function. In the systems where stable fixed points exist the inflection points of potential are the natural guidance to the equilibria. If the trajectory starts from the inflection, it will converge through the shortest path (in the sense of energy) to the stable solution. This connection between perpetual and inflection points may clarify the reasons why the former ones can be useful in finding the attractors.

The application of perpetual points to the systems of complex dynamics, for which the potential is unknown, can bring useful and valuable results. Some of these are shown below.

Firstly, we apply the perpetual points for locating hidden and rare attractors in multistable systems. Below we consider an example of non–autonomous system, the externally excited van der Pol–Duffing oscillator. The dynamics is given by equation

$$\ddot{x} - \alpha(1 - x^2)\dot{x} + x^3 = F\sin(\omega t), \tag{43}$$

where x is the state variable and α, F, ω are the parameters, which we have fixed as follow: $\alpha = 0.2, F = 1$, and $\omega = 0.962$. Depending on the value of ω constant system (43) can be monostable, having one self–excited attractor, as well as multistable, having coexisting hidden and self–excited states.

Equation (43) can be easily transformed into a set of first–order autonomous ODEs (the phase space will be three–dimensional), for which the perpetual points can be calculated (the second derivatives of the state variables equal zero). We denote x_1 as the position ($x_1 := x$) and x_2 as the velocity ($x_2 := \dot{x}$) of the oscillator, while t is considered as the individual time–dependent variable, for which the relation $\dot{t} = 1$ occurs. As the result, the equations of perpetual points of the system (43) are given as follows:

$$\begin{cases} \alpha(1 - {x_1}^2)x_2 - {x_1}^3 + F\sin(\omega t) = 0 \\ -2\alpha x_1 {x_2}^2 - 3{x_1}^2 x_2 + \omega F\cos(\omega t) = 0. \end{cases} \tag{44}$$

Relation (44) consists of polynomial equations due to variables x_1, x_2, and is underdetermined – we have 2 equations of 3 variables. The area of searching for solutions has been fixed as the box $(x_1, x_2, t) \in [-2, 2]\times[-3, 3]\times[0, 2\pi/\omega)$, where $\omega = 0.962$. The reason of choosing such boundaries results from the dynamics of the system itself. The considered position–velocity plane intersects with the basins of rare attractors present in the system. The examples and analysis of these states can be found in [25]. On the other hand, periodicity of trigonometric functions present in (44) implicates the area for t variable.

In our considerations we have transformed the equations from (44) into one rational equation due to variable x_1 and then solve it for different values of t (the Newton's method has been used for numerical calculations). Also, to optimize the issue, we have found a simple property of relation (44), i.e. if the point (x_1^*, x_2^*, t^*), where $t^* \in [0, T/2)$ for $T := 2\pi/\omega$ is the perpetual point, then point $(-x_1^*, -x_2^*, t^* + T/2)$ is perpetual also. This observation allows to reduce the boundaries of t variable into $t \in [0, T/2)$. However, both points (x_1^*, x_2^*, t^*) and $(-x_1^*, -x_2^*, t^* + T/2)$ should be examined for the attractors

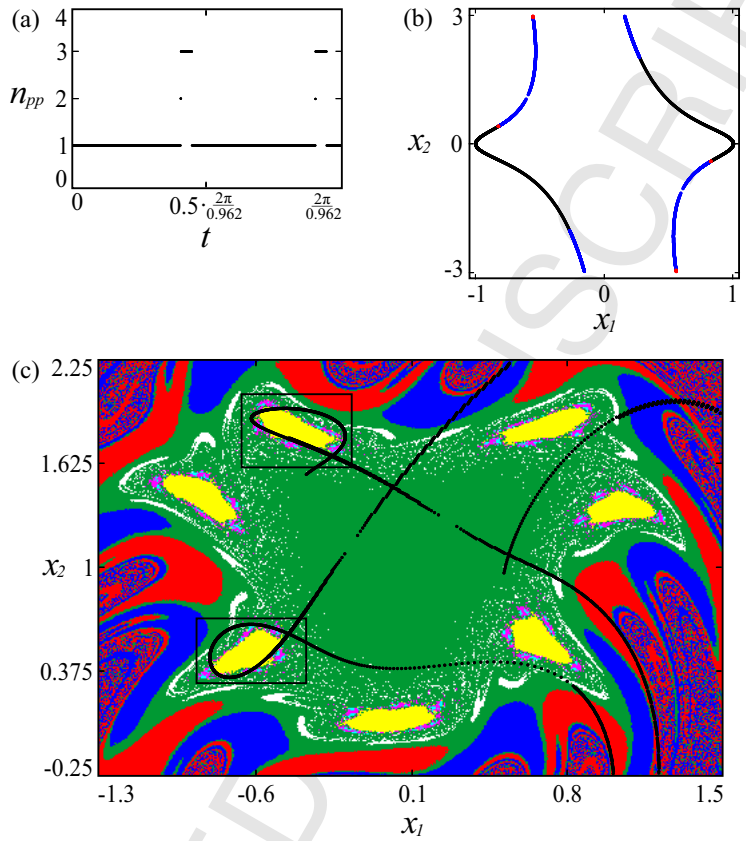

Figure 24: (color online). Perpetual points of system (44) for parameters $\alpha = 0.2, F = 1$, and $\omega = 0.962$. In (a) the number of coexisting points as a function of time is shown, while in (b) their projection on (x_1, x_2) plane is presented. The basins of attraction for single oscillator and the trajectory points (marked as black dots) when crossing the $t = 2\pi/\omega$ plane are shown in (c) [52].

because the basins of attraction are asymmetric and the points may lead to different states.

The results of our calculations are shown in Fig. 24. The number of coexisting perpetual points as the function of variable t is presented in Fig. 24(a). n_{pp} parameter denotes the number of existing solutions. As can be seen, there are 3 possibilities. The perpetual points can be unique, which is observed for the widest range of t variable values but there can also coexist 2 or 3 such points. As one can observe, there are two very narrow time intervals for $n_{pp} = 2$ and two wider for $n_{pp} = 3$. The obtained points are presented in Fig. 24(b), where the projection of calculated solutions of relation (44) on

(x_1, x_2) plane is shown. The black color of the curves refers to the solutions that are unique, while the red and the blue ones to the coexistence of two and three points respectively.

To determine the states to which the obtained perpetual points lead, we have run the system from each one of them (initial conditions) and saved the space coordinates when the trajectory crosses surface $t = 2\pi/\omega$. The results of this procedure are shown in Fig. 24(c). As the background we have used the basins of attraction of system (43) (these change periodically with the period of the excitation), where each color correspond to the basin of different attractors. The dynamics of each state is determined using Poincare sections and the number of the points on the map equals the periodicity of solution (infinitely many for irregular ones). In the considered example, the red, blue and green basins are the dominant ones and refer to two 9 periodic and a quasiperodic attractor respectively. Other solutions can be considered as the rare attractors as their occurence for randomly chosen initial conditions is significantly less probable than for the dominating states (for more see Sec. 3 where the concept of rare attractors has been introduced). The dynamics is as follows. The white region leads to a 25 periodic solution and the pink to 35 periodic one. The cyan color refers to two coexisting attractors of period 70 (their basins can not be separated due to the applied resolution and limitations of calculations). Likewise, in the yellow region three possible states can be obtained – two symmetrical 49–periodic and 63–periodic one. System (43) has one unstable fixed point $(x_1, x_2) = (0, 0)$, which neighbourhood leads to a quasiperiodic solution (green basin). Hence, the torus is a self–excited attractor, while the remaining states are hidden. The points of the trajectories when they cross $t = 2\pi/\omega$ surface are marked as black dots in Fig. 24(c). As one can observe, the points intersect with many regions of different colors, including the ones where initial conditions of rare attractors are located (the examples are marked as black insets in the Figure). This allows to observe so many states of different behaviour. Indeed, using perpetual points we have found ten attractors of the model (43) – nine periodic and one quasiperiodic.

As the second example, let us consider the system in three–dimentional

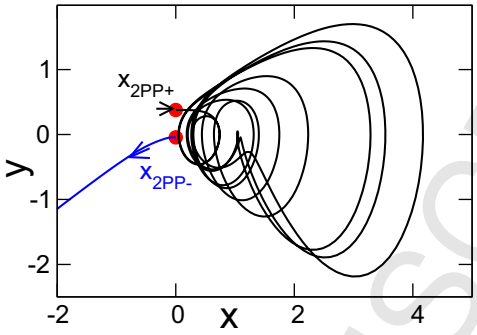

Figure 25: (color online). The transient trajectories starting from perpetual points (red circles) for system (45) at parameter $\alpha = -0.05$ [51].

phase space, described by equations

$$\begin{aligned} \dot{x} &= y, \\ \dot{y} &= z, \\ \dot{z} &= -y + 3y^2 - x^2 - xz + \alpha. \end{aligned} \tag{45}$$

System (45) has no fixed point for $\alpha < 0$ but has one chaotic hidden attractor. It has two perpetual points, $(0, x_{2PP+}, 0)$ and $(0, x_{2PP-}, 0)$, $x_{2PP\pm} = (1 \pm \sqrt{1 - 12\alpha})/6$. These are shown in Fig. 25 with red–circles. The transient trajectories starting from these PPs are shown in Fig. 25. It clearly shows that the trajectories starting from the former one goes to the hidden chaotic attractor (Fig. 25), while the latter one goes to infinity [68]. This confirms that perpetual point $(0, x_{2PP+}, 0)$ is useful to locate the hidden attractor.

All the results that have been shown suggest that the concept of perpetual points is correct and can be useful in the studies of hidden attractors in dynamical systems, especially the ones with complex behaviour. However, we can easily imagine extremally multistable systems, for which the number of coexisting attractors exceeds the number of perpetual points. What is more, recently Hoover *et al.* [148] have described the system with chaotic attractor, for which neither fixed nor perpetual points exist. This suggest that the connection between the perpetual points and the hidden attractors may be correct in one way, i.e. if the system has perpetual points, then they may lead to its hidden states.

As it can be seen, the perpetual points give only some possibilities in the research of dynamical systems. They are not the comprehensive method in finding hidden attractors but rather represent another imperfect concept

that we can apply in our studies. The concept still requires more analysis and investigations to be well understood.

4.2. Controlling evolution of hidden attractors

Over the last few decades the control of oscillating motions in dynamical systems has been the topic of intense research from both theoretical and experimental points of view [149–154]. In many practical situations fixed point solution is desirable, as for example in laser applications [155–160] where a constant output is needed and fluctuations should be avoided. There are also other situations where oscillations need to be maintained, as for instance in brain functioning [161, 162]. In some systems the regular oscillation is necessary rather than the irregular one, e.g. beating of heart [163]. Similarly, in telecommunication chaotic signal is used as a carrier signal rather than a periodic one [164]. These different requirements for specific types of motion suggest that appropriate control strategies are necessary. In this section we report the recent works which have been used to control the hidden motions.

The control of chaotic motion to periodic one is the most difficult due to an extreme sensitivity to initial conditions. However, various approaches have been established to control such motion. Foremost is the OGY method (named after Ott, Grebogi, and Yorke [165]) where unstable periodic orbits are stabilized using a linear feedback method. This method generated widespread interest and its applications can be found in almost all branches of science [150]. Another technique for chaos control is the time–delay feedback (Pyragus method [153, 154]) where unstable periodic orbits of a chaotic system are stabilized by the use of a specially designed external oscillator or by delayed self–controlling feedback without using any external force. There are other equally important methods, e.g. linear and nonlinear, adaptive control etc. (see for extensive review of various control schemes in [166]).

Over the last two decades, controlling oscillating motion to the unstable fixed points has also been a topic of intense research from both theoretical and experimental points of view [149–152, 167]. This control of chaotic dynamics to the fixed points is important in many experimental studies; for example, the removal of power fluctuation in the coupled laser systems [156–158, 160]. One of the important schemes for the stabilization of the fixed point can be done by using the phenomenon of amplitude or oscillation death [168, 169] due to interactions between the coupled oscillators. Here the interaction between two oscillators causes a pair of fixed points to become stable and attracting. These fixed points can either be the unstable fixed point of the

uncoupled system, or these can be entirely new fixed points created by the coupling (recent review of these phenomena can be found in [168, 169]).

Note that all these schemes for controlling dynamical motion have been developed and used on the systems having self–excited oscillation. How will these methods perform and what type of appropriate modifications are required for controlling the hidden attractors is yet to be explored. How to control hidden motion to another hidden one, e.g. hidden chaotic to hidden periodic motion? How are unstable periodic orbits organized within a hidden chaotic attractor and how are these different from that of self–excited chaotic attractor? These are the questions which need to be answered for proper understanding of hidden attractors. Since the concept of the hidden attractor is in itself new therefore understanding its motion and its control strategies is very challenging.

Recently, a simple and effective scheme has been proposed to stabilize the fixed points of a nonlinear oscillatory system by a suitable design of coupling with a linear dynamical system (termed as scheme of linear augmentation [170, 171]. Here, the oscillator dynamics is stabilized at the fixed–point state without changing the internal parameters of the oscillators. This method has been used for both the self–excited attractors [171–173] as well as the hidden attractors [118, 174]. We review this method below for controlling the hidden motions.

Consider a general nonlinear oscillator (2) (cf. Sec. 2). In the scheme of linear augmentation [171] the system is coupled with linear dynamical system (U) as

$$\begin{aligned} \dot{X} &= F(X,p) + \epsilon U, \\ \dot{U} &= -kU - \epsilon(X - B) \end{aligned} \tag{46}$$

Here $\dot{U} = -kU$ is linear system with decay parameter k and ϵ describes the coupling strength between the oscillator and the linear system. B is the other coupling parameter of the augmented system and can be used to locate the position of the fixed points [171]. In the absence of coupling the linear system settles at $U = 0$ for positive k. However, for nonzero coupling strength full system becomes higher dimensional. This scheme has been used rigorously for controlling the oscillating dynamics to the fixed point as well as converting multistable to monostable oscillations. In order to demonstrate this scheme let us consider the system having the hidden attractor with no fixed point, coupled with the linear system, as

$$\begin{aligned}
\dot{x} &= y, \\
\dot{y} &= z, \\
\dot{z} &= -y + 3y^2 - x^2 - xz + \alpha + \epsilon u, \\
\dot{u} &= -ku - \epsilon(z - \beta).
\end{aligned} \tag{47}$$

For $\epsilon = 0$ and $\alpha < 0$ the nonlinear system does not have any fixed point. However at $\alpha = -0.02$ it shows chaotic motion as shown in Fig. 26 (a). Since there is no fixed point therefore this chaotic motion is termed as a hidden attractor.

Due to the presence of coupling, full system (47) becomes 4–dimensional and a new set of fixed points, $x^* = \pm\sqrt{\alpha + \frac{\epsilon^2\beta}{k}}$, $y^* = 0$, $z^* = 0$, is created. Since $\alpha = -0.02$, the condition for a real fixed point solution is $\frac{\epsilon^2\beta}{k} > \alpha$. The existence and stability of these fixed points depend on the values of parameters, k, ϵ and β. Shown in Fig. 26 (b) is the phase space diagram scanned for parameters β and ϵ for $k = 0.5$. Here, the blank region represents the condition where $\frac{\epsilon^2\beta}{k} > \alpha$ does not hold and therefore in this regime the fixed points do not exist. However, the hidden chaotic attractor (Fig. 26 (a)) does continue to exist with small modification due to the presence of the linear term (Eq. (47)). In the regions of brushup (shaded) by filled–black and hatched–red colors, the condition $\frac{\epsilon^2\beta}{k} > \alpha$ is satisfied and thus it leads to the generation of new fixed points. However, the fixed point is stable in the dark regime (black color) while it is unstable in the sketched (red color) regime – the stability is estimated from real part of the largest eigenvalue of the linearized system i.e. filled–black (stable fixed points – SFP) and hatched–red (unstable fixed points – UFP) regions correspond to the negative and positive real parts of the largest eigenvalues respectively. Shown in Fig. 26 (c) is the limit cycle in the hatched–red region at parameters $\beta = 0.5 = \epsilon$ where the fixed point is unstable. This shows that the hidden chaotic attractor is converted to the limit cycle oscillation. Due to the presence of unstable fixed points this limit cycle is a self–excited attractor. At higher values of ϵ the newly created fixed point becomes stable as shown in Fig. (d) where the transient trajectory at parameter values $\beta = 0.5$ and $\epsilon = 1$. Therefore, using this scheme of linear argumentation hidden motion, if it exists, can be controlled to either limit cycle or fixed point. Note that the routes of transition from oscillating motion to the periodic and from periodic to fixed

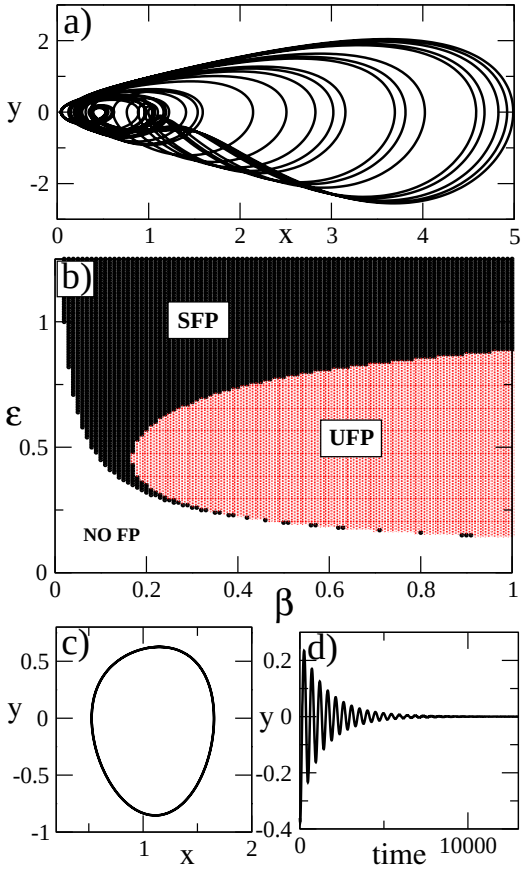

Figure 26: (color online). (a) Hidden chaotic attractor for system, Eq. (47), for $\epsilon = 0$ (uncoupled). (b) Phase space diagram in parameter space (β, ϵ) at $k = 0.5$. In blank regime the fixed point doesn't exist while filled–black and hatched–red regions correspond to the presence of unstable and stable fixed points respectively. (c) Periodic attractor and (d) fixed point solution (transient motion) for coupling strengths $\epsilon = 0.5$ and 1 respectively at $\beta = 0.5$.

point solutions are different in different regions of parameter space (for details see [118]).

In dynamical systems, multistability means the coexistence of several possible asymptotic states for a given set of parameters. These asymptotic states depend crucially on the initial conditions. The basins (the set of initial conditions which go to the same attractors) may be very complicated, e.g. fractal, riddled basins [68, 175–180]. These complicated basins make the understanding of the systems more difficult. Since this phenomenon of multistability has been found in almost all areas of science and nature last few decades have seen great interest in understanding such systems. The detailed study of multistability and its applications can not be neglected in a sense that by applying some control scheme one may use multistability to induce switches between different coexisting states in order to obtain different system performance. As multistability creates a dilemma to decide the final asymptotic state of the system a proper control technique is required for practical situations, particularly for engineering systems where a target dynamics is required. Hence, for a certain desired performance of a system control of multistability is essential. Out of several multistability control schemes [68, 118, 173, 174], the most effective way to ensure a predefined behavior of the system is to annihilate all undesired states. However, in practice, an external control is always a better choice as it may not require accessibility of the internal parameters of the system.

Considering the importance of understanding the multistability and its control several attempts have been made in the last decades. An extensive review of control of multistability has been published by Pisarchik and Feudel [24] for the self–excited multistable attractors. These schemes of control have not been used for hidden attractors so far. Recently, the presence of coexisting hidden attractors with riddled basins has been reported in [68]. It is shown that chaotic as well as periodic hidden attractors may coexist in single or coupled systems with interesting basins. These types of multistable hidden attractors are found in many systems. How to control multistability is challenging. Recently, to control such multistable hidden attractors the same linear augmentation (Eq. (46)) is used to remove multistability. It is found that linear augmentation scheme can drive the multistable hidden attractors to monostable state – for details, see [118, 173].

5. Dynamics of coupled systems with hidden attractors

The studies of the coupled systems with hidden attractors are the natural consequence of the development of research in the topic of hidden states. However, the knowledge in this area is still insufficient and the results are in very early stage. Some considerations on the issue have been shown in [68]. In the [118, 174] authors discuss the possibility of control of multistability in the systems where the unit with hidden attractor is coupled with the linear system. Recently, hidden attractors have been found in coupled systems with only self–excited attractors [181].

Although we still stand at the beginning of the road to learn and understand the behaviour of the coupled systems with hidden states, the results obtained so far are very promising. Among the standard types of synchronization that can be found in basic models, we have observed more complex patterns like clustering of the oscillators or the chimera states [182–191]. The latter ones are quite new phenomenon in dynamical systems and are very intensively studied by the researchers. Originally chimera states have been discovered by Kuramoto [182] in his studies about non–locally coupled phase oscillators. Nowadays, chimeras are being described in many different areas of science, e.g., in the mentioned phase oscillators [183–185], chemical oscillators [186, 187], neural models [188] or experimental works [189, 190]. The review of the history and basic properties of chimera states can be found in [191].

All the phenomena that we have observed in the coupled systems with hidden attractors (and also the ones that still need to be identified and described) arise from the complex nature of the systems themselves. If each unit that creates the network has hidden attractors itself, it is hard to overestimate how many possibilities of dynamics the whole system can exhibit. What we present in this Section is only the small sample of behaviour that can be found in the described models.

5.1. Identical systems – types of synchronization, clustering, chimera states with hidden heads

In our research we have focused on the coupled systems which consist of identical units with hidden attractors. We present the results obtained for the smallest possible group, i.e., two coupled oscillators, as well as the effects of our investigations in large networks. In all our considerations we have used van der Pol–Duffing oscillator as the basic unit of the studied models.

5.1.1. System of two coupled oscillators

Let us consider the system of two coupled van der Pol–Duffing oscillators, which are externally excited by the sine functions. The dynamics is given by equations

$$\begin{cases} \ddot{x} - \alpha(1-x^2)\dot{x} + x^3 + \varepsilon(y-x) = F\sin(\omega t) \\ \ddot{y} - \alpha(1-y^2)\dot{y} + y^3 + \varepsilon(x-y) = F\sin(\omega t), \end{cases} \tag{48}$$

where x and y are the state variables which describe the position in phase space of the corresponding oscillator, $\alpha = 0.2, F = 1.0, \omega = 0.962$ are fixed parameters and ε is the coupling coefficient. The latter value can be identified as the stiffness of the spring that couples oscillators in our simulation. The basins of attraction of coexisting states for such defined van der Pol–Duffing units can be found in Fig. 24(c) (cf. Sec. 4.1).

In our analysis of possible dynamics we have used the concept of perpetual points described in Sec. 4.1. The method applied to equations (48) is similar to the one presented in the quoted Section. Here, we denote x_1 (y_1) as the position of first (second) oscillator and x_2 (y_2) as its velocity. t is identified as the new time–dependent variable.

Perpetual points of the system (48) are given as the solutions of the set of equations

$$\begin{cases} \alpha(1-{x_1}^2)x_2 - {x_1}^3 + F\sin(\omega t) + \varepsilon(x_1 - y_1) = 0 \\ -2\alpha x_1 {x_2}^2 - 3{x_1}^2 x_2 + \omega F\cos(\omega t) + \varepsilon(x_2 - y_2) = 0 \\ \alpha(1-{y_1}^2)y_2 - {y_1}^3 + F\sin(\omega t) + \varepsilon(y_1 - x_1) = 0 \\ -2\alpha y_1 {y_2}^2 - 3{y_1}^2 y_2 + \omega F\cos(\omega t) + \varepsilon(y_2 - x_2) = 0. \end{cases} \tag{49}$$

Relation (49) consists of polynomials due to the variables x_1, x_2, y_1 and y_2 and is underdetermined (4 equations of 5 variables). The area of searching for solutions in five–dimensional phase space is given by $(x_1, x_2, y_1, y_2, t) \in [-2,2] \times [-3,3] \times [-2,2] \times [-3,3] \times [0, 2\pi/\omega)$. However, it should be noted that the presented equations can be simplified into two polynomial equations due to variables x_1, x_2 (or y_1, y_2, depending on the transformation) and then solved for fixed t.

To optimize the issue of finding solutions of relation (49) some useful properties of these equations can be found, i.e.:
(i) if point $(x_1^*, x_2^*, y_1^*, y_2^*, t^*)$, where $t^* \in [0, T/2)$ for $T := 2\pi/\omega$ is perpetual one, then point $(-x_1^*, -x_2^*, -y_1^*, -y_2^*, t^* + T/2)$ is perpetual also;
(ii) if (x_1^*, x_2^*, t^*) is a perpetual point of a single oscillator (without coupling),

then point $(x_1^*, x_2^*, x_1^*, x_2^*, t^*)$ is a perpetual point of the coupled system for any value of coupling coefficient ε;
(iii) for the fixed value of ε, if $(x_1^*, x_2^*, y_1^*, y_2^*, t^*)$ is a perpetual point, then point $(y_1^*, y_2^*, x_1^*, x_2^*, t^*)$ is also a perpetual one.

In our calculations, Newton's method for solving nonlinear systems of equations has been used.

The results are presented in Fig. 27. The number of calculated perpetual points is shown in the left panel of the Figure. Time variable t is fixed for each plot and the number of points corresponding to the coupling strenth $\varepsilon \in [0, 2]$ is denoted by n_{pp} parameter. In the first subfigure, for $t = 0.1 \cdot 2\pi/\omega$ (Fig. 27(a)) only three states are possible. When the coupling is small, perpetual points can be unique or five of them can coexist. After reaching some threshold value, the number of points stabilize on three. When t value increases, more complex behaviour occurs. In the Fig. 27(b), for $t = 0.25 \cdot 2\pi/\omega$ n_{pp} parameter varies from one to nine, while in Fig. 27(c), for $t = 0.95 \cdot 2\pi/\omega$ it changes from one to seven. As one can observe, the size of intervals of coupling parameter values where the given number of perpetual points coexist can change from quite wide to extremely narrow. Also, value of n_{pp} parameter is even in all presented examples, which is a simple conclusion from the properties (ii)–(iii) described above and the results obtained for the single oscillator in Sec. 2.2 (for t values considered in Fig. 27 a single system has one unique perpetual point). In the right panel in Fig. 27 the corresponding projections of perpetual points on position–velocity plane are marked by blue dots. The position of points in phase space (on curves) changes continuously with increasing ε. In addition, we present the trajectory points of system (48) when they cross fixed subspace $t = 2\pi/\omega$ – these points are shown as red dots in figure. The distribution of these points in space suggests, that they intersect with basins of different attractors that coexist in the system.

Considering calculated perpetual points as the initial conditions of system (48) we have obtained the attractors that appear only for the coupled oscillators and have not been found for the single ones, for the same parameter values (i.e., $\alpha = 0.2, F = 1$ and $\omega = 0.962$). The examples of dynamics and types of synchronization for fixed coupling parameter values are shown in Figs. 28–29. In both figures Poincare maps are presented in the left panel and the projections of trajectories on position–velocity plane in the right one. The colors on the plots correspond to the legend on the axes (red and blue colors are used in the case of anti–phase synchronization and the green one

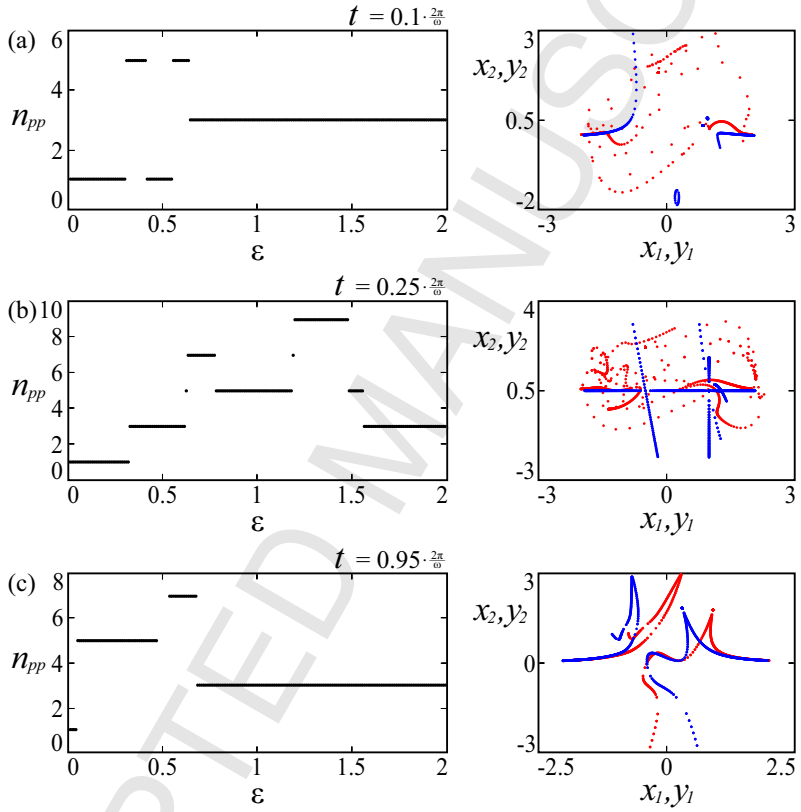

Figure 27: (color online). The number of coexisting perpetual points (n_{pp} parameter) in the function of coupling strength ε (left panel) and projection of these points on position–velocity plane (blue dots in the right panel) for system (49). Variable t is fixed for each diagram and increases from the top to the bottom, $t = 0.1 \cdot 2\pi/\omega, 0.25 \cdot 2\pi/\omega, 0.95 \cdot 2\pi/\omega$ respectively. The points of trajectories (starting from perpetual points) while crossing $t = 2\pi/\omega$ surface are marked as red dots in the right panel [52].

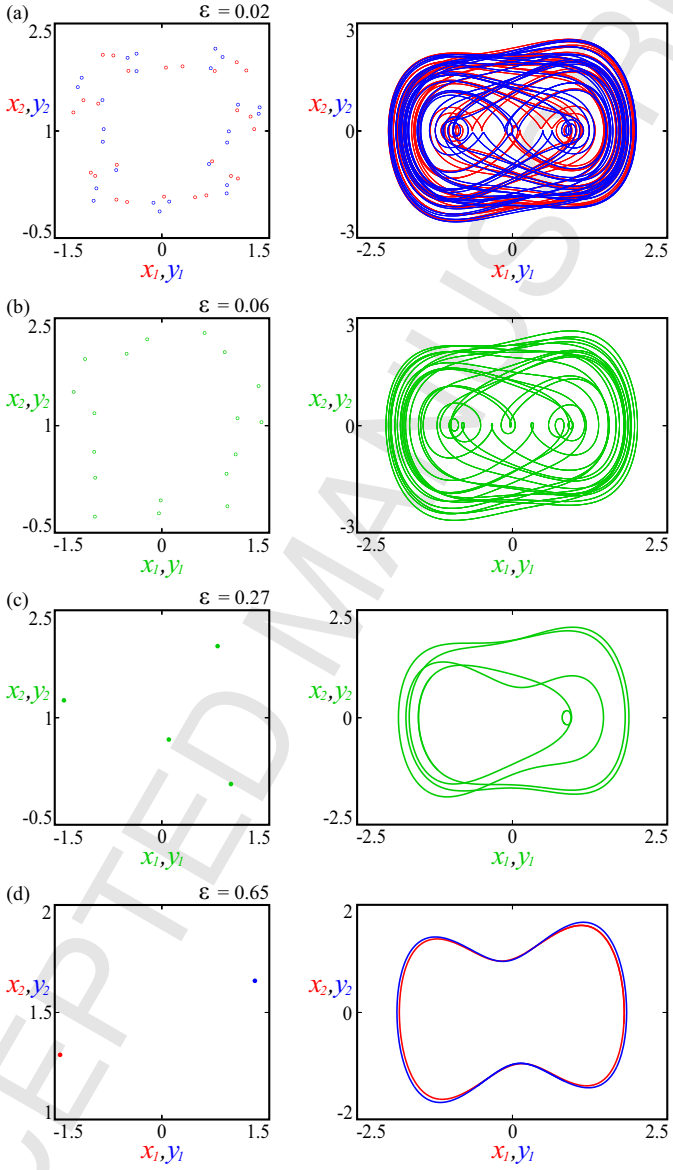

Figure 28: (color online). Poincare maps (left panel) and trajectories (right panel) of regular attractors obtained from perpetual points, that exist only for coupled oscillators system (48). Increasing from the top to the bottom, $\varepsilon = 0.02$ (coexisting attractors of period 25), $\varepsilon = 0.06$ (one common attractor of period 18), $\varepsilon = 0.27$ (one common attractor of period 4) and $\varepsilon = 0.65$ (coexisting attractors of period 1) [52].

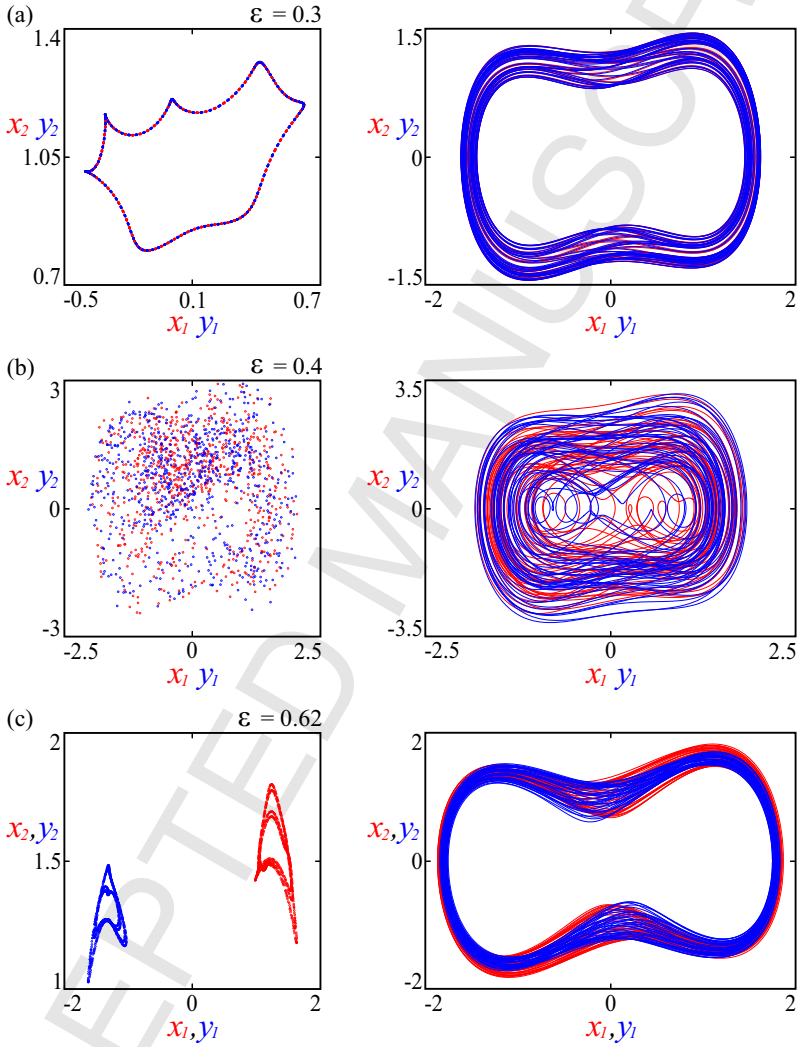

Figure 29: (color online). Poincare maps (left panel) and trajectories (right panel) of irregular attractors obtained from perpetual points, that exist only for coupled oscillators system (48). Increasing from the top to the bottom, $\varepsilon = 0.3$ (one common quasiperiodic attractor), $\varepsilon = 0.4$ (coexisting chaotic attractors) and $\varepsilon = 0.62$ (coexisting quasiperiodic attractors) [52].

in the case of in–phase synchronization).

In Fig. 28 the examples of periodic solutions are presented. In Fig. 28(a) two states of period 25 coexist, where the trajectories are symmetric around the origin of the coordinate system and the oscillators are anti–phase synchronized. The example of synchronization is shown in Fig. 28(b), where subsystems get attracted to 18 period orbit. In both these examples, the attractors bifurcate from the original ones, that can be found in the single van der Pol–Duffing oscillator (where one 25 period attractor and two 9 period attractors coexist). Another new states are shown in Fig. 28(c–d), where one attractor of period 4 (in–phase synchronization) and two solutions of period 1 (anti–phase synchronization) are shown respectively. On the other hand, irregular attractors for coupled system (48) are shown in Fig. 29. In Fig. 29(a) a torus is presented, on which both units are lag synchronized. The chaotic behaviour can be found in Fig. 29(b), where oscillators are desynchronized, although the coexisting states seem to have similar structure. Another example of quasiperiodic dynamics is shown in Fig. 29(c), where subsystems are anti–phase synchronized on two tori.

It should be emphasized, that no state shown in Figs. 28–29 (in the sense of attractor on which the first or the second oscillator is – red, blue and green curves in Figures) has been observed for a single system using perpetual points. This suggests that these states can be born only when the oscillators are coupled and what is more, that the study of perpetual points allows us to identify new local behaviour of the dynamical systems.

The presented results have been obtained for the simpliest coupling variant, where only the linear coupling of the units appears in the equations. We can generalize the issue by considering other, more complex coupling patterns, although for such systems the obtained equations for perpetual points can be much more complicated to solve.

5.1.2. Network of oscillators

To investigate more complex behaviour of the coupled dynamical systems with hidden attractors we have considered the network of coupled van der Pol–Duffing oscillators introduced above.

In this case, the system is given by equations

$$\begin{cases} \dot{x}_i = y_i + \frac{d}{2P} \sum\limits_{j=i-P}^{i+P} [x_j - x_i] \\ \dot{y}_i = \alpha(1 - {x_i}^2)y_i - {x_i}^3 + \mathrm{F}\sin\omega t + \frac{d}{2P} \sum\limits_{j=i-P}^{i+P} [y_j - y_i] \end{cases} \tag{50}$$

where x_i and y_i are real dynamic variables (position and velocity of i–th oscillator respectively), $i = 1, \ldots, N$, N is the size of the network, d is the coupling parameter, $2P$ is the number of neighbors in both directions coupled with the i–th unit (symmetric coupling), and α, F, ω are the local parameters. An additional parameter connected with the considered system is the coupling radius, defined as $r = P/N$. When $r = 1/N$, the oscillators are locally coupled and when $r = 0.5$ we obtain global coupling, otherwise the units are non–locally coupled. Also, one can observe that there are two coupling components in system (50) – one for the position coordinates (coupling by x variables) and the second for the velocity (coupling by y variables).

For our calculations we have fixed $\alpha = 0.2, F = 1.0$ and $\omega = 0.94$, for which values the dynamics of van der Pol–Duffing oscillator is bi–stable and each unit has exactly two coexisting attractors – chaotic one, which is self–excited, and period 7 orbit, which is the hidden attractor. The basins of these are shown in Fig. 30, where the Poincare map of chaotic state is presented by blue dots, with the corresponding grey basin, while the periodic attractor is marked by yellow dots, with the corresponding red basin. The size of the considered network is $N = 100$.

To analyze the possible behaviour of system (50) we have prepared simulations with many different, randomly chosen initial conditions. These, for a single simulation, have been prepared as follows: For each oscillator we have drawn one of two black boxes shown in Fig. 30, which intersect only with the basin of one of the attractors and from the chosen area the initial conditions have been taken randomly, using uniform distribution. The examples of the observed states for fixed coupling radius $r = 0.3$ and changing coupling strength are shown in Fig. 31.

In each subfigure 31(a–e) the snapshot of position in space of each oscillator is shown in the upper left panel (the (i, x_i) graph), while in the lower left panel one can observe the snapshot of mean velocity of each unit (the $(i, \tilde{y}_i)$ graph), both plots calculated after fixed transient time. On the other

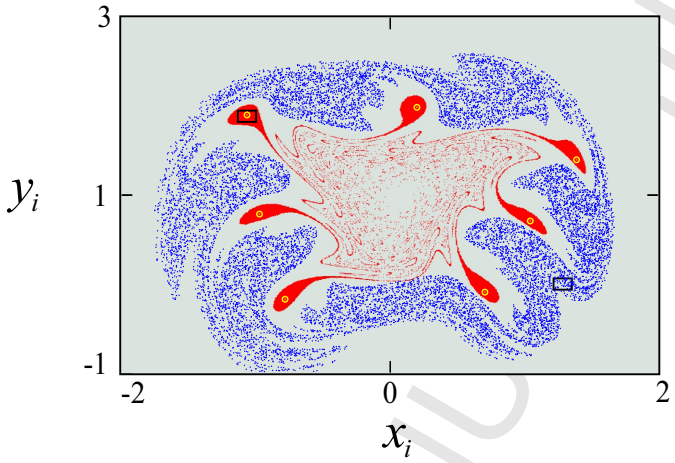

Figure 30: (color online). Poincare maps and corresponding basins of attraction of bi–stable van der Pol–Duffing oscillator. Chaotic attractor is marked by blue dots with corresponding grey basin, while period 7 orbit is marked by yellow dots with corresponding red basin. Initial conditions for oscillators have been taken from the black boxes marked in the figure. Parameters: $\alpha = 0.2, F = 1.0$ and $\omega = 0.94$.

hand, in the right panel of each subfigure the space–time mean velocity plot is presented. The colors marked on the snapshots correspond to the local dynamics of each unit creating the network (50), hence they determine the groups of different local behaviour of the oscillators.

First, when the coupling value is small (Fig. 31(a), $d = 0.005$), two different solutions of period 7 and one chaotic state are born. Each oscillator gets attracted to one of them, depending on the color of corresponding dot (blue and red dots refer to periodic orbits, while the black ones to the chaotic). The oscillators with regular local dynamics create two branches on the snapshots of position and mean velocity (the velocity is also fixed in time), while the rest of them are located randomly – we can observe here typical spatial chaos structure [192–194]. What should be noted, the blue attractor is the original state that has been found for the single oscillator (shown in Fig. 30 as yellow dots), while the second periodic attractor and the chaotic one are new states that do not appear in the original system for given parameter values. When the coupling strength increases to $d = 0.01$, in Fig. 31(b) more complex behaviour occurs. The oscillators corresponding to red, blue and black dots are on two periodic (period 7) and one chaotic attractors respectively, and the structure of these states is very similar to the ones observed for $d = 0.005$. A chimera state with chaotic head (black dots) and spatial chaos regions (in-

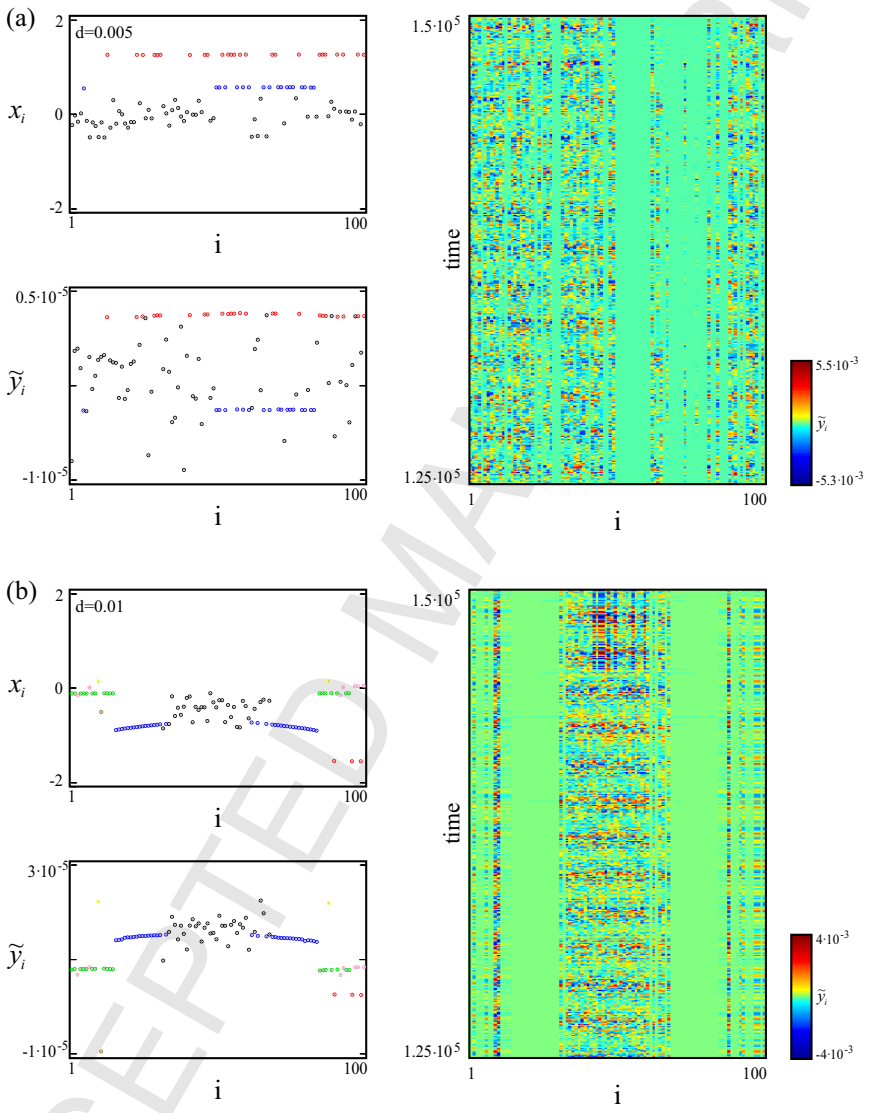

Figure 31: (color online). The examples of dynamics of the system (50) for fixed coupling radius $r = 0.3$ and different coupling coefficients. In each subfigure (a)–(e) the snapshots of position (upper left panel) and mean velocity (lower left panel), and the space–time mean velocity plot (right panel) are shown. The colors marked on the snapshots correspond to local dynamics of the oscillators. Coupling strength d increases from the top to the bottom, $d = 0.005, 0.01, 0.02, 0.025, 0.3$ respectively.

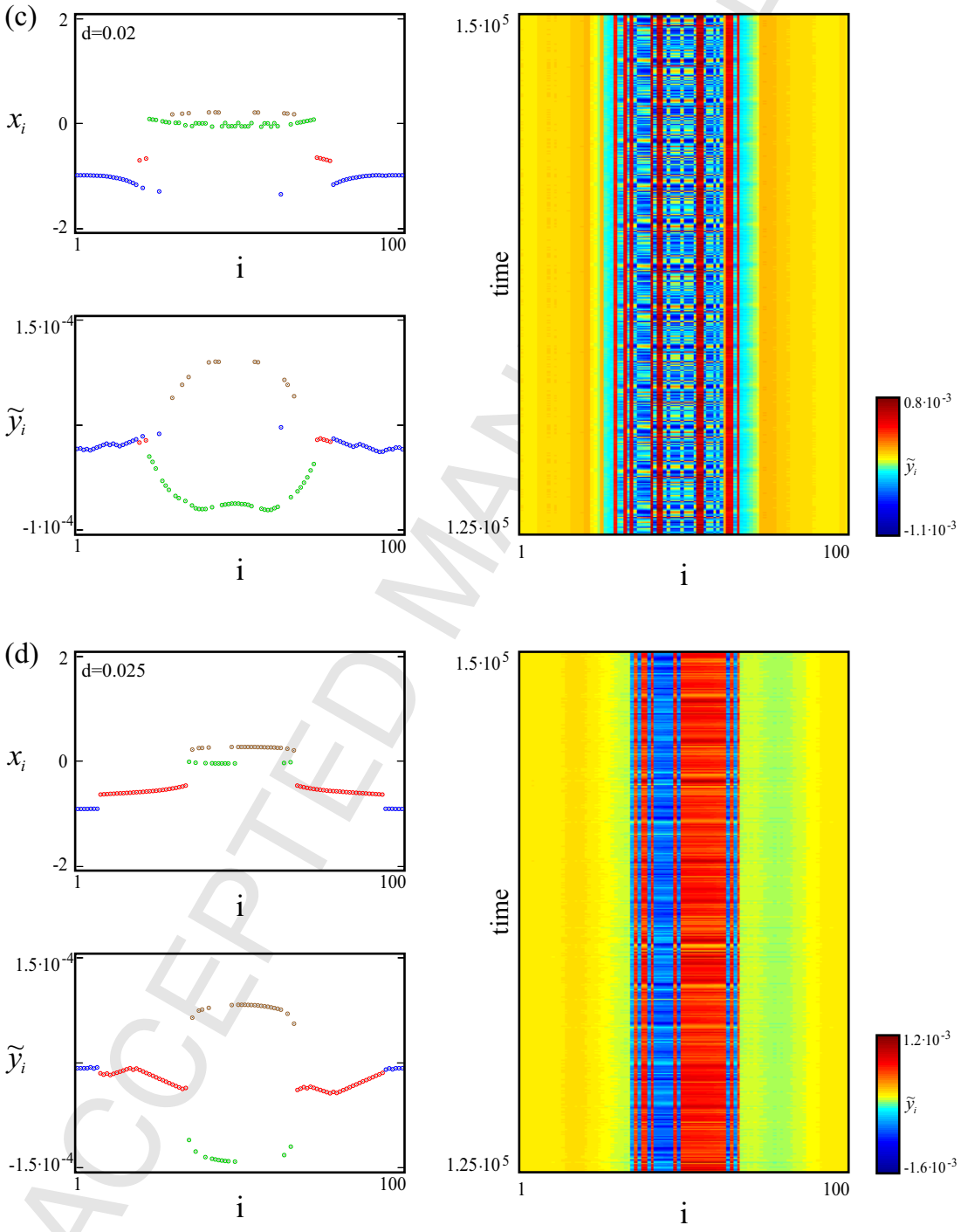

Fig. 31 (continued)

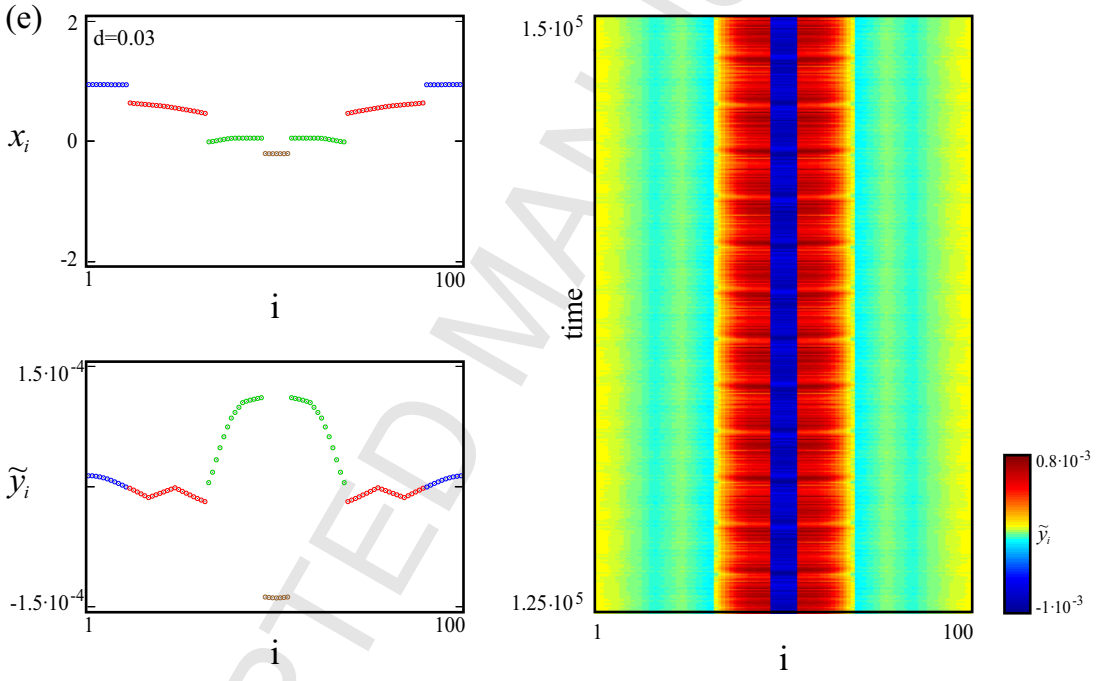

Fig. 31 (continued)

tersections between black and blue dots) is born. The rest of the oscillators is devided into four groups of different local dynamics, where the green ones are on quasiperiodic state, while the pink, yellow and brown are on chaotic attractors (but none of them is similar to the chaotic attractor in the original van der Pol–Duffing system). The structure of the mean velocity is similar to the snapshot of position, and the velocity changes in time according to the local behaviour of units creating the network. Another example of chimera state is presented in Fig. 31(c), for $d = 0.02$. Here, we can observe the state where all the oscillators are moving periodically. The ones corresponding to red and blue branches are on period 7 attractors, while the ones marked by green and brown dots are on period 14 orbits. The chimera consist of spatial pattern between green and brown clusters, also with two units (that belong to the red branch) in between those clusters. What is more, the green structure seems to contain two levels of oscillators, with slight difference in position between them (what can be seen on the snapshot of the position in Fig. 31(c)). The portrait of mean velocity shows a continuous pattern for each group of oscillators. Similar network state has been observed for $d = 0.025$ in Fig. 31(d), although in this case the oscillators from green and brown branches behave quasiperiodically (the ones from red and blue clusters are still on period 7 orbits). Also, these two groups are now separated from the others and there are no oscillators in between like it was in the previous scenario. Finally, when the coupling is large enough (Fig. 31(e), $d = 0.03$) chimera states disappear and we can observe only clusters of solutions. The local dynamics of oscillators in each of these branches is regular (red, blue – period 7, green, brown – period 14) and the portrait of mean velocity corresponds to the snapshot of position. It should be emphasized, that for each color group described above, the oscillators that belong to one chosen structure represent the same local dynamics in the qualitative sense. The attractors on which these oscillators are can exhibit some slight quantitative differences, e.g., in the position in space or in the rotation around some point. Nevertheless, we can suitably describe a sort of representative attractor, which can properly describe the local behaviour of each oscillator belonging to the group.

5.2. Influence of parameters mismatch

In Sec. 5.1 the examples of dynamics of coupled systems with hidden attractors have been shown, both for the smallest system of two and for the network of hundred units. In all these examples the initial conditions have

been arbitrary chosen. Although such calculations give us some idea about the typical behaviour and dynamical properties of the considered systems, the scenario by which the network transforms from one state to another is still unknown. Only the bifurcation analysis allows to explain and possibly understand the issue.

In this Section we have focused on network (50) described above, without changing the oscillators' coefficients and the size of the system ($\alpha = 0.2, F = 1.0, \omega = 0.94$ and $N = 100$). As bifurcation parameters we have chosen the coupling strength d and the coupling radius r. In each simulation the state presented in Fig. 31(b) for $d = 0.01$ and $r = 0.3$ has been used as a starting point for further changes in the networks' parameters.

The results for fixed coupling radius $r = 0.3$ and coupling strength d considered as the bifurcation parameter are shown in Fig. 32.

As mentioned above, the starting point is state in Fig. 32(a) for $d = 0.01$, and in the first step the coefficient is increased. The color code of the units on the snapshots is the same as in Fig. 31(b). For $d = 0.012$ (Fig. 32(b)) the oscillators marked by pink, yellow and brown dots get attracted to the green cluster. As a result, we obtain a chimera state with two coherent branches (green and blue), a chaotic head (black oscillators) and a few units separated from the main structures (red ones). The spatial chaos regions between blue and black parts also survived. With further increase to $d = 0.021$, in Fig. 32(c) one can observe that oscillators from the chaotic part of chimera are forming a kind of spatial pattern. The units no longer oscillate randomly in space like in the previous case, but they have been transformed into two intersecting levels. What is more, the blue cluster gets narrower due to the fact that some units escaped to the green one. The described behaviour occurs for higher values of d. With the increase of the coupling strength the length of the intersecting region gets smaller (oscillators begin to form one common branch), and even more units leave the blue cluster. Finally, for $d = 0.028$ (Fig. 32(d)) the spatial chaos disappears and a new cluster is born (the black one). Also, the solitary red units stick to one of the main branches. With further increase of d parameter the spatial chaos regions between black and blue structures get smaller and shrink, forming three separated clusters' patterns in space. When the coupling is large enough ($d = 0.032$), in Fig. 32(e) these clusters glue together and form common oscillating wave, on which all oscillators are synchronized.

On the other hand, in the next step we have decreased coupling d, also starting from the state for $d = 0.01$. At the beginning, the network behaves

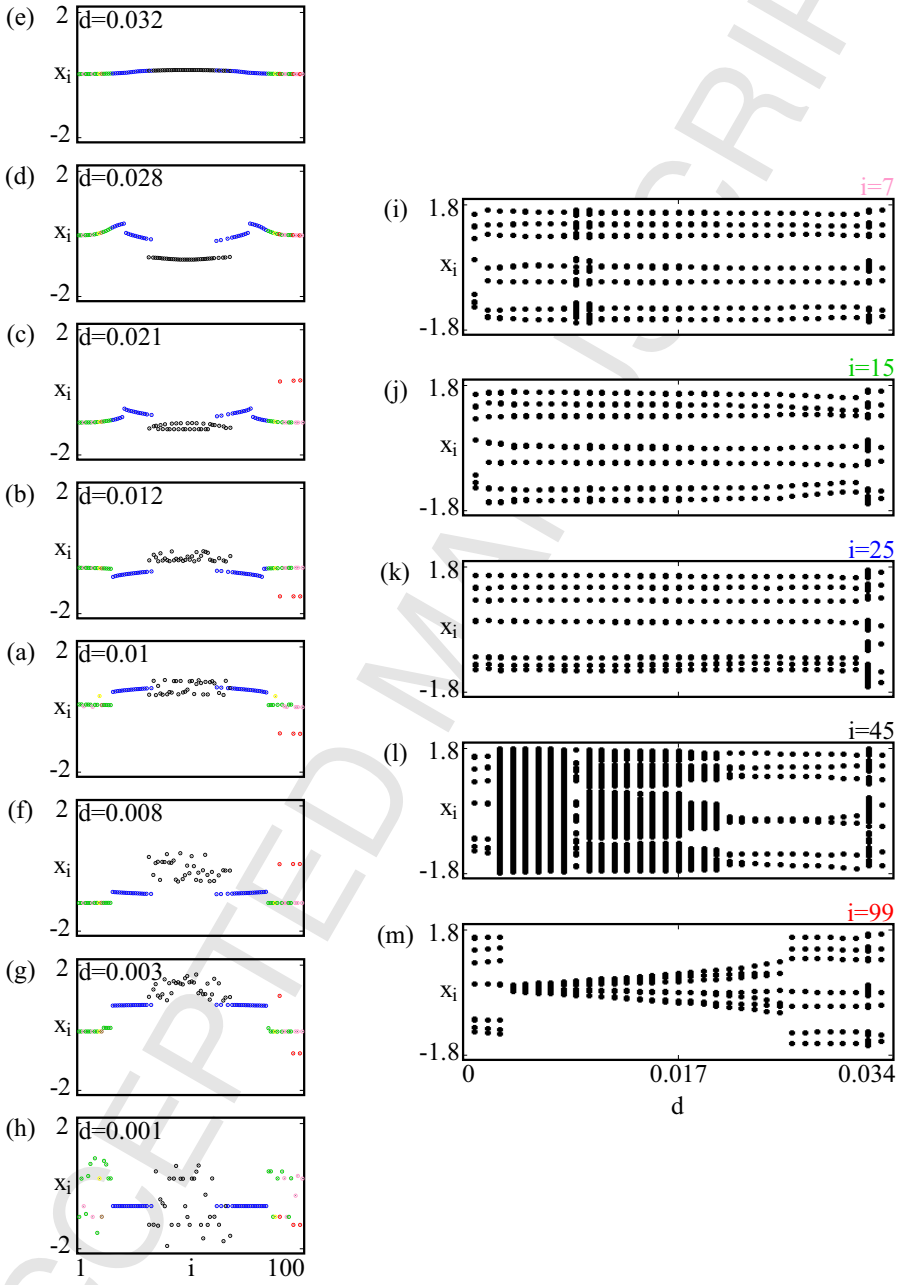

Figure 32: (color online). Bifurcation scenario for network (50) with fixed coupling radius $r = 0.3$. In the left panel the snapshots for each value of the coupling strength d (increasing from the bottom to the top, $d = 0.001, 0.003, 0.008, 0.01, 0.012, 0.021, 0.028, 0.032$ respectively) have been shown. In the right panel the bifurcation diagrams for chosen oscillators i (increasing from the top to the bottom, $i = 7, 15, 25, 45, 99$ respectively) have been presented.

similarly as in the previous procedure. For $d = 0.008$ in Fig. 32(f) the oscillators pink, yellow and brown stick to the green cluster and the rest remains the same. The differences occur with further decrease of the coupling strength. In Fig. 32(g), $d = 0.003$, the green cluster (with single pink, yellow and brown units) starts to fall apart. As it can be observed on the snapshot, four units from the left part and one unit from the right one leave the structure. Also, the red dots divide into two subgroups and no longer oscillate on the same level. Finally, when the coupling is very small at $d = 0.001$, the green branch gets destroyed and in Fig. 32(h) we obtain coherent blue clusters of oscillators and incoherent state of the remaining part of the system.

To follow the dynamics of the oscillators from one state of the network to another, in Fig. 32(i–m) bifurcation diagrams have been presented. The color code of the chosen units refers to the one used on the snapshots in Fig. 32(a–h). As one can see, oscillators 7th, 15th and 25th (pink, green and blue dots respectively) behave similarly, i.e. for increasing as well as decreasing coupling strength d they bifurcate through quasiperiodic and periodic attractors of similar structures to the final states. The dynamics of oscillator 45th (black dot on the snapshot) remains chaotic in the wide interval aroud $d = 0.01$, but finally transforms into regular one, which remains mostly for the rest of coupling values. In the case of unit 99th (red one) the amplitude of the oscillations changes (increases/decreases) in the same direction as the value of coupling, until the bifurcation parameter reaches threshold value for which it stabilizes (approximately $d = 0.026$ ($d = 0.003$) for increase (decrease) of the coupling strength). All the oscillators synchronize on chaotic state for $d = 0.032$ (Fig. 32(e)), which then bifurcate at $d = 0.033$ to periodic solution. What should be noted, also in the case $d = 0.001$ the final attractors obtained by the considered oscillators seem to be qualitatively similar.

Next, in Fig. 33 we present the results of our analysis for fixed coupling strength $d = 0.01$ and coupling radius r considered as the bifurcation parameter.

Likewise, the starting point is the state Fig. 33(a) for $r = 0.3$, and in the first step the radius is increased. The color code of the units on the snapshots is the same as previously. For $r = 0.32$ in Fig. 33(b) only the oscillators corresponding to pink dots get attracted to the green ones, while the pattern of the remaining part of the network does not change. The yellow and brown units remain solitary until $r = 0.38$ case in Fig. 33(c), when they also stick to the green cluster, creating one common branch (filled with a

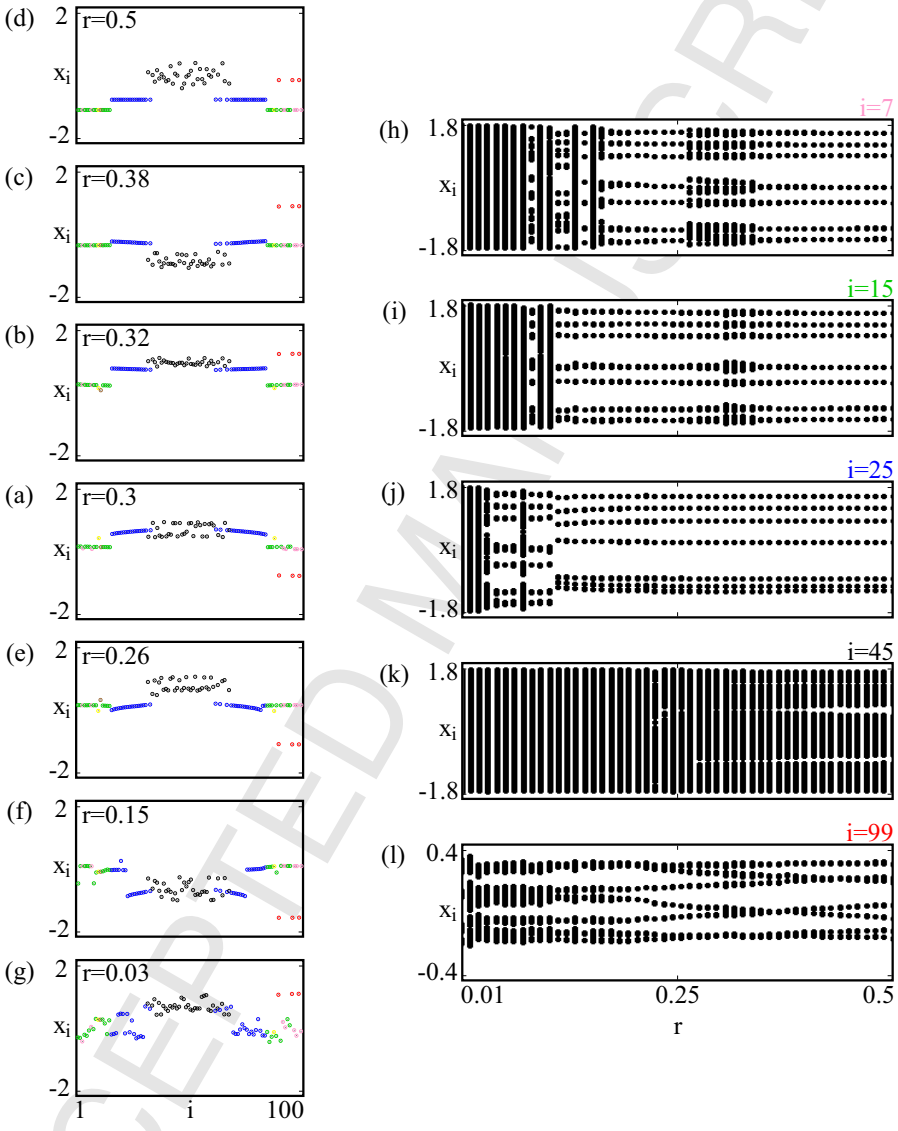

Figure 33: (color online). Bifurcation scenario for the network (50) with fixed coupling strength $d = 0.01$. In the left panel the snapshots for each value of the coupling radius r (increasing from the bottom to the top, $r = 0.03, 0.15, 0.26, 0.3, 0.32, 0.38, 0.5$ respectively) have been shown. In the right panel the bifurcation diagrams for chosen oscillators i (increasing from the top to the bottom, $i = 7, 15, 25, 45, 99$ respectively) have been presented.

few gaps corresponding to the separated red dots). Further increase of the bifurcation parameter does not change the spatial pattern of the network but the larger the coupling radius r is, the less the coherent branches wave in time. In the extreme case, for global coupling in Fig. 33(d) ($r = 0.5$) blue and green clusters only oscillate (at any moment of time t they are placed horizontally in space). As one can observe, in this case the spatial behaviour of most of the oscillators has remained unchanged.

For the case of decreasing radius r the results are as follows (likewise, we have begun the bifurcations from the network state for $r = 0.3$). The initial behaviour is identical as in the previous considerations, i.e. for $r = 0.26$ (Fig. 33(e)) the pink oscillators stick to the green ones and nothing else changes. However, with further decrease of the radius the structures begin to fall apart. As can be seen in Fig. 33(f) for $r = 0.15$, the oscillators get separated for the blue clusters to the green one, which in fact starts to become filled with more gaps and discontinuities and loses its stability. The process of destruction continues and an example of possible final state of the system is shown in Fig. 33(g) for $r = 0.03$. The whole pattern has become incoherent.

The bifurcation diagrams of a few chosen oscillators are presented in Fig. 33(h–l) (we have chosen exactly the same units as in the case of bifurcations with parameter d). The diagrams of oscillators 7th, 15th and 25th (pink, green and blue dots respectively) while increasing the bifurcation parameter are quite similar – all of them transform through chaotic and quasiperiodic/periodic states to obtain the final attractor. In the reverse bifurcations from $r = 0.3$ to $r = 0.01$ the oscillators get attracted to chaotic and quasiperiodic states (quasiperiodic windows can be seen). On the other hand, the dynamics of unit 45th (black dots) is completely different. We can observe only chaotic behaviour all the way through the bifurcation parameters. Also for oscillator 99th (red one) the transformation from one state to another proceeds differently. The curves on the diagram intersect and change their direction. Also the amplitude in much lower than in the previous examples. What should be noted, the final dynamics of the oscillators is also not the same, as it was the case with the bifurcation parameter d. For $r = 0.5$ only the 7th and 15th oscillators are on the same quasiperiodic attractor, while the 25th and 99th present different local dynamics. In contrast, the 45th unit remains on the chaotic state. For $r = 0.01$ 7th, 15th, 25th and 45th oscillators exhibit similar chaotic behaviour, while the dynamics of the 99th one seems quasiperiodic.

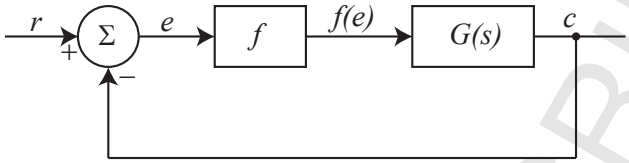

Figure 34: Nonlinear control system. $G(s)$ is a linear transfer function, $f(e)$ is a single–valued, continuous, and differentiable [195].

6. Experimental observations of hidden attractors

Hidden attractors can be observed in various nonlinear control systems, like this schematically shown in Fig. 34. In 1950s–1960s, the studies of the well–known Markus–Yamabe's [196], Aizerman's [197], and Kalman's [195] conjectures on absolute stability led to the discovery of the possible coexistence of a hidden periodic oscillation and a unique stable stationary point in automatic control systems (see [42, 44, 48, 198–202]; the corresponding discrete examples were considered in [203]). In 1957 R.E. Kalman stated the following [195]: "*If $f(e)$ in Fig. 1* [see Fig. 34] *is replaced by constants K corresponding to all possible values of $f'(e)$, and it is found that the closed–loop system is stable for all such K, then it is intuitively clear that the system must be monostable; i.e., all transient solutions will converge to a unique, stable critical point.*" Kalman's conjecture is a strengthening of Aizerman's conjecture [197], which considers nonlinearities belonging to the sector of linear stability. Note that these conjectures are valid from the standpoint of simplified analysis such as the linearization, harmonic balance, and describing function methods (DFM), which explains why these conjectures were put forward.

Nowadays, various counterexamples to these conjectures (nonlinear systems where the only equilibrium, which is stable, coexists with a hidden periodic oscillation) are known (see [42, 44, 48, 198–201, 204]; the corresponding discrete examples are considered in [203, 205]). For example, the system:

$$\begin{aligned} \dot{x}_1 &= -x_2 - 10f(e), \\ \dot{x}_2 &= x_1 - 10.1f(e), \\ \dot{x}_3 &= x_4, \\ \dot{x}_4 &= -x_3 - x_4 + f(e), \end{aligned} \tag{51}$$

where $e = x_1 - 10.1x_3 - 0.1x_4$ and $f(e) = \tanh(e)$ has the only equilibrium (green dot in Fig. 35(a)) which is stable, while the nonlinearity (blue curve

in Fig. 35(c)) and its derivative belong to the linear stability sector ($K \in (0, 9.9)$, red lines in Fig. 35(c)). At the same time the system admits a stable periodic solution, which is the hidden attractor (blue curve in Fig. 35(b) and the projection of the attractor on the plane (x_1, x_2) shown as green curve in Fig. 35(a)).

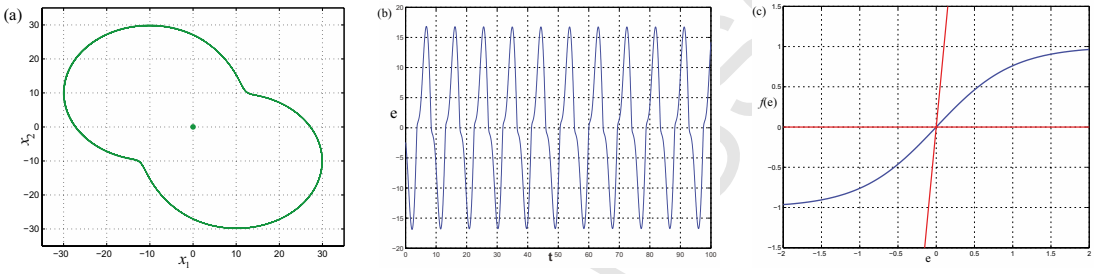

Figure 35: (color online). System (51) as the counterexample to the Kalman conjecture. In (a) the stable fixed point (green dot) and the projection of periodic solution (green curve) are shown, while in (b) the periodic behavior of e component is presented. The nonlinearity (blue curve) and the linear stability sector (red lines) are shown in (c).

Similar situation with linear stability and hidden oscillations occurs in the analysis of aircrafts and launchers control systems with saturation [206, 207]. In [33] the crash of aircraft YF–22 Boeing in April 1992, caused by the difficulties of rigorous analysis and design of nonlinear control systems with saturation, is discussed and the conclusion is drawn that *"since stability in simulations does not imply stability of the physical control system (an example is the crash of the YF22), stronger theoretical understanding is required"*.

Hidden attractors can be easily observed in various simple electronic circuits. As the first example let us consider the circuit shown in Fig.36 This circuit is the realization of the chaotic flow with a line equilibrium [132] described in Sec. 2. The equations are as follows:

$$\begin{aligned} \frac{d\nu_{c_1}}{dt} &= \frac{1}{R_1 C_1}\frac{R_8}{R_7}\nu_{c_2}, \\ \frac{d\nu_{c_2}}{dt} &= -\frac{1}{R_2 C_2} + \frac{1}{10R_3 C_2}\nu_{c_2}\nu_{c_3}, \\ \frac{d\nu_{c_3}}{dt} &= -\frac{1}{R_4 C_3} - \frac{1}{10R_5 C_3} - \frac{1}{10R_6 C_3}\nu_{c_1}\nu_{c_3}. \end{aligned} \tag{52}$$

This circuit includes four operational amplifiers, eight resistors, three capacitors and three analog multipliers. The values of electronic components are selected as $R_1 = R_2 = R_4 = R_7 = R_8 = 100k\Omega$, $R_3 = R_6 = 10k\Omega$,

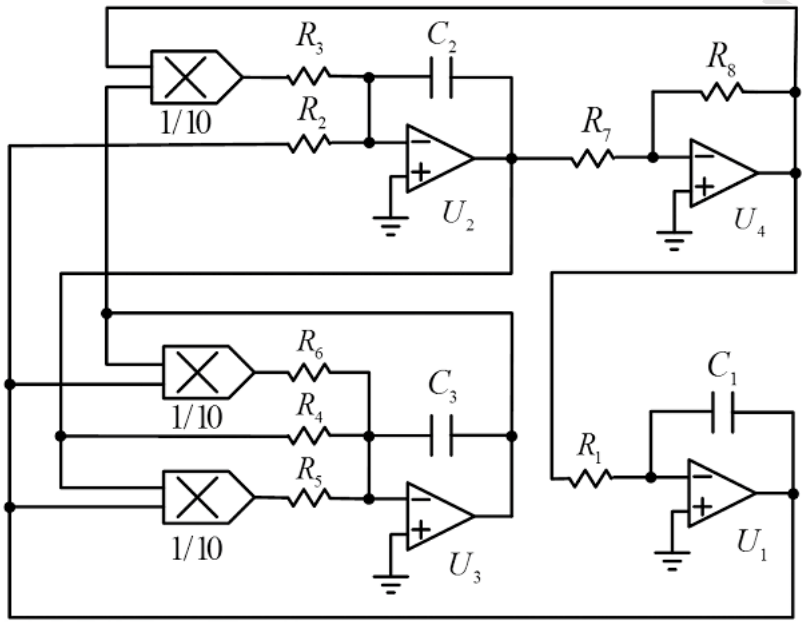

Figure 36: Circuit exhibiting hidden attractors with a line equilibrium.

$R_7 = 0.588k\Omega$ and $C_1 = C_2 = C_3 = 1nF$. The Multisim results are shown in Fig. 37 which display the hidden chaotic attractor in different planes.

As the second example consider the circuit illustrated in Fig. 38. The circuit is the realization of a four–dimensional continuous–time autonomous system without equilibrium [71]. The circuital equations are given by:

$$\begin{aligned}
\frac{d\nu_{c1}}{dt} &= -\frac{1}{R_7C_1}\nu_{c1} + \frac{1}{R_7C_1}\left(\frac{R_5}{R_4}\nu_{c2} - \frac{R_5}{R_1}\nu_{c1} + \frac{R_5}{R_3}\nu_{c1}\right), \\
\frac{d\nu_{c2}}{dt} &= -\frac{1}{R_{15}C_2}\nu_{c2} + \frac{1}{R_{15}C_2}\left(-\frac{R_{13}}{R_8}\nu_{c2} + \frac{R_{13}}{10R_{11}}\nu_{c1}\nu_{c2} + \frac{R_{13}}{R_{12}}\nu_{c4} + \frac{R_{13}}{R_{10}}\nu_{c2}\right), \\
\frac{d\nu_{c3}}{dt} &= -\frac{1}{R_{22}C_3}\nu_{c2} + \frac{1}{R_{22}C_3}\left(\frac{R_{20}}{R_18}V_1 - \frac{R_{20}}{10R_{17}}\nu_{c1}\nu_{c2} + \frac{R_{20}}{R_{19}}\nu_{c2}\right), \\
\frac{d\nu_{c4}}{dt} &= -\frac{1}{R_{27}C_4}\nu_{c4} + \frac{1}{R_{27}C_4}\left(-\frac{R_{25}}{R_{23}}\nu_{c1} + \frac{R_{25}}{R_{24}}\nu_{c4}\right).
\end{aligned} \tag{53}$$

The circuit is implemented by using common off–the–shelf components such as: operational amplifiers, resistors, capacitors and analog multipliers. The values of electronic components in Fig. 38 are chosen as follows $R_1 = R_4 = 114.94k\Omega$, $R_2 = R_3 = R_5 = R_6 = R_{10} + R_{16} = R_{18} = R_{19} = R_{20} = R_{24} = R_{25} = 100k\Omega$, $R_7 = R_{15} = R_{22} = R_{27} = 1k\Omega$, $R_8 = R_{14} = R_{23} = R_{26} =$

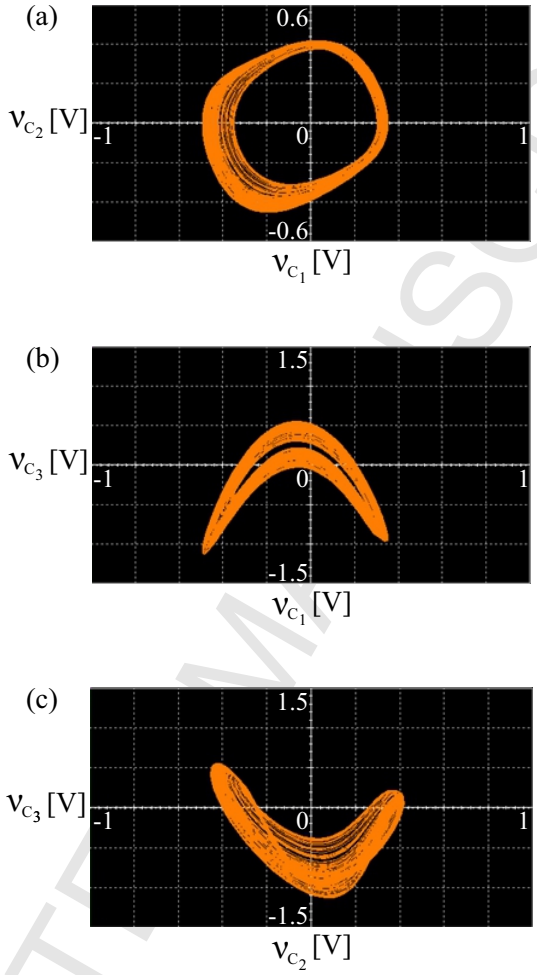

Figure 37: (color online). Hidden chaotic attractors of the circuit (52) with a line equilibrium in different planes: (a) $\nu_{c_1}\nu_{c_2}$, (b) $\nu_{c_1}\nu_{c_3}$, (c) $\nu_{c_2}\nu_{c_3}$.

$200k\Omega$, $R_9 = 9.8k\Omega$, $R_{11} = R_{17} = R_{21} = 10k\Omega$, $R_{12} = 500k\Omega$, $V_1 = 1V_{DC}$ and $C_1 = C_2 = C_3 = C_4 = 100nF$. We use the oscilloscope to display the hidden chaotic attractors. The experimental results are shown in Fig. 39.

There are some precautions for designing an analog circuit that emulates the dynamics of chaotic flow, especially when the attractor is hidden:
(a) The components of the analog circuit must be selected carefully to match the mathematical model. Choosing correct off–the–shelf discrete components is a practical challenge. For example, it is easy to change the parameters and the eigenvalues of the chaotic system with one stable equilibrium when in-

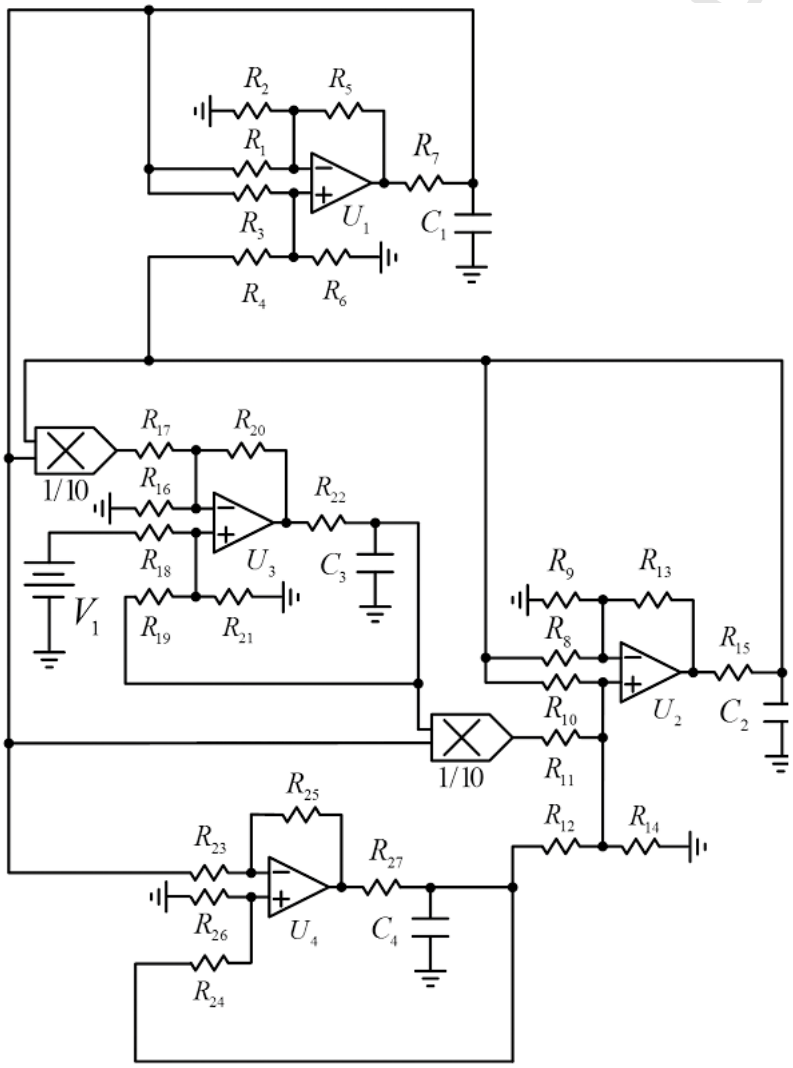

Figure 38: Circuit exhibiting hidden attractors without equilibrium.

appropriate values of the electronic components are used. In such cases, the dynamics of the system can change radically.

(b) The limits of operational amplifiers and analog multipliers, such as saturation, power supply voltages, nonlinearities, frequency limitations and acceptable inputs must be considered. For example, in a chaotic system like

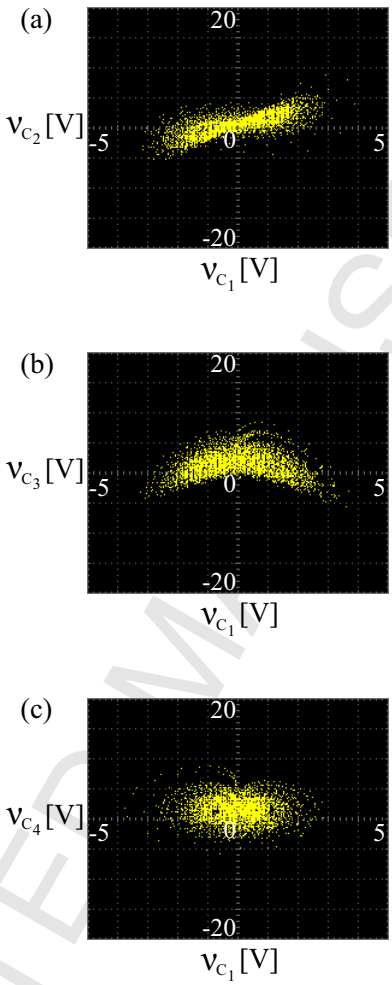

Figure 39: (color online). Hidden chaotic attractors of the circuit (53) without equilibrium in different planes: (a) $\nu_{c_1}\nu_{c_2}$, (b) $\nu_{c_1}\nu_{c_3}$, (c) $\nu_{c_1}\nu_{c_4}$.

NE_4 [66], the amplitudes of the variables are much greater than the other cases (see Fig.1 in [66]).

7. Conclusions

We give evidence that the hidden attractors can be expected in a great number of dynamical systems ranging from low–dimensional (2–dimensional) ones to the high–dimensional networks of coupled oscillators. Recently, these state have been also observed in maps (see, e.g. [203, 205, 208]). In many

cases hidden attractors have small basins of attractions and the system's evolution on them is very sensitive towards external perturbations (noise), initial conditions and small changes of the system's parameters. Typically even small perturbation can lead to an unexpected switch to a different attractor. In applied systems this switch is equivalent to the catastrophic bifurcation from the desired to the undesired regime. Such bifurcations in ecological or climate models can explain the events like the collapse of an overharvested population or ancient climatic changes. In engineering systems the catastrophic bifurcations can lead to the damages of the commercial devices. To avoid such unexpected events one needs to identify all hidden attractors, estimate its basins of attraction and apply an appropriate controlling scheme.

Contrary to the self–excited attractors the hidden attractors do not touch unstable fixed points in their basins of attractions. To localize them one cannot use transient processes leading to the attractors from the neighborhoods of the unstable fixed points. For numerical uncovering of hidden attractors it is necessary to develop special analytical–numerical procedures (e.g. evolutionary algorithms [209, 210]). Typically such procedures are based on the knowledge of the system topology. As this knowledge can be very limited, particularly in the case of high–dimensional systems an approach based on perpetual points (defined in Sec. 4) has been proposed. We give evidence that if the system has perpetual points, then the transient processes initiating from them lead to hidden attractors.

The dynamics of the network consisting of such units with hidden attractors can become very complex. Chimera states, cluster synchronization and other dynamical structures are only a few patterns that can be found in such systems. Here, we have only scratched the surface and all the analysis presented in the Sec. 5 are the prelude to more complex considerations. These can include different types and sizes of networks, methods of coupling as well as systems which dynamics exhibit high multistability (a great number of coexisting self–excited and hidden attractors).

Hidden atttractors are robust and can be observed experimentally. We briefly describe the cases of the occurences of such attractors in experimental systems. The examples of the circuit implementations of the systems with hidden attractors are given.

Acknowledgements DD and TK thank the Polish National Science Centre for supporting the project (MAESTRO Programme – Project No 2013/08/A/ST8/00/780). GL and NK thank the Russian Scientific Foun-

dation (project 14-21-00041). AP thanks DST, Government of India for financial support and TU, Lodz for warm hospitality. The authors would like to thank Dr. Viet Thanh Pham, Professor J. C. Sprott, Professor Seyed Mohammad Reza Hashemi Golpayegani, Dr. Sifeu Takougang Kingni, Mrs. Fahimeh Nazarimehr, for help and comments which enhanced the quality of this paper.

8. References

[1] M. Scheffer, Critical Transitions in Nature and Society, Princeton University Press, 2009.

[2] T. M. Lenton, H. Held, E. Kriegler, J. W. Hall, W. Lucht, S. Rahmstorf, H. J. Schellnhuber, Tipping elements in the earth's climate system, Proc. Natl. Acad. Sci. USA 105 (2008) 1786.

[3] N. Boers, B. Bookhagen, H. M. J. Barbosa, N. Marwan, J. Kurths, J. A. Marengo, Prediction of extreme floods in the eastern Central Andes based on a complex networks approach, Nat. Commun. 5 (2014) 5199.

[4] N. Boers, A. Rheinwalt, B. Bookhagen, H. M. J. Barbosa, N. Marwan, J. Marengo, J. Kurths, The South American rainfall dipole: A complex network analysis of extreme events, Geophys. Res. Lett. 41 (2014) 7397.

[5] N. Boers, B. Bookhagen, N. Marwan, J. Kurths, J. Marengo, Complex networks identify spatial patterns of extreme rainfall events of the South American Monsoon System, Geophys. Res. Lett. 40 (2013) 4386.

[6] M. Scheffer, S. Carpenter, J. A. Foley, C. Folke, B. Walker, Catastrophic shifts in ecosystems, Nature 413 (2001) 591.

[7] L. Da Silveira Lobo Sternberg, Savanna-forest hysteresis in the tropics, Glob. Ecol. Biogeogr. 10 (2001) 369.

[8] M. Hirota, M. Holmgren, E. H. Van Nes, M. Scheffer, Global resilience of tropical forest and savanna to critical transitions, Science 334 (2011) 232.

[9] R. M. May, Thresholds and breakpoints in ecosystems with a multiplicity of stable states, Nature 269 (1977) 471.

[10] A. Babloyantz, A. Destexhe, Low-dimensional chaos in an instance of epilepsy, Proc. Natl. Acad. Sci. USA 83 (1986) 3513.

[11] W. W. Lytton, Computer modelling of epilepsy, Nature Rev. Neurosci. 9 (2008) 626.

[12] B. Litt, R. Esteller, J. Echauz, M. D'Alessandro, R. Shor, T. Henry, P. Pennell, C. Epstein, R. Bakay, M. Dichter, G. Vachtsevanos, Epileptic seizures may begin hours in advance of clinical onset: a report of five patients, Neuron 30 (2001) 51.

[13] P. E. Mc Sharry, L. A. Smith, L. Tarassenko, Prediction of epileptic seizures: are nonlinear methods relevant?, Nature Med. 9 (2003) 241.

[14] H. Erzgraber, D. Lenstra, B. Krauskopf, E. Wille, M. Peil, I. Fisher, W. Elsaer, Mutually delay-coupled semiconductor lasers: Mode bifurcation scenarios, Opt. Commun. 255 (2005) 286.

[15] J. Kambhu, S. Weidman, N. Krishnam, New Directions for Understanding Systemic Risk: A Report on a Conference Cosponsored by the Federal Reserve Bank of New York and the National Academy of Sciences, The National Academies Press, 2007.

[16] R. M. May, G. Levin, S. A. Sugihara, Ecology for bankers, Nature 451 (2008) 893.

[17] P. J. Menck, J. Heitzig, J. Kurths, H. J. Schellnhuber, How dead ends undermine power grid stability, Nat. Commun. 5 (2014) 3969.

[18] M. Kapitaniak, K. Czolczynski, P. Perlikowski, A. Stefanski, T. Kapitaniak, Synchronous states of slowly rotating pendula, Phys. Rep. 541 (2014) 1.

[19] M. Kapitaniak, M. Lazarek, M. Nielaczny, P. Perlikowski, T. Kapitaniak, Synchronization extends the life time of the desired behavior of globally coupled systems, Sci. Rep. 4 (2014) 4391.

[20] J. Machowski, B. J. W., J. R. Bumby, Power System Dynamics: Stability and Control, Wiley, 2008.

[21] U. Feudel, Complex dynamics in multistable systems, Int. J. Bifurcat. Chaos 18 (2008) 1607.

[22] M. D. Shrimali, A. Prasad, R. Ramaswamy, U. Feudel, The nature of attractor basins in multistable systems, Int. J. Bifurcat. Chaos 18 (2008) 1675.

[23] S. Kraut, U. Feudel, Multistability, noise, and attractor hopping: The crucial role of chaotic saddles, Phys. Rev. E 66 (2002) 015207.

[24] A. N. Pisarchik, U. Feudel, Control of multistability, Phys. Rep. 540 (2014) 167.

[25] A. Chudzik, P. Perlikowski, A. Stefanski, T. Kapitaniak, Multistability and rare attractors in van der Pol-Duffing oscillator, Int. J. Bifurcat. Chaos 21 (2011) 1907.

[26] S. L. T. de Souza, A. M. Batista, I. L. Caldas, R. L. Viana, T. Kapitaniak, Noise-induced basin hopping in a vibro-impact system, Chaos Soliton. Fract. 32 (2007) 758.

[27] B. Blazejczyk-Okolewska, T. Kapitaniak, Co-existing attractors of impact oscillator, Chaos Soliton. Fract. 9 (1998) 1439.

[28] B. Blazejczyk-Okolewska, T. Kapitaniak, Dynamics of impact oscillator with dry friction, Chaos Soliton. Fract. 7 (1996) 1455.

[29] T. Kapitaniak, Generating strange nonchaotic trajectory, Phys. Rev. E 47 (1993) 1408.

[30] T. Kapitaniak, Stochastic response with bifurcations to non-linear Duffing's oscillator, J. Sound Vib. 102 (1985) 440.

[31] A. Silchenko, T. Kapitaniak, V. S. Anishchenko, Noise-enhanced phase locking in a stochastic bistable system driven by a chaotic signal, Phys. Rev. E 59 (1999) 1593.

[32] M. Scheffer, J. Bascompte, W. A. Brock, V. Brovkin, S. R. Carpenter, V. Dakos, H. Held, E. H. van Nes, M. Rietkerk, G. Sugihara, Early-warning signals for critical transitions, Nature 461 (2009) 53.

[33] T. Lauvdal, R. Murray, T. Fossen, Stabilization of integrator chains in the presence of magnitude and rate saturations: a gain scheduling approach, in: Proc. IEEE Control and Decision Conference, Vol. 4, 1997, p. 4404.

[34] H. E. Nusse, J. A. Yorke, E. J. Kostelich, Dynamics: Numerical Explorations, Springer New York, 1982.

[35] T. S. Parker, L. O. Chua, Numerical Algorithms for Chaotic Systems, Springer New York, 1989.

[36] Y. Ueda, N. Akamatsu, C. Hayashi, Computer simulations and non-periodic oscillations, Trans. IEICE Japan 56A (1973) 218.

[37] N. V. Kuznetsov, G. A. Leonov, V. I. Vagaitsev, Analytical-numerical method for attractor localization of generalized Chua's system, IFAC Proceedings Volumes (IFAC-PapersOnline) 4 (2010) 29.

[38] G. A. Leonov, N. V. Kuznetsov, V. I. Vagaitsev, Localization of hidden Chua's attractors, Phys. Lett. A 375 (2011) 2230.

[39] G. A. Leonov, N. V. Kuznetsov, V. I. Vagaitsev, Hidden attractor in smooth Chua systems, Physica D 241 (2012) 1482.

[40] G. A. Leonov, N. V. Kuznetsov, Hidden attractors in dynamical systems. From hidden oscillations in Hilbert-Kolmogorov, Aizerman, and Kalman problems to hidden chaotic attractors in Chua circuits, Int. J. Bifurcat. Chaos 23 (2013) 1330002.

[41] G. A. Leonov, V. I. Vagaitsev, N. V. Kuznetsov, Algorithm for localizing Chua attractors based on the harmonic linearization method, Dokl. Math. 82 (2010) 693.

[42] N. V. Kuznetsov, G. A. Leonov, S. M. Seledzhi, Hidden oscillations in nonlinear control systems, IFAC Proceedings Volumes (IFAC-PapersOnline) 18 (2011) 2506.

[43] G. A. Leonov, N. V. Kuznetsov, O. A. Kuznetsova, S. M. Seledzhi, V. I. Vagaitsev, Hidden oscillations in dynamical systems, Trans. Syst. Control 6 (2011) 54.

[44] V. O. Bragin, V. I. Vagaitsev, N. V. Kuznetsov, G. A. Leonov, Algorithms for finding hidden oscillations in nonlinear systems. The Aizerman and Kalman conjectures and Chua's circuits, J. Comput. Sys. Sc. Int. 50 (2011) 511.

[45] N. Kuznetsov, O. Kuznetsova, G. Leonov, V. Vagaitsev, Analytical-numerical localization of hidden attractor in electrical Chua's circuit, Informatics in Control, Automation and Robotics, Lecture Notes in Electrical Engineering 174 (2013) 149.

[46] G. A. Leonov, N. V. Kuznetsov, Prediction of hidden oscillations existence in nonlinear dynamical systems: analytics and simulation, Adv. Intell. Syst. Comput. 210 (2013) 5.

[47] R. N. Madan, Chua's Circuit: A Paradigm for Chaos, World Scientific, Singapore, 1993.

[48] G. A. Leonov, N. V. Kuznetsov, Algorithms for searching for hidden oscillations in the Aizerman and Kalman problems, Dokl. Math. 84 (2011) 475.

[49] S. Brezetskyi, D. Dudkowski, T. Kapitaniak, Rare and hidden attractors in van der Pol-Duffing oscillators, Eur. Phys. J. Spec. Top. 224 (2015) 1459.

[50] P. J. Menck, J. Heitzig, N. Marwan, J. Kurths, How basin stability complements the linear-stability paradigm, Nat. Phys. 9 (2013) 89.

[51] A. Prasad, Existence of perpetual points in nonlinear dynamical systems and its applications, Int. J. Bifurcat. Chaos 25 (2015) 1530005.

[52] D. Dudkowski, A. Prasad, T. Kapitaniak, Perpetual points and hidden attractors in dynamical systems, Phys. Lett. A 379 (2015) 2591.

[53] G. Leonov, N. Kuznetsov, T. Mokaev, Homoclinic orbits, and self-excited and hidden attractors in a Lorenz-like system describing convective fluid motion, Eur. Phys. J. Spec. Top. 224 (2015) 1421.

[54] D. Hilbert, Mathematical problems, Bull. Amer. Math. Soc. (1901-1902) 437.

[55] N. N. Bautin, On the number of limit cycles generated on varying the coefficients from a focus or centre type equilibrium state, Doklady Akademii Nauk SSSR (in Russian) 24 (1939) 668.

[56] G. A. Leonov, O. A. Kuznetsova, Lyapunov quantities and limit cycles of two-dimensional dynamical systems. Analytical methods and symbolic computation, Regul. Chaotic Dyn. 15 (2010) 354.

[57] N. V. Kuznetsov, O. A. Kuznetsova, G. A. Leonov, Visualization of four normal size limit cycles in two-dimensional polynomial quadratic system, Diff. Equat. Dynam. Systems 21 (2013) 29.

[58] S. Nose, A molecular dynamics method for simulations in the canonical ensemble, Mol. Phys. 52 (1984) 255.

[59] W. Hoover, Canonical dynamics: Equilibrium phase-space distributions, Phys. Rev. A 31 (1985) 1695.

[60] H. Posch, W. Hoover, F. Vesely, Canonical dynamics of the Nosé oscillator: Stability, order, and chaos, Phys. Rev. A 33 (1986) 4253.

[61] J. C. Sprott, Some simple chaotic flows, Phys. Rev. E 50 (1994) R647.

[62] J. Sprott, W. Hoover, C. Hoover, Heat conduction, and the lack thereof, in time-reversible dynamical systems: Generalized Nosé-Hoover oscillators with a temperature gradient, Phys. Rev. E 89 (2014) 042914.

[63] C. Sprott, Strange attractors with various equilibrium types, Eur. Phys. J. Spec. Top. 224 (2015) 1409.

[64] X.-S. Y. Lei Wang, The invariant tori of knot type and the interlinked invariant tori in the Nose-Hoover oscillator, Eur. Phys. J. B 88 (2015) 78.

[65] Z. Wei, Dynamical behaviors of a chaotic system with no equilibria, Phys. Lett. A 376 (2011) 102.

[66] S. Jafari, J. Sprott, S. Golpayegani, Elementary quadratic chaotic flows with no equilibria, Phys. Lett. A 377 (2013) 699.

[67] D. Cafagna, G. Grassi, Chaos in a new fractional-order system without equilibrium points, Commun. Nonlinear Sci. 19 (2014) 2919.

[68] U. Chaudhuri, A. Prasad, Complicated basins and the phenomenon of amplitude death in coupled hidden attractors, Phys. Lett. A 378 (2014) 713.

[69] A. Kuznetsov, S. Kuznetsov, E. Mosekilde, N. Stankevich, Co-existing hidden attractors in a radio-physical oscillator system, J. Phys. A - Math. Theor. 48 (2015) 125101.

[70] V.-T. Pham, S. Jafari, C. Volos, X. Wang, S. Golpayegani, Is that really hidden? The presence of complex fixed-points in chaotic flows with no equilibria, Int. J. Bifurcat. Chaos 24 (2014) 1450146.

[71] V.-T. Pham, F. Rahma, M. Frasca, L. Fortuna, Dynamics and synchronization of a novel hyperchaotic system without equilibrium, Int. J. Bifurcat. Chaos 24 (2014) 1450087.

[72] V.-T. Pham, C. Volos, S. Jafari, Z. Wei, X. Wang, Constructing a novel no-equilibrium chaotic system, Int. J. Bifurcat. Chaos 24 (2014) 1450073.

[73] X. Wang, G. Chen, Constructing a chaotic system with any number of equilibria, Nonlinear Dynam. 71 (2013) 429.

[74] X. Wang, G. Chen, A chaotic system with only one stable equilibrium, Commun. Nonlinear Sci. 17 (2014) 1264.

[75] S. Huan, Q. Li, X.-S. Yang, Horseshoes in a chaotic system with only one stable equilibrium, Int. J. Bifurcat. Chaos 23 (2013) 1350002.

[76] S. Jafari, J. C. Sprott, V.-T. Pham, S. M. R. H. Golpayegani, A. H. Jafari, A new cost function for parameter estimation of chaotic systems using return maps as fingerprints, Int. J. Bifurcat. Chaos 24 (2014) 1450134.

[77] S. Kingni, S. Jafari, H. Simo, P. Woafo, Three-dimensional chaotic autonomous system with only one stable equilibrium: Analysis, circuit design, parameter estimation, control, synchronization and its fractional-order form, Eur. Phys. J. Plus 129 (2014) 76.

[78] S.-K. Lao, Y. Shekofteh, S. Jafari, J. Sprott, Cost function based on Gaussian mixture model for parameter estimation of a chaotic circuit with a hidden attractor, Int. J. Bifurcat. Chaos 24 (2014) 1450010.

[79] S. Vaidyanathan, Anti-synchronization of Wang-Chen chaotic systems via sliding mode control, in: IEEE International Conference on Computational Intelligence & Computing Research (ICCIC), 2012, p. 1.

[80] W. X., G. Chen, Symmetrical multi-petal chaotic attractors in a 3D autonomous system with only one stable equilibrium, in: Proceedings of the 2011 Fourth International Workshop on Chaos-Fractals Theories and Applications, IEEE Computer Society, 2011, p. 82.

[81] Z. Wei, R. Wang, A. Liu, A new finding of the existence of hidden hyperchaotic attractors with no equilibria, Math. Comput. Simulat. 100 (2014) 13.

[82] Z. Wei, W. Zhang, Hidden hyperchaotic attractors in a modified Lorenz-Stenflo system with only one stable equilibrium, Int. J. Bifurcat. Chaos 24 (2014) 1450127.

[83] M. Molaie, S. Jafari, J. Sprott, S. Golpayegani, Simple chaotic flows with one stable equilibrium, Int. J. Bifurcat. Chaos 23 (2013) 1350188.

[84] A. Sommerfeld, Beitrage zum dynamischen ausbau der festigkeitslehre, Zeitschrift des Vereins deutscher Ingenieure 46 (1902) 391.

[85] R. Evan-Iwanowski, Resonance Oscillations in Mechanical Systems, Elsevier, 1976.

[86] M. Eckert, Arnold Sommerfeld: Science, Life and Turbulent Times 1868-1951, Springer, 2013.

[87] A. Fradkov, O. Tomchina, D. Tomchin, Controlled passage through resonance in mechanical systems, J. Sound Vib. 330 (2011) 1065.

[88] M. Kiseleva, N. Kuznetsov, G. Leonov, Self-excited and hidden oscillations in electromechanical systems, IFAC International Workshop on Periodic Control Systems(accepted, http://arxiv.org/).

[89] N. Mihajlovic, A. van Veggel, N. van de Wouw, H. Nijmeijer, Analysis of friction-induced limit cycling in an experimental drill-string system, J. Dyn. Syst. Meas. Control 126 (2004) 709.

[90] J. de Bruin, A. Doris, N. van de Wouw, W. Heemels, H. Nijmeijer, Control of mechanical motion systems with non-collocation of actuation and friction: A Popov criterion approach for input-to-state stability and set-valued nonlinearities, Automatica 45 (2009) 405.

[91] M. Kiseleva, N. Kuznetsov, G. Leonov, P. Neittaanmaki, Hidden oscillations in drilling system actuated by induction motor, IFAC Proceedings Volumes (IFAC-PapersOnline) 5 (2013) 86.

[92] G. A. Leonov, N. V. Kuznetsov, M. A. Kiseleva, E. P. Solovyeva, A. M. Zaretskiy, Hidden oscillations in mathematical model of drilling system actuated by induction motor with a wound rotor, Nonlinear Dynam. 77 (2014) 277.

[93] M. Kiseleva, N. Kondratyeva, N. Kuznetsov, G. Leonov, E. Solovyeva, Hidden periodic oscillations in drilling system driven by induction motor, IFAC Proceedings Volumes (IFAC-PapersOnline) 19 (2014) 5872.

[94] M. Kiseleva, N. Kondratyeva, N. Kuznetsov, G. Leonov, Hidden oscillations in drilling systems with salient pole synchronous motor, IFAC Proceedings Volumes (IFAC-PapersOnline) 48 (2015) 700.

[95] N. V. Kuznetsov, G. A. Leonov, T. N. Mokaev, Hidden attractor in the Rabinovich system(http://arxiv.org/pdf/1504.04723v1.pdf).

[96] M. Rabinovich, Stochastic autooscillations and turbulence, Uspehi Physicheskih Nauk [in Russian] 125 (1978) 123.

[97] A. S. Pikovski, M. I. Rabinovich, V. Y. Trakhtengerts, Onset of stochasticity in decay confinement of parametric instability, Sov. Phys. JETP 47 (1978) 715.

[98] G. A. Leonov, V. A. Boichenko, Lyapunov's direct method in the estimation of the Hausdorff dimension of attractors, Acta Appl. Math. 26 (1992) 1.

[99] E. N. Lorenz, Deterministic nonperiodic flow, J. Atmos. Sci. 20 (1963) 130.

[100] V. A. Boichenko, G. A. Leonov, V. Reitmann, Dimension Theory for Ordinary Diff. Equat., Teubner, Stuttgart, 2005.

[101] N. Kuznetsov, Hidden attractors in fundamental problems and engineering models. A short survey., AETA 2015: Recent Advances in Electrical Engineering and Related Sciences, Lecture Notes in Electrical Engineering 371 (2016) 13.

[102] G. Leonov, N. Kuznetsov, T. Mokaev, Homoclinic orbit and hidden attractor in the Lorenz-like system describing the fluid convection motion in the rotating cavity, Commun. Nonlinear Sci. 28 (2015) 166.

[103] A. B. Glukhovskii, F. V. Dolzhanskii, Three-component geostrophic model of convection in a rotating fluid, Academy of Sciences, USSR, Izvestiya, Atmospheric and Oceanic Physics (in Russian) 16 (1980) 311.

[104] M. I. Rabinovich, A. L. Fabrikant, Stochastic self-modulation of waves in nonequilibrium media, J. Exp. Theor. Phys. 77 (1979) 617.

[105] M.-F. Danca, G. Chen, Bifurcation and chaos in a complex model of dissipative medium, Int. J. Bifurcat. Chaos 14 (2004) 3409.

[106] C. Meador, A comparison of two 4th-order numerical ordinary differential equation methods applied to the Rabinovich-Fabrikant equations(http://scottsarra.org/math/papers/ClydeMeador_SeniorCapstone_2009.pdf).

[107] M.-F. Danca, M. Feckan, N. Kuznetsov, G. Chen, Looking more closely to the Rabinovich-Fabrikant system, Int. J. Bifurcat. Chaos(accepted, http://arxiv.org/pdf/1509.09206v1.pdf).

[108] V.-T. Pham, C. Volos, L. Gambuzza, A memristive hyperchaotic system without equilibrium, Scientific World J. 2014 (2014) 368986.

[109] F. Tahir, S. Jafari, V.-T. Pham, C. Volos, X. Wang, A novel no-equilibrium chaotic system with multiwing butterfly attractors, Int. J. Bifurcat. Chaos 25 (2015) 1550056.

[110] S. Vaidyanathan, C. K. Volos, V. Pham, Analysis, control, synchronization and SPICE implementation of a novel 4-D hyperchaotic Rikitake dynamo system without equilibrium, J. Eng. Sci. Technol. Rev. 8 (2015) 232.

[111] D. Cafagna, G. Grassi, Fractional-order systems without equilibria: The first example of hyperchaos and its application to synchronization, Chinese Phys. B 24 (2015) 080502.

[112] G. A. Leonov, N. V. Kuznetsov, Hidden oscillations in dynamical systems. 16 Hilbert's problem, Aizerman's and Kalman's conjectures, hidden attractors in Chua's circuits, J. Math. Sci. 201 (2014) 645.

[113] G. A. Leonov, M. A. Kiseleva, N. V. Kuznetsov, P. Neittaanmäki, Hidden oscillations in drilling systems: torsional vibrations, J. Appl. Nonlinear Dyn. 2 (2013) 83.

[114] J. Sprott, X. Wang, G. Chen, Coexistence of point, periodic and strange attractors, Int. J. Bifurcat. Chaos 23 (2013) 1350093.

[115] N. Kuznetsov, G. Leonov, Hidden attractors in dynamical systems: systems with no equilibria, multistability and coexisting attractors, IFAC Proceedings Volumes (IFAC-PapersOnline) 19 (2014) 5445.

[116] Z. Zhusubaliyev, E. Mosekilde, Multistability and hidden attractors in a multilevel DC/DC converter, Math. Comput. Simulat. 109 (2015) 32.

[117] Z. Wang, W. Sun, Z. Wei, S. Zhang, Dynamics and delayed feedback control for a 3D jerk system with hidden attractor, Nonlinear Dynam. 82 (2015) 577.

[118] P. Sharma, M. Shrimali, A. Prasad, N. Kuznetsov, G. Leonov, Controlling dynamics of hidden attractors, Int. J. Bifurcat. Chaos 25 (2015) 1550061.

[119] X.-Y. Dang, C.-B. Li, B.-C. Bao, H.-G. Wu, Complex transient dynamics of hidden attractors in a simple 4D system, Chin. Phys. B 24 (2015) 050503.

[120] V.-T. Pham, C. Volos, S. Jafari, X. Wang, S. Vaidyanathan, Hidden hyperchaotic attractor in a novel simple memristive neural network, Optoelectron. Adv. Mat. 8 (2014) 1157.

[121] C. Li, J. C. Sprott, Coexisting hidden attractors in a 4-D simplified Lorenz system, Int. J. Bifurcat. Chaos 24 (2014) 1450034.

[122] Z. Wei, I. Moroz, A. Liu, Degenerate Hopf bifurcations, hidden attractors and control in the extended Sprott E system with only one stable equilibrium, Turkish J. Math. 38 (2014) 672.

[123] V.-T. Pham, C. Volos, S. Vaidyanathan, T. Le, V. Vu, A memristor-based hyperchaotic system with hidden attractors: Dynamics, synchronization and circuital emulating, J. Eng. Sci. Technol. Rev. 2 (2015) 205.

[124] M. Chen, J. Yu, B.-C. Bao, Finding hidden attractors in improved memristor-based Chua's circuit, Electron. Lett. 51 (2015) 462.

[125] M. Chen, M. Li, Q. Yu, B. Bao, Q. Xu, J. Wang, Dynamics of self-excited attractors and hidden attractors in generalized memristor-based Chua's circuit, Nonlinear Dynam. 81 (2015) 215.

[126] Z. Wei, W. Zhang, Z. Wang, M. Yao, Hidden attractors and dynamical behaviors in an extended Rikitake system, Int. J. Bifurcat. Chaos 25 (2015) 1550028.

[127] I. Burkin, N. Khien, Analytical-numerical methods of finding hidden oscillations in multidimensional dynamical systems, Diff. Equat. 50 (2014) 1695.

[128] Q. Li, H. Zeng, X.-S. Yang, On hidden twin attractors and bifurcation in the Chua's circuit, Nonlinear Dynam. 77 (2014) 255.

[129] H. Zhao, Y. Lin, Y. Dai, Hidden attractors and dynamics of a general autonomous van der Pol-Duffing oscillator, Int. J. Bifurcat. Chaos 24 (2014) 1450080.

[130] V.-T. Pham, C. Volos, S. Jafari, X. Wang, Generating a novel hyperchaotic system out of equilibrium, Optoelectron. Adv. Mat. 8 (2014) 535.

[131] C. Li, J. Sprott, Chaotic flows with a single nonquadratic term, Phys. Lett. A 378 (2014) 178.

[132] S. Jafari, J. Sprott, Simple chaotic flows with a line equilibrium, Chaos Soliton. Fract. 57 (2013) 79.

[133] Z. Wei, P. Yu, W. Zhang, M. Yao, Study of hidden attractors, multiple limit cycles from Hopf bifurcation and boundedness of motion in the generalized hyperchaotic Rabinovich system, Nonlinear Dynam. 82 (2015) 131.

[134] Z. T. Zhusubaliyev, E. Mosekilde, V. G. Rubanov, R. A. Nabokov, Multistability and hidden attractors in a relay system with hysteresis, Physica D 306 (2015) 6.

[135] B. Bao, F. Hu, M. Chen, Q. Xu, Y. Yu, Self-excited and hidden attractors found simultaneously in a modified Chua's circuit, Int. J. Bifurcat. Chaos 25 (2015) 1550075.

[136] M. Zakrzhevsky, I. Schukin, V. Yevstignejev, Rare attractors in driven nonlinear systems with several degree of freedom, Scientific Proc. Riga Technical Univ. Transp. Engin. 6 (2007) 79.

[137] H. K. Khalil, Nonlinear Systems, Prentice Hall, 2002.

[138] N. Levinson, Transformation theory of non-linear Diff. Equat. of the second order, Ann. Math. 45 (1944) 723.

[139] T. Yoshizawa, Stability theory by Liapunov's second method, Math. Soc. Japan, 1966.

[140] G. Leonov, V. Reitman, Attraktoreingrenzung fur nichtlineare Systeme, Teubner, 1987.

[141] V. A. Yakubovich, Method of matrix unequalities in theory of nonlinear control systems stability. I. Forced oscillations absolute stability, Autom. Remote Control 25 (1964) 905.

[142] G. A. Leonov, I. M. Burkin, A. I. Shepelyavy, Frequency Methods in Oscillation Theory, Kluwer, 1996.

[143] V. Rasvan, Three lectures on dissipativeness, in: IEEE International Conference on Automation, Quality and Testing, Robotics, Vol. 1, 2006, p. 167.

[144] G. A. Leonov, V. Reitmann, Das Rössler-System ist nicht dissipativ im Sinne von Levinson, Math. Nachr. 129 (1986) 31.

[145] V. N. Belykh, Qualitative methods of the theory of nonlinear oscillations in point systems (in Russian), Gorki University Press, Gorki, 1980.

[146] G. A. Leonov, On the global stability of the Lorenz system, J. Appl. Math. Mech. 47 (1983) 861.

[147] A. Prasad, A note on topological conjugacy for perpetual points, Int. J. Nonlinear Sci. (in press).

[148] W. G. Hoover, C. G. Hoover, J. C. Sprott, Nonequilibrium systems: hard disks and harmonic oscillators near and far from equilibrium, Mol. Simulat. 20 (2015) 1.

[149] E. Ott, Chaos in Dynamical Systems, Cambridge University Press, 1993.

[150] I. B. Schwartz, T. W. Carr, I. Triandaf, Tracking controlled chaos: Theoretical foundations and applications, Chaos 7 (1997) 664.

[151] I. Triandaf, I. B. Schwartz, Tracking sustained chaos: A segmentation method, Phys. Rev. E 62 (2000) 3529.

[152] S. Sinha, J. S. Rao, R. Ramaswamy, Adaptive control in nonlinear dynamics, Physica D 43 (1990) 118.

[153] K. Pyragas, F. Lange, T. Letz, J. Parisi, A. Kittel, Stabilization of an unstable steady state in intracavity frequency-doubled lasers, Phys. Rev. E 61 (2000) 3721.

[154] K. Pyragas, Continuous control of chaos by self-controlling feedback, Phys. Lett. A 170 (1992) 421.

[155] M.-Y. Kim, Ph. D. Thesis, University of Maryland, 2005.

[156] M.-Y. Kim, R. Roy, J. L. Aron, T. W. Carr, I. B. Schwartz, Scaling behavior of laser population dynamics with time-delayed coupling: theory and experiment, Phys. Rev. Lett. 94 (2005) 088101.

[157] P. Kumar, A. Prasad, R. Ghosh, Stable phase-locking of an external-cavity diode laser, J. Phys. B 41 (2008) 135402.

[158] P. Kumar, A. Prasad, R. Ghosh, Strange bifurcation and phase-locked dynamics in mutually coupled diode laser systems, J. Phys. B 42 (2009) 145401.

[159] V. P. Gangwar, A. Prasad, R. Ghosh, Optical phase dynamics in mutually coupled diode laser systems exhibiting power synchronization, J. Phys. B 44 (2011) 235403.

[160] A. Prasad, Y. C. Lai, A. Gavrielides, V. Kovanis, Amplitude modulation in a pair of time-delay coupled external-cavity semiconductor lasers, Phys. Lett. A 318 (2003) 71.

[161] J. C. Sackellares, L. D. Iasemidis, R. L. Gilmore, S. N. Roper, Chaos in the Brain?, World Scientific, Singapore, 2000.

[162] L. D. Iasemidis, Epileptic seizure prediction and control, IEEE Trans. Biomed. Eng. 50 (2003) 549.

[163] D. J. Christini, K. M. Stein, S. M. Markowitz, S. Mittal, D. J. Slotwiner, M. A. Scheiner, S. Iwai, B. B. Lerma, Nonlinear-dynamical arrhythmia control in humans, P. Natl. Acad. Sci. USA 98 (2001) 5827.

[164] M. Kennedy, R. Rovatti, G. Setti, Chaotic Electronics in Telecommunications, CRC Press, 2000.

[165] E. Ott, C. Grebogoi, J. A. Yorke, Controlling chaos, Phys. Rev. Lett. 64 (1990) 1196.

[166] E. Schöl, H. G. Schuster, Handbook of Chaos Control, Wiley-VCH, 2007.

[167] E. R. Rosa, E. Ott, M. H. Hess, Transition to phase synchronization of chaos, Phys. Rev. Lett. 80 (1998) 1642.

[168] G. Saxena, A. Prasad, R. Ramaswamy, Amplitude death: The emergence of stationarity in coupled nonlinear systems, Phys. Rep. 251 (2012) 205.

[169] A. Koseska, E. Volkov, J. Kurths, Oscillation quenching mechanisms: Amplitude vs. oscillation death, Phys. Rep. 531 (2013) 173.

[170] V. Resmi, G. Ambika, R. E. Amritkar, Synchronized states in chaotic systems coupled indirectly through a dynamic environment, Phys. Rev. E 81 (2010) 046216.

[171] P. R. Sharma, A. Sharma, M. D. Shrimali, A. Prasad, Targeting fixed-point solutions in nonlinear oscillators through linear augmentation, Phys. Rev. E 83 (2011) 067201.

[172] P. R. Sharma, M. D. Shrimali, A. Prasad, U. Feudel, Controlling bistability by linear augmentation, Phys. Lett. A 377 (2013) 2329.

[173] P. R. Sharma, A. Singh, A. Prasad, M. D. Shrimali, Controlling dynamical behavior of drive-response system through linear augmentation, Eur. Phys. J. Spec. Top. 223 (2014) 1531.

[174] P. R. Sharma, M. D. Shrimali, A. Prasad, N. V. Kuznetsov, G. A. Leonov, Control of multistability in hidden attractors, Eur. Phys. J. Spec. Top. 224 (2015) 1485.

[175] S. W. McDonald, C. Grebogi, E. Ott, J. A. Yorke, Fractal basin boundaries, Physica D 17 (1985) 125.

[176] C. Grebogi, E. Kostelich, E. Ott, J. A. Yorke, Multi-dimensioned intertwined basin boundaries: basin structure of the kicked double rotor, Physica D 25 (1987) 347.

[177] J. F. Heagy, T. L. Carroll, L. M. Pecora, Experimental and numerical evidence for riddled basins in coupled chaotic systems, Phys. Rev. Lett. 73 (1994) 3528.

[178] J. C. Alexander, J. A. Yorke, Z. You, I. Kan, Riddled basins, Int. J. Bifurcat. Chaos 2 (1992) 795.

[179] E. Ott, J. C. Alexander, I. Kan, J. C. Sommerer, J. A. Yorke, A transition to chaotic attractors with riddled basins, Physica D 76 (1994) 384.

[180] Y.-C. Lai, R. L. Winslow, Riddled parameter space in spatiotemporal chaotic dynamical systems, Phys. Rev. Lett. 72 (1994) 1640.

[181] G. Leonov, N. Kuznetsov, M. Yuldashev, R. Yuldashev, Hold-in, pull-in, and lock-in ranges of PLL circuits: rigorous mathematical definitions and limitations of classical theory, IEEE Trans. Circuits Syst. – I: Regular Papers 62 (2015) 2454.

[182] Y. Kuramoto, D. Battogtokh, Coexistence of coherence and incoherence in nonlocally coupled phase oscillators, Nonl. Phen. Compl. Syst. 5 (2002) 380.

[183] C. R. Laing, The dynamics of chimera states in heterogeneous Kuramoto networks, Physica D 238 (2009) 1569.

[184] D. M. Abrams, S. H. Strogatz, Chimera states in a ring of nonlocally coupled oscillators, Int. J. Bifurcat. Chaos 16 (2006) 21.

[185] D. M. Abrams, S. H. Strogatz, Chimera states for coupled oscillators, Phys. Rev. Lett. 93 (2004) 174102.

[186] M. R. Tinsley, S. Nkomo, K. Showalter, Chimera and phase-cluster states in populations of coupled chemical oscillators, Nat. Phys. 8 (2012) 662.

[187] S. Nkomo, M. R. Tinsley, K. Showalter, Chimera states in populations of nonlocally coupled chemical oscillators, Phys. Rev. Lett. 110 (2013) 244102.

[188] J. Hizanidis, V. Kanas, A. Bezerianos, T. Bountis, Chimera states in networks of nonlocally coupled Hindmarsh-Rose neuron models, Int. J. Bifurcat. Chaos 24 (2014) 1450030.

[189] E. A. Martens, S. Thutupalli, A. Fourriere, O. Hallatschek, Chimera states in mechanical oscillator networks, P. Natl. Acad. Sci. 110 (2013) 10563.

[190] T. Kapitaniak, P. Kuzma, J. Wojewoda, K. Czolczynski, Y. Maistrenko, Imperfect chimera states for coupled pendula, Sci. Rep. 4 (2014) 6379.

[191] M. J. Panaggio, D. M. Abrams, Chimera states: coexistence of coherence and incoherence in networks of coupled oscillators, Nonlinearity 28 (2015) R67.

[192] S.-N. Chow, J. Mallet-Paret, Pattern formation and spatial chaos in lattice dynamical systems - part I, IEEE T. Circuits - I 42 (1995) 746.

[193] P. Coullet, C. Elphick, D. Repaux, Nature of spatial chaos, Phys. Rev. Lett. 58 (1987) 431.

[194] I. Omelchenko, Y. Maistrenko, P. Hovel, E. Scholl, Loss of coherence in dynamical networks: Spatial chaos and chimera states, Phys. Rev. Lett. 106 (2011) 234102.

[195] R. E. Kalman, Physical and mathematical mechanisms of instability in nonlinear automatic control systems, Transactions of ASME 79 (1957) 553.

[196] L. Markus, H. Yamabe, Global stability criteria for differential systems, Osaka Math. J. 12 (1960) 305.

[197] M. A. Aizerman, On a problem concerning the stability in the large of dynamical systems, Uspekhi Mat. Nauk (in Russian) 4 (1949) 187.

[198] V. A. Pliss, Some Problems in the Theory of the Stability of Motion, Izd LGU, 1958.

[199] R. E. Fitts, Two counterexamples to Aizerman's conjecture, IEEE Trans. Autom. Control 11 (1966) 553.

[200] N. E. Barabanov, On the Kalman problem, Sib. Math. J. 29 (1988) 333.

[201] J. Bernat, J. Llibre, Counterexample to Kalman and Markus-Yamabe conjectures in dimension larger than 3, Dyn. Contin. Discret. I. 2 (1996) 337.

[202] G. A. Leonov, N. V. Kuznetsov, Analytical-numerical methods for investigation of hidden oscillations in nonlinear control systems, IFAC Proceedings Volumes (IFAC-PapersOnline) 18 (2011) 2494.

[203] R. Alli-Oke, J. Carrasco, W. Heath, A. Lanzon, A robust Kalman conjecture for first-order plants, in: Proc. IEEE Control and Decision Conference, 2012.

[204] G. A. Leonov, V. O. Bragin, N. V. Kuznetsov, Algorithm for constructing counterexamples to the Kalman problem, Dokl. Math. 82 (2010) 540.

[205] W. P. Heath, J. Carrasco, M. de la Sen, Second-order counterexamples to the discrete-time Kalman conjecture, Automatica 60 (2015) 140.

[206] B. R. Andrievsky, N. V. Kuznetsov, G. A. Leonov, A. Y. Pogromsky, Hidden oscillations in aircraft flight control system with input saturation, IFAC Proceedings Volumes (IFAC-PapersOnline) 5 (2013) 75.

[207] B. R. Andrievsky, N. V. Kuznetsov, G. A. Leonov, S. M. Seledzhi, Hidden oscillations in stabilization system of flexible launcher with saturating actuators, IFAC Proceedings Volumes (IFAC-PapersOnline) 19 (2013) 37.

[208] S. Jafari, V.-T. Pham, S. Golpayegani, M. Moghtadaei, S. T. Kingni, The relationship between chaotic maps and some chaotic systems with hidden attractors, Int. J. Bifurcat. Chaos (private communication).

[209] I. Zelinka, A survey on evolutionary algorithms dynamics and its complexity – Mutual relations, past, present and future, Swarm Evol. Comput. 25 (2015) 2.

[210] I. Zelinka, Evolutionary identification of hidden chaotic attractors, Eng. Appl. Artif. Intel.(private communication).